THE EFFECT OF CT DISPLAY WINDOW AND IMAGE PLANE ON DIAGNOSTIC CERTAINTY FOR CHARACTERISTICS OF CANINE ELBOW DYSPLASIA

by

Tonya C. Tromblee, DVM, MS, Dipl. ACVR

Thesis submitted to the faculty of the Virginia Polytechnic Institute and State University

in partial fulfillment of the requirements for the degree of

MASTER OF SCIENCE

IN

BIOMEDICAL AND VETERINARY SCIENCES

Jeryl C. Jones, DVM, PhD, Dipl. ACVR, Chair

Peter K. Shires, BVSc, MS, Dipl. ACVS

Anne M. Bahr, DVM, MS, Dipl. ACVR

May 11, 2006

Blacksburg, Virginia

Keywords: canine elbow dysplasia, computed tomography, CT display window, CT reformatted image plane

THE EFFECT OF CT DISPLAY WINDOW AND IMAGE PLANE ON DIAGNOSTIC CERTAINTY FOR CHARACTERISTICS OF CANINE ELBOW DYSPLASIA

by

Tonya C. Tromblee, DVM, MS, Dipl. ACVR

Jeryl C. Jones, DVM, PhD, Dipl. ACVR, Chair

Department of Small Animal Clinical Sciences

VA-MD Regional College of Veterinary Medicine, Blacksburg, VA

(ABSTRACT)

Computed tomography (CT) is an established diagnostic modality for evaluation of canine elbow dysplasia. However, diagnostic sensitivity for elbow abnormalities may be affected by variations in CT image quality. Currently there are no data-based recommendations for elbow CT image display parameters. The purpose of this study was to test the effect of CT display parameters on observers' diagnostic certainty for CT abnormalities reportedly associated with canine elbow dysplasia. Fifty dysplastic elbows and ten clinically normal elbows were selected for imaging. Computed tomographic image data from selected elbows were filmed in transverse, sagittal and dorsal planes, with each plane filmed in window widths of 1500, 2500, and 3500 HU. Two veterinary radiologists independently evaluated each set of images for the presence or absence of hypoattenuating MCP subchondral defects, *in situ* MCP fissures, discrete MCP fragments, irregularity of the radial incisure of the ulna, subchondral sclerosis of the

trochlea humeri, osteochondrosis or kissing lesions, and joint incongruity. Level of diagnostic certainty for each CT abnormality was recorded for each observer using a visual analog scale system. The effect of elbow status, plane, and window on the degree of observer certainty was tested. Overall, observers demonstrated higher diagnostic certainty for normal elbows than dysplastic elbows. Observer certainty for the presence of altered subchondral density (presumed osteomalacia or sclerosis) was primarily affected by window width, whereas certainty for structural defects of the MCP, radial incisure, trochlea humeri, and joint incongruity was primarily affected by image plane.

DEDICATION

This thesis is dedicated to my mom who believed in me before I believed in myself. Your unconditional love and endless support has given me strength and allowed me to become who I am. You are my angel and my inspiration.

ACKNOWLEDGMENTS

Dr. Jeryl Jones- for her infinite wisdom, organization, and always knowing how to phrase words better than I ever could. Many thanks for your gentle prodding and encouragement, and helping me through all the baby steps.

Dr. Anne Bahr- for her contributions to the study design, enduring the teleconferences, and reading all those CT images!

Dr. Peter Shires- for contributing his clinical perspectives to the study.

Dr. Martha Larson- for her endless generosity, kindness, and understanding. Thanks for being there for me and covering floor duty when I needed time off.

Dr. Chris Ober, Jeremy Lewis, and Terry Lovern- for helping me maintain my sanity by providing daily humor and allowing me to vent.

SusieAyers (Miss Susie)- for being an ally and endless source of e-mail funnies, advice, and patience. Your laugh always makes me smile.

Susanne Aref- for making sense of all the data.

Donna Hanover and Jennifer Hanke- for the many hours they spent creating CT images.

Dr. George Lees- for use of his research dogs.

Dr. Sharon Kerwin and Galen Pahl- for their assistance with physical examinations and anesthesia.

Tim Spotswood- for his faith in me and providing the incentive to complete this.

Virginia Veterinary Medical Association Veterinary Memorial Fund- for financial support of this project.

TABLE OF CONTENTS

TABLE OF FIGURES

CHAPTER 1

OVERVIEW OF THE STUDY

This thesis contains a complete review of the literature and a manuscript in journal format that includes the description of the experimental design, results, and discussion of the findings. Appendices in this text include normal computed tomographic images of the canine elbow and a sectional anatomic atlas of the normal canine elbow obtained from a pilot study. The manuscript is a collaboration of multiple authors, however the primary author was responsible for the creation of the thesis, manuscript, and appendices. Dr. Jeryl Jones served as committee chair and primary research advisor and is credited in part for the experimental design, image interpretation, data analysis, and editorial review. Drs. Anne Bahr and Peter Shires served as committee members and also contributed to the experimental design. In addition, Dr. Bahr contributed to CT image interpretation. Dr. Susanne Aref provided data analysis and interpretation for this study. Their contributions are greatly appreciated.

1.1 INTRODUCTION

Elbow dysplasia is the most common cause of forelimb lameness in popular large and giant-breed dogs. Canine elbow dysplasia (CED) is a term used to describe a group of developmental abnormalities of the elbow which includes the well-known

lesions fragmented medial coronoid process (FCP), ununited anconeal process (UAP), osteochondrosis (OC) and/or osteochondritis dissecans (OCD), and elbow joint incongruity, but CED also includes the lesser known conditions of patella cubiti and ununited medial epicondyle.[1-7] Of all these conditions, FCP is the most common. Elbow dysplasia typically afflicts young, rapidly growing large breed dogs and frequently results in progressive and debilitating osteoarthritis. Because osteoarthritis is irreversible, early diagnosis and surgical intervention has been advocated to provide the best possible clinical outcome.[3,4,7-11]

Computed tomography (CT) is a non-invasive imaging technique that uses x-rays and computers to create sectional images of anatomic structures. Because of the complexity of the canine elbow joint, CT has become an established tool for diagnosis and treatment planning in dogs with lameness localized to the elbow.[12-16] Compared to other x-ray imaging modalities, CT has the highest diagnostic accuracy and sensitivity for FCP.[17] However, in our hospital, we have observed that CT images of canine elbows may be misinterpreted and clinically significant lesions overlooked if images are displayed using inappropriate window settings or without planar reformatted images. Previous studies have demonstrated that observers' ability to detect lesions is affected by CT image display.[18-23] However, to our knowledge, there are no published guidelines for displaying canine elbow CT images and no published reports that have investigated the effect of window settings or use of multi-planar reconstruction in observer performance for lesion detection.

The objective of this thesis was to test the effects of CT image window and plane on observers' diagnostic certainty for the presence or absence of CT characteristics reportedly associated with canine elbow dysplasia. Another objective of the study was to provide display parameter guidelines to optimally display individual CT characteristics of canine elbow dysplasia.

1.2 METHODS

The medical records at Texas A&M University College of Veterinary Medicine were reviewed for dogs evaluated for elbow dysplasia. Criteria for inclusion were: large breed dogs (>20 kg) with lameness and pain isolated solely to one or both elbows, original archived CT image data of the elbows, and recorded arthroscopic or surgical findings from at least one elbow. Fifty arthroscopically explored elbows and ten clinically normal elbows without arthroscopic confirmation were selected for the study. Original CT image data from selected elbows were reformatted and filmed in transverse, sagittal and dorsal planes. Each plane was filmed in window widths of 1500 and 2500 HU at a level of 300 HU, and 3500 HU at a level of 500 HU. Two board-certified veterinary radiologists, unaware of surgical findings, independently evaluated each set of films for: 1) hypoattenuating MCP subchondral defects, 2) *in situ* MCP fissure(s), 3) discrete MCP fragment(s) (i.e. fragmented coronoid process), 4) irregularity and/or hypoattenuating defects of the radial incisure (RI), 5) subchondral sclerosis of the trochlea humeri, 6) flattening and/or hypoattenuating defects of the trochlea humeri, and 7) joint incongruity. Evaluators recorded their

level of diagnostic certainty for the presence or absence of each CT abnormality using a visual analog scale system (VAS). The effect of status (normal/abnormal), plane, or window on the degree of certainty was tested. Arcsin square root transformation of VAS scores provided estimation of observer diagnostic certainty for each CT abnormality.

1.3 RESULTS

Data analysis revealed that elbow status and observer had a significant effect on diagnostic certainty. Overall, observers demonstrated a higher degree of certainty for determining normal elbows as normal rather than dysplastic elbows as abnormal. Diagnostic certainty for normal MCP status was greatest in the transverse plane at 1500 HU and least at 3500 HU. In contrast, in dysplastic elbows, diagnostic certainty for the presence or absence of an MCP *in situ* fissure was greatest at 3500 HU and least at 1500 HU. An unexpected finding was that for dysplastic elbows, the transverse plane had no effect on diagnostic certainty for *in situ* fissures. Certainty for the presence or absence of discrete MCP fragmentation was high in both the transverse and sagittal planes, regardless of window. However, given a dysplastic elbow, the sagittal plane was associated with higher diagnostic certainty for FCP than the transverse plane. Irregularity of the RI was detected with highest certainty in the transverse plane regardless of window. Determination of trochlear sclerosis was affected by both plane and window. For a given plane and window, the dorsal plane at 1500 HU had the greatest diagnostic certainty for subchondral sclerosis of the trochlea

humeri but the least diagnostic certainty for normal status. Conversely, the dorsal plane at 3500 HU was associated with the greatest diagnostic certainty for normal status but the least diagnostic certainty for subchondral sclerosis. Diagnostic certainty for the presence or absence of flattening and/or hypoattenuating defects of the trochlea humeri differed between observers. For one observer, certainty for the presence of this characteristic was highest in the dorsal plane regardless of window. Diagnostic certainty for joint incongruity was highest in the sagittal plane regardless of window.

1.4 CONCLUSIONS

For most CT abnormalities of the canine elbow, diagnostic certainty is more dependent on image plane or combination of plane and window, than window level alone. Detection of shape and margination abnormalities of the MCP, radial incisure, and joints were most influenced by image plane. However, window width does affect the perceived alteration in subchondral bone opacity (attenuation) for the MCP and trochlea humeri. To maximize diagnostic certainty for CED lesions, the authors feel the transverse plane in 3500 HU is optimal for diagnosing hypoattenuating MCP subchondral defects and *in situ* fragments and the dorsal plane in 1500 HU for detection of subchondral sclerosis. Regardless of display window, the dorsal plane is recommended for detection of flattening or articular defects of the trochlea humeri; transverse plane for detection of RI irregularity; transverse and sagittal plane for detection of MCP fragments; and sagittal plane for detection of humeroulnar, humeroradial, or radioulnar joint incongruity.

CHAPTER 2

REVIEW OF THE LITERATURE

2.1 NORMAL ANATOMY AND DEVELOPMENT OF THE CANINE ELBOW

The elbow is an articulation of three bones which distribute weight-bearing forces in three dimensions. The humerus has one distal condyle that consists of a lateral, flattened capitulum (capitulum humeri) and a medial, narrow ridged trochlea (trochlea humeri) that articulates with the radius and ulna. The medial compartment of the elbow joint (humeroulnar) is an articulation between the trochlea humeri and medial coronoid process (MCP) of the ulna. The lateral compartment of the elbow (humeroradial joint) is formed by articulation between the capitulum and radial head. The capitulum humeri articulates only with the cranially sloping lateral part of the radial head hence, the majority of weight-bearing forces are transferred through this joint.[9,24,25] The ulna contributes only minor weight-bearing support. The olecranon and proximal ulna provides attachment for the triceps muscles and acts as a lever arm for the extensor muscles of the antebrachium. The anconeal process forms the proximal extent of the trochlear notch and fits into the olecranon fossa of the humerus during limb extension. It has no muscular or ligamentous attachments, but aids in preventing rotary and lateral instability of the elbow when loaded.[26,27] The range of motion of the elbow can vary from 170-180º in extension to 30-40º in flexion.[28,29] The trochlear notch is the concave portion of the proximal ulna that articulates with the trochlea humeri. It is measured from the anconeal process to the lateral coronoid

process. Humeroulnar contact areas at the trochlear notch tend to become more circular during growth in non-arthritic large and giant breeds. Conversely, the trochlear notch of smaller breeds typically remain more elliptical (height is greater than depth) than large breeds.[30] The medial coronoid process (MCP) forms the distomedial edge of the trochlear notch and serves to increase articular contact area.[31,32] The normal radioulnar articular surface is a transition from the trochlear notch of the ulna to the horizontally oriented articular surface of the radial head, and from the radius onto the downward medial slope of the MCP.[24,25] The radial head articulates with the ulna at the radial incisure. The two bones are secured by a transverse annular ligament with attachments to the lateral and medial coronoid processes under the corresponding collateral ligaments. The articular circumference of the radial head is larger than the corresponding radial incisure, thereby allowing pronation and supination of the antebrachium.

2.1.1 Development and Ossification of the Elbow

2.1.1.1 The Humerus

The distal humerus has three principal centers of ossification: one for the capitulum and lateral aspect of the trochlea, one for the trochlea and medial aspect of the condyle, and one for the medial epicondyle. Articular cartilage is thickest at the humeral condyle during development, and up to 20 weeks of age, the articular cartilage of the trochlea is thicker than that of the capitulum.[33-35] The ossification

center for the capitulum and trochlea appear at 2-3 weeks of age, however the center for the medial epicondyle does not appear until approximately 6-8 weeks of age.[35-37] As ossification progresses, the medial and lateral aspects of the humeral condyle are separated by a thin cartilaginous plate that is radiographically visible as a radiolucent line.[38] Fusion of the condyle normally occurs at 10-12 weeks of age, and physeal closure of the medial epicondyle occurs at approximately 6 months of age.[39]

2.1.1.2 The Radius

The radius develops from 3 principal ossification centers: one for the proximal epiphysis (radial head), one for the diaphysis, and one for the distal epiphysis and styloid process.[37] At birth, the epiphyses are cartilaginous but the diaphysis is well developed. The distal epiphysis is radiographically apparent generally between 2-4 weeks of age, and the proximal epiphysis appears at 3-5 weeks of age.[37,40] Under normal conditions, the distal physis of the radius contributes 70% of bone length while 30% is attributed to the proximal physis.[40] In large breed dogs, radiographic closure of the distal physis occurs between 8 and 12 months of age, and is the age at which maximum radial length is achieved.[41-43] Increased limb length has been demonstrated in gonadectomized dogs when compared to intact dogs due to delayed physeal closure in the absence of gonadal hormones.[44]

2.1.1.3 The Ulna

The ulna also has 3 principal centers of ossification: one for the proximal epiphysis (tuberis olecrani, an apophysis), one for the diaphysis, and one for the distal epiphysis. Like the radius, the diaphysis of the ulna is well developed at birth and the epiphyses are cartilaginous. Ossification of the distal epiphysis appears at 2-3 weeks of age, whereas the proximal epiphysis does not ossify until 5-8 weeks of age.[37,40] In dogs, the distal epiphysis is elongated and conical-shaped, which differs from other species that tend to have a discoid shaped physis and epiphysis.[45] The distal growth plate is responsible for 85% of the length of the ulna. Therefore in immature animals, it must grow at least 15% faster than the combined proximal and distal radial physes to maintain equivalent length between bones.[40,46] Accelerated physeal growth in the dog is accomplished by the unique conical shape and the increased diameter of the ulnar metaphysis and diaphysis. The surface area of a conical growth plate is 1.5 times that of a flat growth plate of the same diameter. Furthermore, the increased diameter of the metaphysis and diaphysis in large and giant breeds accommodates rapid endochondral ossification.[40] During the most rapid phase of growth, (4-5 months of age) the diameter of the ulna may be 1.5 times that of the radius. Approximately 90% of the ulnar length is achieved by 7 months of age, but radiographic closure of the distal physis generally does not occur until 9-12 months of age.[40,41,47] At skeletal maturity, cortical and metaphyseal remodeling are complete, and the metaphyseal and diaphyseal diameters are less than those of the radius.

2.1.1.3.1 Ossification of the Anconeal Process

The proximal epiphysis of the ulna usually forms from a single ossification center and grows proximally toward the tip of the olecranon, but contributes little to overall bone length.[40] Hare noted that in some dogs ossification within the proximal epiphysis began simultaneously at more than one site.[37] When this occurred, the foci of ossification tended to be in close proximity and united shortly after their appearance.

The anconeal process (AP) of the ulna is completely cartilaginous at birth, but was once considered the fourth ossification center of the ulna in some breeds.[48,49] In a study of three litters of German shepherd dogs (15 dogs) and 2 litters of greyhounds (17 dogs), Van Sickle described that the bones of all elbows developed similarly. Several independent foci of ossification appeared radiographically within the cartilaginous model at 11 to 12 weeks of age, then enlarged and coalesced into a single center separated from the trochlear notch by a thin plate of cartilage.[49] However, a recent study of 142 juvenile dogs disputes that the smaller foci of ossification cannot be seen radiographically until they coalesce into a larger, 'blackberry-shaped' center, which may potentially mimic the appearance of smaller individual centers.[50] The onset of ossification of separate centers is widely varied, and has been reported to occur from 7-8 weeks,[35] 11-12 weeks,[49,51] or 12-14 weeks.[7] It is generally agreed that complete ossification does not occur before 14 weeks of age.[50] Distinct and separate ossification centers of the AP often occur in the GSD and other large breed dogs, but have also been documented in a 7 week old

Dachshund.[50] Separate ossification centers may be unilateral or bilateral. Radiographically, an ossification center is delineated by a radiolucent fissure that represents the peripheral cartilaginous portion of the AP. Anatomical sections show the single ossification center is concave along the cranioproximal margin and union occurs adjacent to the articular cartilage of the trochlear notch.[50] In dogs with separate ossification centers, fusion of the AP center begins at the trochlear notch by 7-8 weeks, progresses along the superficial margins, and fuses lastly in the center.[35] Development of the lateral aspect of the AP always occurs before the medial aspect.[32] This is a presumed adaptation to increased loading forces that occur at the craniolateral aspect of the AP. A recent study confirmed an impression along the inner side of the lateral epicondyle within the olecranon fossa that has increased subchondral density to support this idea.[52] There is no normal articulation between the medial aspect of the AP and trochlea humeri, which likely explains the reduced development of this side.[50]

Depending on the breed or individual, the AP may develop in one of two ways; a direct extension of the diaphysis via appositional ossification or as one or more separate ossification centers.[35,49,50,53] Appositional ossification is characterized primarily by the absence of separate ossification centers, and cranial shifting and alteration of the fusion line of the AP as it develops from the diaphysis.[50] This mode of development occurs mostly in small and medium breeds.

2.1.1.3.2 Fusion of the Anconeal Process

The AP is one of the last structures of the elbow to form, but its growth plate is the first to close.[35] By whatever means of ossification, fusion of the AP to the olecranon should be complete by 5 months of age in the normal dog. Fusion of the AP has been reported to be as early as 14-15 weeks in greyhounds, but generally does not occur before 16-20 weeks in the GSD.[29,31,49,51,54] Non-union of the AP is characterized by a persistent radiolucent fissure between the AP and trochlear notch. If radiographic union is not present by 20 weeks of age, spontaneous fusion will not occur.[27,28,31] Dogs with larger ossification centers (GSD and other large and giant breeds) are predisposed to ununited anconeal process (UAP). Van Sickle hypothesized that the increased size of the cartilaginous model of the AP in these breeds may account for the delayed rate of endochondral ossification and fusion.[49] However, genetic, hormonal, or metabolic factors may also be responsible for delayed union of the AP in GSD.[31,49]

2.1.1.3.3 Ossification of the Medial Coronoid Process

The MCP is also cartilaginous at birth but does not have a separate center of ossification.[35,50] Ossification begins at approximately 4 weeks of age; from the base toward the apex, and center toward the periphery to form a sloped, slightly concave, pyramidal structure.[50,55,56] The articular surface at the apex is positioned below the articular surface of the radial head. Endochondral ossification continues from the MCP toward the radial incisure.[55,56] Ultrastructural studies of subchondral bone

formation have demonstrated asynchronous ossification between the MCP and radial incisure. Wolschrijn *et al* have shown the lateral aspect of the MCP (humeral articular side) develops before the portion adjacent to the radial incisure.[55,56] This has been described as an adaptive response of the subchondral bone to increased weight bearing forces due to increased locomotor activity. The MCP is covered with cortical bone by 8-18 weeks of age but the radial incisure is incompletely ossified even at 24 weeks. Radiographic ossification of the MCP is usually complete by 20-22 weeks[7] but may be as long as 24 weeks in large breed dogs.[57] However, Breit *et al* demonstrated that ossification of the MCP occurred significantly earlier in small and chondrodystrophic breeds of dogs than GSD and rottweilers.[50] In that study, ossification in the small breeds was complete by 16 weeks, an average of 4 weeks earlier than the large breeds. It is thought that maturation of the anconeal process generally coincides with the maturation the MCP. However in the same study, Breit *et al* demonstrated that in some large breed dogs, ossification of the AP can precede the MCP by as much as 6 weeks. Particularly between the ages of 16-24 weeks, large breeds (GSD and Rottweilers) had a higher prevalence of immature MCP when compared to small and chondrodystrophic breeds. Timing of ossification of MCP subchondral bone in relation to increases in body weight and locomotor activities is critical. Because the MCP completes ossification later than all other articular surfaces in the elbow, it is particularly vulnerable to mechanical overloading. Asynchronous development coinciding with an immature MCP can predispose them to fragmentation.[10,11,24,25,58,59]

2.1.2 Subchondral Bone Formation and Remodeling

Articular cartilage and the subchondral bone plate serve to distribute forces within joints and the loading capacity is related to their ultrastructural architecture.[60-63] Subchondral bone plates are formed by the coalescence of islands of trabeculae created during endochondral ossification.[64,65] Although endochondral ossification ceases at skeletal maturity, subchondral bone remodeling remains possible when a joint is exposed to sustained increases in load.[66,67] Remodeling produces subchondral bone that is thicker and denser with greater strength, stiffness, and hardness in an attempt to reduce strain to preset levels.[60,62,68] During development, subchondral bone must fulfill two requirements; providing resistance to compressive articular forces while simultaneously promoting endochondral ossification and longitudinal growth until skeletal maturity. According to the mechanostat hypothesis, as body weight increases during growth, there is progressively increased loading strain on bone. Therefore, the thickness of the subchondral bone is an adaptive response to sustained pressures.[69-71] It has been previously reported that subchondral remodeling occurs earlier in dogs than other species,[71] and trabecular structure of the canine MCP displays distinct alignment earlier than in other bones.[64,72-74]

Microtomography (microCT) is a fast, non-destructive, microscopic imaging technique to evaluate small biopsy specimens (<14 mm).[75,76] It operates the same as conventional CT, except the unit is small enough to sit on a countertop. The spatial resolution is as fine as 5 microns and provides precise 3-D reconstruction of internal architecture. It is commonly used to study the effects of mechanical stimuli on

trabecular bone remodeling *in vitro*.[75,76] MicroCT has been used to describe subchondral and trabecular bone formation of the MCP in normal dogs.[55,56,77] At 6 weeks of age, the MCP trabeculae are primarily oriented perpendicular to the humeroulnar joint. This is a presumed adaptation to forces exerted by the humerus onto the MCP during the push off phase of locomotion when the elbow is in extension.[78,79] At a young age, subchondral bone density was also increased in the trochlea humeri directly across from the MCP.[80] Schön *et al* postulated that the direction of stress acting on a concave joint surface is indicated by the prevailing alignment of collagen fibrils and osteons in subchondral bone.[53,81] Split lines refer to the orientation and direction of collagen fibrils and osteons and signify areas of he highest strength within bone.[53,81] Tensile bone strength is higher when parallel to the prevailing direction of split lines rather than perpendicular to them, whereas compressive strength is highest when perpendicular to the split lines.[82] Altered or abnormal mechanical loading on subchondral bone is correlated with a change in alignment of split lines.[53] However, the distribution of subchondral bone density does not always correlate with the distribution of compressive loads in concave joint surfaces. Some authors believe the orientation of split lines more appropriately reflects stress distribution.[53,68] Maierl *et al* found the split lines of the trochlear notch to be primarily oriented in a sagittal or longitudinal direction, i.e. connecting the anconeal process with the MCP.[53,80] A smaller percentage of ulnar trabeculae are oriented along a craniocaudal axis in response to tensile forces applied by the annular ligament during mechanical loading.[55,56] Orientation of trabeculae toward the radial

incisure has not been found, which suggests that compression at the radioulnar joint is negligible.[55,56] Gait analyses have shown that at mid-stance loading, there is a long lever arm from the ground toward the center of the trochlear notch that is subjected to a medially oriented, transverse force. This force tends to rotate the antebrachium inward to create a bending moment at the elbow to produce increased forces at the MCP and AP. The increased bending and sagittal loading forces through the elbow are believed responsible for subchondral remodeling of the MCP and AP and predispose these structures to damage.[52]

2.1.3 Articular Cartilage

Epiphyseal cartilage is vascular hyaline cartilage that forms the articular-epiphyseal cartilage complex.[83] It is responsible for the formation and shaping of the ends of bones via endochondral ossification. Epiphyseal cartilage differentiates into four zones, each of which is physiologically and morphologically distinct during the process of maturation; reserve cartilage, proliferation, hypertrophy, and calcification and degeneration. Calcified cartilage is separated from articular cartilage by the tidemark. The articular-epiphyseal cartilage complex is supplied by cartilage canals that contain small vessels arising from the perichondrium.[84] These small vessels provide nutrients to deeper cartilage layers that cannot receive nourishment by synovial fluid. Attrition of cartilage canal vessels occurs normally with age as epiphyseal cartilage becomes thinner and less reliant on blood supply.[85] Articular

hyaline cartilage remains after completion of endochondral ossification, and its thickness varies with the joint.

Hyaline cartilage exists only at locations where exerted forces are within specific, predetermined ranges. If forces are less than threshold then the cartilage will naturally atrophy or not form at all.[86,87] These cartilage free areas, also known as synovial fossae or cartilage atrophy, are believed to represent normal macroscopic interruptions of articular cartilage.[86] Cartilage atrophy is the progressive thinning of articular cartilage resulting in full thickness defects during the normal maturation of the normal elbow joint. This has been described in normal young Golden Retrievers and young humans,[86,88] but has also been described in both normal adult dogs and those with pathological changes.[24,25] In humans, cartilage atrophy of the trochlear notch begins at 12-15 years of age.[88] In dogs, atrophy begins at approximately 8 weeks of age, and at predictable locations: the lateral aspect of the trochlear notch continuing toward the base of the anconeal process; the base of the lateral coronoid process; small area between medial and lateral coronoid processes; and the edge of the capitulum humeri.[86] Reddish discoloration of the articular cartilage of the trochlea humeri has been also reported to be associated with cartilage atrophy.[86] Histologically, the subchondral bone underneath these cartilage defects is covered by a thin layer of normal synovial cells without evidence of inflammatory cellular infiltrate. The discolored cartilage of the trochlea humeri was described as fibrocartilage, also without evidence of inflammatory infiltrate.[86] If forces are greater

than a physiologically determined threshold, the cartilage may develop nutritional deficits and/or ischemia with subsequent pathological atrophy.[87]

2.1.4 Physiological Joint Incongruity

Heterogeneous distribution of forces over articular cartilage, as seen in joint incongruity, can also lead to formation of abnormal synovial fossae or cartilage atrophy.[87] In human elbow joints, the trochlear notch is deeper than necessary to be perfectly congruent with the humeral trochlea, and deformation during loading results in tensile stress.[89] Ecktsein *et al* found this type of physiological concave incongruity produces bicentric transmission of forces at low loads, where a state of congruence is achieved during maximal loading and forces are transmitted more uniformly.[68,89-91] It has been postulated that physiological geometric incongruity optimizes stress distribution during cyclic loading, and this is thought to promote optimal chondrocyte nutrition, metabolism, and lubrication.[89,91] Bicentric concave humeroulnar incongruity has been demonstrated in normal canine and human elbows.[32,90-92] Radiographic evidence of radioulnar incongruity has been reported as early as 24 weeks of age.[24,25] In the dog, subchondral bone density was found to be highest within the radius, MCP and AP but not the trochlear notch, indicative of bicentric transmission through the elbow.[93] A recent study demonstrated that geometric incongruity of the elbow is extremely variable as evidenced by the distribution of articular cartilage along the trochlear notch of the ulna.[94] In that study, the highest prevalence of concave incongruity occurred in heavy-set breeds with foci of cartilage

atrophy within the trochlear notch. In contrast, dogs with lower body weight had more uniformly distributed articular cartilage which was postulated as an indicator for complete physiological joint congruence.[94] Cartilage atrophy is believed to occur at the trochlear notch because insufficient mechanical force is transmitted through this structure. Cartilage atrophy may also contribute to joint incongruence but may not impair weight bearing function. Atrophy in the center of the trochlear notch may be a normal adaptation to the absence of loading forces in this region.[32,91,92] This is substantiated by absence of inflammation in the subchondral bone. Similarly, the degree of humeroulnar incongruity has been found to be positively correlated with body weight and is commonly seen in large and giant breeds.[53] This supports the theory that bicentric transmission of loads is optimized for stress distribution in larger or heavier breeds.[94] However, it is generally accepted that atrophy or cartilaginous defects at critical weight bearing locations likely contributes to elbow pathology. The role of cartilage atrophy in dogs with CED remains unknown as it has been found both in normal dogs[86,94,95] and dogs with concomitant elbow dysplasia.[10,24,25] Normal development of structures that form the articular surfaces is critical to preserve joint function. Furthermore, dysplasia of the trochlear notch and/or asynchronous growth between the radius and ulna may also contribute to abnormal humeral forces on an immature MCP.

2.2 CANINE ELBOW DYSPLASIA

Canine elbow dysplasia (CED) is a term adopted by the International Elbow Working Group (IEWG) that refers to a group of developmental abnormalities of the elbow that result in progressive and irreversible osteoarthrosis. Originally, CED was used to describe ununited anconeal process (UAP), but was later expanded to include osteochondrosis and osteochrondritis (OCD) of the trochlea humeri, fragmented medial coronoid process (FCP) of the ulna, ununited medial epicondyle, and most recently, elbow joint incongruity (JI).[1,7,10,24,25,29,34,96,97] Therefore, CED is considered to encompass four primary lesions: UAP, osteochondrosis and/or OCD, FCP, and JI. There remains some uncertainty as to the underlying cause of CED, but there is general agreement that disturbed endochondral ossification of articular or physeal cartilage, dysplasia of trochlear notch, and asynchronous growth of the radius and ulna are considered as primary causes of CED.[7,10,24,25,97]

Incomplete ossification of the humeral condyle (IOHC) is another condition that is not technically considered a form of CED, but also affects rapidly growing, large breed dogs that are predisposed to CED and has been reported to occur concurrently with FCP.[38,98] Incomplete ossification of the humeral condyle has been reported mostly in spaniel breeds which are breeds with chondrodystrophism: Cocker, Brittany, Springer, Cavalier King Charles, and Clumber Spaniels.[38,99] The recent discovery of IOHC in large breeds (Labrador Retrievers and Rottweilers) suggests the possibility of a common pathogenesis.[98,100,101] This condition should be considered

as a differential for elbow lameness when all other developmental orthopedic diseases have been excluded.[100]

2.2.1 Genetics and Heritability of CED

A complex genetic inheritance for CED has been determined with a heritability index that varies from 0.10-0.77, an average of 0.45 for females and 0.77 for males.[102-105] Heritability estimates are population-based measures that determine the proportion of observed phenotypic variance that can be attributed to additive genetic factors.[105] It has been shown the traits of UAP are inherited independently of those for OCD, and FCP is inherited independently from OCD and JI.[104,105] The risk of developing elbow arthrosis is higher in dogs with affected parents than unaffected parents.[102,106] The risk of inheritance correlates with the severity of arthrosis (RR=1.6).[102] Heritability is reported to be strong in the Labrador Retriever, Rottweiler, and Bernese Mountain Dog, with a heritability index of 0.3-0.4.[107-110] In Rottweilers and Bernese Mountain Dogs, the offspring from normal breeding parents had a 31% incidence of CED. Breeding one normal with one affected produced 44-48% affected offspring, and breeding two affected parents produced 59-62% affected offspring.[6] CED predominantly affects males; the male to female ratio ranges from 2:1 to 5:1.[8,29,103,104,110-116]

Many authors agree that males develop clinical and radiographic signs of CED earlier than females, have more rapid progression of osteoarthrosis, and have more severe arthrosis scores (based on IEWG criteria) when compared to

females.[102,103,106,110,114,116-118] The delayed onset and clinical severity of CED in females is attributed to higher levels of serum estrogen that retards cartilage growth and skeletal maturation in juvenile animals.[105]

2.2.1.1 CED Screening Programs

With high heritability estimates, selection of superior (unaffected) sires and dams is imperative to reduce the prevalence of CED. The International Elbow Working Group (IEWG) was established in 1989 to coordinate international efforts to lower the incidence and prevalence of CED. The IEWG coordinates research and dissemination of information regarding CED, establishes scoring guidelines for national screening registries, and provides education and international discussions about elbow osteoarthrosis.[117,119] The Orthopedic Foundation for Animals (OFA) also has an elbow screening program and provides information on the incidence of elbow dysplasia in dogs.[120] Together, with the cooperative efforts of other international groups and breeders, these organizations help provide information regarding breed incidence of CED. Because heritability is a definite factor in the development of elbow arthrosis, susceptible breeds should have elbows radiographed at a young age. Breeding animals of susceptible breeds should be carefully selected by the elbow status and pedigree of the parents, grandparents, and siblings.[104] But owners or breeders should be reminded that normal radiographic findings do not exclude the presence of elbow disease, particularly in females. Until genetic testing

is available to eliminate CED carriers, alternative imaging methods such as CT may be helpful for detection of lesions in young patients prior to breeding.

2.2.2 Ununited Anconeal Process

2.2.2.1 Signalment and Predisposed Breeds

In 1959 Cawley and Archibald identified and described the anatomical defect known as ununited anconeal process (UAP).[48] They considered the anconeal process to be the fourth center of ossification in some breeds, including German shepherd dogs. This was later confirmed by Van Sickle in 1966.[49] Initial reports of UAP found it occurred in closely related German shepherd dogs and heredity was assumed to be a major etiological factor.[48,49] Shortly thereafter, UAP was determined to have a dominant, non-sex linked mode of inheritance[121,122] but other studies have implicated hormonal factors, metabolic defects, nutritional deficiencies, and physeal trauma as etiological factors.[31,48,123,124 125] Classic UAP is a disease of large to giant breed dogs in which a separate center of ossification has been documented. The German shepherd was the first breed in which UAP was described, and is reported to have the highest incidence.[28,29,126,127] However, UAP has also been identified in the St. Bernard, Irish Wolfhound, Great Dane, Great Pyrenees, Labrador Retriever, Pointer, Weimaraner, Newfoundland, Bloodhound, and some chondrodystrophoid breeds; the Bassett Hound, Dachshund, and French Bulldog.[51] In chondrodystrophoid breeds however, premature closure of the distal ulnar physis causes caudal subluxation of the

proximal ulna and shearing stress of the anconeal process.[127] It has been suggested that AP separation in these breeds should be considered a type of fracture rather than classic UAP.[128] Ununited anconeal process is bilateral in 20-35% of affected dogs.[47,48,129,130] Male dogs are twice as likely to be affected as females, possibly because of more rapid growth and greater body size of male dogs.[128]

2.2.2.2 Etiology and Pathogenesis

The pathogenesis of UAP is not completely understood and likely has a multifactorial etiology. Inherited developmental anomaly,[122,127] nutritional deficiency or metabolic defect,[131,132] and trauma[49] have all been incriminated. UAP has been considered to be a manifestation of osteochondrosis with weakening of the attachment of the anconeal process, and the stress of weight bearing prevents union with the proximal ulna.[29,125] In chondrodystrophic dogs, the phenotype predisposes them to premature closure of the distal ulnar physes which may result in UAP.[127] More recently, Olsson has postulated that asynchronous growth between the radius and ulna, particularly overgrowth of the radius with a shortened ulna is the cause of UAP.[125] In such cases, the radius forces the humeral trochlea in a proximal direction, placing abnormal pressure against the developing anconeal process. If this occurs early enough in the ossification of the AP, or if osteochondrosis is present, the entire structure is more susceptible to trauma, and tearing of the weakened cartilage prevents osseous bridging of the gap.[7,28,126] Alternatively, Wind proposed that an abnormally developed, elliptical shaped trochlear notch may cause abnormal forces

placed onto the anconeal process by the humeral condyle.[24,25] The UAP may be connected to the olecranon via fibrous or fibrocartilaginous tissue,[31] or it may be completely separated from the parent bone, producing gross lateral instability.[127] The loss of stability, and free articular bone fragment initiates synovial inflammation, swelling, and pain. In cases with bilateral involvement, one side is typically more severely affected. Early changes include joint effusion, disruption of articular cartilage, joint capsule thickening, and periarticular osteophytosis. If left untreated, older dogs invariably demonstrate advanced degenerative joint disease, characterized by loss of articular cartilage along the trochlear notch, eburnation of subchondral bone, progressive synovial proliferation and prominent joint capsule thickening, progressive osteophytosis, and reduced range of motion.

2.2.2.3 Clinical Findings

Dogs usually exhibit clinical signs between 6 and 12 months of age, but some dogs may not demonstrate lameness until much later. Intermittent weight bearing lameness exacerbated by exercise is the most frequent presenting complaint. If disease is present bilaterally, lameness may shift between forelimbs or may be difficult to detect when elbows are equally affected. Lameness in older dogs is progressive and insidious due to progression of osteoarthrosis. Gait analysis generally reveals a characteristic weight bearing lameness with abduction or "winging out" of affected elbows as the limb is advanced, and external rotation of the foot and splaying of toes at standing.[127] Pain and crepitation are easily elicited during flexion

and extension of the elbow, and thickening of the joint capsule may be palpable. Depending on duration and severity of lameness, disuse muscle atrophy may also be seen. Occasionally, the loose anconeal fragment can be palpated on either side of the triceps tendon.[128]

2.2.3 Osteochondrosis and Osteochondritis Dissecans

In 1974 Olsson first described the clinical and radiographic appearance of osteoarthrosis in 17 juvenile dogs.[133] Necropsy examination of the elbows of these dogs revealed severe osteoarthrosis due to severe erosion of articular cartilage and subchondral bone of the medial aspect of the humeral condyle caused by a loosely attached ossicle to the MCP, then described as ununited coronoid process.[133] Surgical examination via arthrotomy of an elbow of a different dog of the same study revealed lesions of osteochondritis dissecans (OCD). Olsson considered these lesions to be new forms of elbow dysplasia, but also thought they, as well as ununited anconeal process, were merely different manifestations of osteochondrosis.[134]

2.2.3.1 Pathogenesis

Osteochondrosis is a disorder of the articular-epiphyseal cartilage and/or physeal cartilage that occurs in humans and many animal species.[33,135-143] Although somewhat inaccurate because the initial lesion does not involve bone, the term *osteochondrosis* is the most widely accepted term in both veterinary and human

literature to describe the failure of endochondral ossification. Lesions in dogs and humans are site specific and, in the forelimb, occur at areas with thickened articular cartilage or areas that are subject to greater pressure such as the humeral head or humeral condyle.[10,107,143,144] The primary defect occurs at the zone of hypertrophy, where there chondrocytes fail to differentiate or produce the proper extracellular matrix that promotes matrix calcification and vascular penetration of epiphyseal cartilage. This failure results in regional retention of proliferating chondrocytes and thickening of epiphyseal cartilage rather than conversion to bone. With continued thickening, the center undergoes ischemic necrosis because it lies beyond the boundary of nutrient diffusion from synovial fluid or physeal capillaries. Ultimately, the failure of endochondral ossification occurs when the front of ossification reaches the area of necrotic cartilage, creating a zone of necrosis that extends to the subchondral bone.[118,145] The altered matrix and collagen fibril pattern of necrotic cartilage is similar to hyaline cartilage, therefore it is weaker, more vulnerable to trauma, and never undergoes ossification.[34,83]

As the disease process progresses, damage to articular cartilage initially manifests as softening and fibrillation that, with continued use and weight-bearing, progresses to cracks and fissures. With exposure to synovial fluid, the fissures may enlarge and extend to the subchondral bone, where cartilage may then separate from the underlying subchondral bone to form an elevated cartilaginous flap. The formation of the cartilaginous flap with secondary synovitis and osteoarthrosis is known as *osteochondritis dissecans* (OCD).[7,10,34,125,146,147] Following cartilage cleavage or flap

formation, exposure of collagen and collagen degradation products initiates synovitis, joint effusion, pain, lameness, and osteoarthritis.[10,118,134,142,148,149]

Formation of subchondral cyst-like lesions secondary to advanced degenerative joint disease is thought to share a similar pathogenesis. With synovial effusion, intra-articular pressure is elevated. During motion, the synovial fluid may be 'injected' through existing clefts within articular cartilage which result in ischemia and necrosis of underlying bone.[150] Alternatively, when there is loss of protective articular cartilage, direct pressure on subchondral bone induces contusions, ischemia, and subchondral necrosis. The necrotic centers may undergo granulation, fibrosis, and metaplastic cartilage remodeling to form a cyst-like structure that communicates with the joint space.[150]

Joint pain is elicited by chemical stimulation of nociceptors by inflammatory cytokines and cartilage degradation products. Nociceptors are also mechanically stimulated by physical movement of the osteochondral fragment. The severity of the condition is dependent on the size and fate of the flap. Cartilaginous or osteocartilaginous flaps may remain attached or may separate from the adjacent cartilage to float freely in the synovial fluid. The loose fragment may be degraded by proteolytic enzymes and completely resorbed, causing little problem. If however, the fragment attaches to the synovial membrane, it may receive nourishment to continue endochondral ossification and formation of a 'joint mouse'.[118,134] *In situ* movement of the osteochondral or cartilaginous fragment prevents healing of the subchondral

bone and also serves as a constant irritant, and perpetuates pain, lameness, and progression of osteoarthrosis.[3]

2.2.3.2 Etiology

The etiology of osteochondrosis and OCD in dogs is considered by most to be multifactorial, but trauma, ischemia, hereditary factors, rapid growth, and nutrition have been considered the most important.[143,148,151] Human and canine OCD may share a similar etiopathogenesis, and accepted theories include those of microtrauma and disruption of local or epiphyseal vasculature.[143,152-155] Histopathological analysis of cartilaginous flaps from chronic lesions in the horse has supported the theory of trauma, because predilection sites are in areas of increased biomechanical stress.[140,141] In contrast, the histopathology of human OCD lesions is consistent with primary osteonecrosis of subchondral bone secondary to repetitive microtrauma, however the articular cartilage may remain intact.[143,156] Articular cartilage may become damaged secondarily from inadequate mechanical support by softened subchondral bone, and a partially attached or free osteochondral fragment may form.[143,157] In contrast to dogs, human OCD lesions are found in the capitellum humeri far more often than the trochlea humeri.[143,157] The incidence at this site reflects biomechanical stresses and precarious vascular anatomy. The human radiocapitellar joint bears 60% of axial compressive loads during extension.[143,157] The greater stiffness of the radial head over that of the capitellum, and predominance of capitellar involvement supports microtrauma as the inciting event.[143] This explains why this condition is seen more

often in highly athletic children and juveniles.[156] In animals, microtrauma is unlikely the sole cause of osteochondrosis but does play a role in the severity of lesions in pigs and calves housed on hard flooring. In both pigs and calves, lesions of medial femoral condyle predominate over those of the lateral condyle.[84,153,155,158] Olsson also postulated that repeated microtrauma at the caudal humeral head and lateral femoral condyle could lead to osteochondrosis lesions.[34]

2.2.3.3 Histopathology

Olsson believed large areas of necrotic cartilage that were subjected to weight bearing forces resulted in the cracking and fissuring of the articular surface, and in some dogs, progressed to a full thickness cleft to the subchondral bone through the zone of necrosis.[7] However, histologic evidence does not support this theory. Guthrie *et al* examined histological samples of 24 OCD flaps using light microscopy and transmission electron microscopy.[147] They described wide zones of proliferating chondrocytes that appeared in pairs rather than columns. The tidemark was irregular and chondrocytes could be found beyond the tidemark in some areas. Densely packed fibrous connective tissue lined the deep surface of the flap and was presumed to be an attempt of repair. Although there was gross evidence of synovitis at surgical debridement of the flaps, inflammatory infiltrate into the flap was lacking. The chondrocytes often showed degenerative changes, but widespread necrosis or non-viable cells were not found. This implied that nutrition of the chondrocytes remained adequate following detachment.[147]

2.2.4 Fragmented Medial Coronoid Process

2.2.4.1 Signalment and Predisposed Breeds

Fragmented medial coronoid process (FCP) is the most commonly recognized developmental disease of the elbow in large- and giant-breed dogs.[4,7,113,134,144] However, one case report of bilateral FCP-like lesions were described in an 8-year-old Persian cat.[159] FCP is a separation of an osteochondral fragment at the apex of the MCP or along the lateral margin adjacent to the radial head. Worldwide, it is a frequent source of lameness and DJD in large and giant breed dogs with a heavy conformation, including Bernese Mountain Dogs, Rottweilers, Boxers, Labrador and Golden Retrievers, Newfoundlands, German shepherds, St. Bernards, Bull Mastiffs, and Chow Chows.[4,6,10,24,25,102,111,114,125,126] Prevalence among certain breeds is high; 15-25% in the Labrador Retriever,[104,115,160,161] 30-50% in the Rottweiler and Newfoundland,[102,103,108] and 36-72% in Bernese Mountain Dogs.[115,162,163] FCP has also been reported in smaller breeds including Beagles, Pomeranians, Shetland Sheepdogs, and Basset Hounds.[164-166] Males are affected in up to 75% of cases,[31,57,112,114,144,167,168] although there was lower male predisposition in a Swedish population of Bernese Mountain Dogs.[106]

Canine elbow dysplasia is bilateral in 33-80% of cases, and various forms can occur simultaneously within the same elbow.[7,8,10,57,111,118,164,167-170] FCP can occur concomitantly with OCD of the humeral condyle and is most commonly found in Labrador Retrievers.[111,134,165,167,170,171] Berzon and Quick reported concurrent osteochondrosis lesions in 100% of elbows surgically explored for FCP.[168]

However, in this report, these lesions were not detected on pre-operative radiographs and may have been erosive chondromalacia of the opposing articular surface of the trochlea humeri incited by a loose FCP rather than true osteochondrosis.[8,164,168] Read *et al* also found similar osteochondrosis-like lesions in dogs with FCP, however microscopic examination confirmed these lesions to represent articular cartilage erosions or so-called 'kissing lesions'.[8] Other combinations also frequently occur. In a study of 92 Bernese Mountain Dogs, co-existing FCP and joint incongruity was seen in over 50% of dogs.[163] Similarly, a recent study investigating the incidence of concomitant FCP in dogs with UAP, surgically confirmed both lesions in 13% of German Shepherd Dogs and 16% of all dogs in the study.[112] In a radiographic study of 500 German Shepherd Dogs, the prevalence of JI, OCD, and FCP were higher than UAP, and combination of at least 2 primary CED lesions were found in 42.2% of dogs.[172] However, diagnosis of primary lesions was made from radiographs, not by surgical confirmation. The prevalence of OCD in this study may have been overestimated, when lesions may have been 'kissing lesions.' The lower than expected UAP prevalence in this study is likely explained by the prescreening process that occurred during subject enrollment, and subjects' radiographs with obvious UAP lesions were not submitted for evaluation for other CED lesions.[172]

2.2.4.2 Etiology and Pathogenesis

The etiology and pathogenesis of FCP remains controversial and poorly understood. FCP is likely a multifactorial disease, influenced by genetics, nutritional

oversupplementation, growth rate, and trauma.[132,173,174] Early studies considered it a manifestation of osteochondrosis,[134,148,175] but this has not been supported by histological evidence.[77,147] In a study of 120 large-breed dogs with elbow osteoarthrosis, *in situ* fissures and fragmentation of the MCP were observed in 41% and 85% of elbows respectively.[10] Cartilaginous MCP fissures ranged from superficial clefts to full-thickness osteochondral cleavages, and therefore were believed to precede fragmentation. Of dogs with discrete fragments, the configuration of fragmentation varied; fragments were single or multiple, 40% were transverse and involved the apex of the MCP, and 60% were more sagittal and paralleled the radial incisure.[10] Another author described up to 7 types of MCP lesions, some of which were exclusively cartilaginous lesions.[176] Schwalter first described 3 different line patterns of fragmentation of the canine MCP: transverse, sagittal fragmentation along the lateral border and involving the apex of the process, and sagittal fragmentation along the lateral border not involving the apex.[177] Kunzel also described 3 types of subchondral split patterns of the MCP that correspond with fissure and fragmentation configuration.[53] Split line patterns were defined as: (1) transverse pattern extending between collateral borders, (2) sagittal pattern aligned with the lateral margin and perpendicular to the apex and medial border of the MCP, and (3) intermediate pattern, a transition between the others with alignment of split lines oblique to the long axis of the MCP, and may predispose to multiple fragments. The intermediate pattern had the highest incidence, and was associated with breeds with the heaviest mean body weight (>42 kg), whereas the transverse pattern had the lowest prevalence, and was

associated with the lowest mean body weight (<34 kg). However, there was no association of breed and pattern type.[53] These findings have been supported by recent reports that state the orientation of fragmentation lines may vary even within a single breed.[163]

Most dogs with developmental FCP are younger than one year of age at the time of diagnosis, however, there have been reports of older dogs (>24 months) with surgically confirmed FCP in the absence of radiographic changes associated with osteoarthrosis. Although histologic corroboration has yet to be determined, it is of the authors' opinion that FCP in these older dogs may result from repetitive microtrauma to the articular cartilage and subchondral bone. It is possible that strain of the joint capsule or periarticular ligaments may induce subclinical joint laxity or incongruity which leads to articular cartilage damage and subchondral bone remodeling. If this were true, FCP in older dogs may share a common etiopathology with human OCD of the capitellum in which trauma is a major factor.

2.2.4.3 Clinical Findings

Like other forms of elbow dysplasia, most dogs present with lameness between 5 and 12 months of age.[7,8,111,118,134,144] Dogs typically exhibit a stiff, stilted gait with a shortened forward stride, slightly abducted forelimbs with inward rotation of the elbows and outward rotation of the paws. Lameness tends to be exacerbated with exercise or minor trauma, and it is important to differentiate elbow pain from shoulder pain. Elbow pain and/or crepitus can be elicited with both flexion and

extension of the elbow, or direct palpation at the medial aspect of the joint. There may also be varying degrees of joint effusion and muscle atrophy depending on the duration of lameness. Lameness may be intermittent or insidious in onset, and may be difficult to recognize especially in cases of bilateral involvement.

2.2.4.4 FCP and Joint Incongruity

Although there remains dispute as to the cause of FCP, there is general agreement that in affected animals, a normal MCP may be subjected to local 'mechanical overloading', or fragmentation may occur through generalized weakness of the cartilage and subchondral bone in combination with mechanical overloading of the MCP.[4,10,147] Excessive focal pressure on articular cartilage has been linked to chondrocyte death, degeneration of cartilage matrix, and initiation of synovitis and osteoarthritis.[32,178] Ultrastructural studies and histological reports suggest FCP lesions represent a failure of subchondral bone leading to an osteochondral fracture.[147,179] Thus, it has been speculated that MCP fissures or fragments may be the result of growth disparities between the radius and ulna (i.e. short-radius syndrome), or between the humeral condyle and trochlear notch of the ulna (i.e. trochlear notch dysplasia).[4,11,24,25,53,180,181] Both types result in joint incongruity, thereby resulting in redistributed weight-bearing forces onto the MCP.[24,25] This 'mechanical overloading' exceeds the load-bearing capacity of the subchondral bone and leads to fragmentation. In 1986, Wind compared the radiographic findings and gross necropsy appearance of normal canine elbow joints to those of Bernese

mountain dogs afflicted with FCP, OCD, and UAP.[24,25] Elbow joint incongruity was seen on lateral radiographs and characterized by (1) proximal displacement of the trochlear notch, creating a step between the lateral coronoid process and the articular surface of the radial head, (2) increased width of humeroulnar and humeroradial joint spaces, and (3) cranial displacement of the humeral condyle on the radius.[24,25] She concluded that incongruity, particularly the humeroulnar joint, was a common denominator between dogs with FCP, OCD, and UAP, and preceded fragmentation of the MCP. Radiographic changes were substantiated by necropsy findings; the MCP was found to lie proximal to the level of the radial head, there was damage to articular cartilage of the humeral condyle opposing the lesions of FCP and UAP, and an elliptical shaped trochlear notch, with a curvature arc too small to accommodate the trochlea humeri. Because the joints of the elbow are incompletely formed at 4-6 months of age (usually the age at which CED manifests), an abnormally small trochlear notch could result in cranial displacement of the trochlea humeri onto the immature MCP lying above the radial head, predisposing to FCP. The same scenario could also explain the development of OCD, caused by interruption of endochondral ossification due to excessive pressure exerted by the MCP onto the immature trochlea humeri. If however, trochlear notch dysplasia occurred after 6 months of age, she postulated FCP would be less likely to occur despite persistent JI, because the MCP would have matured.[24] In an attempt to explain the joint incongruity seen grossly and radiographically in Bernese mountain dogs with CED, Wind examined lateral radiographs of antebrachii from 825 dogs of various breeds.[25] Length measurements

were made during several periods of growth during the first year of life. Analysis of these measurements showed an increase in the relative size of the proximal ulna in medium- and large-breed dogs. It was concluded that this was necessary to provide the trochlear notch sufficient size to encompass the large humeral condyle characteristic of larger breeds. In cases of an insufficient trochlear notch, the humeral condyle was thought to place abnormal stress on the developing coronoid and anconeal process, thereby contributing to FCP and UAP.[25] Wind, however, failed to explain the pathogenesis for the growth disparity between the radius and ulna, but speculated the incongruity was caused by retarded physeal growth of the distal radius.[57]

2.2.4.4.1 Asynchronous Growth of the Radius and Ulna

Asynchronous growth between the radius and ulna with subsequent development of JI was also found in a similar study of 77 Swiss Bernese Mountain Dogs.[182] Compared to normal Swiss Bernese Mountain Dogs, those with FCP had a proportionally shorter radius than its companion ulna, a proportionally longer proximal ulna, and increased distance between the trochlea humeri and radial head. According to the IEWG, this is the most frequent type of dysplasia seen in this breed[170,183] however, the pathogenesis of asynchronous growth in these dogs has not been elucidated.[4] Increased loading of the MCP has been demonstrated in *in vitro* studies as well as clinical reports documenting FCP secondary to premature closure of distal radial physes.[180,181] Radial shortening (or 'short radius syndrome') results in

reduced radial head articulation, increased contact with the distal trochlear notch and lateral coronoid process, and migration of articular contact from the medial aspect of the MCP to the lateral border adjacent to the radial head.[180] Supraphysiologic loading of the lateral margin of the MCP is considered a mechanical cause of FCP.[180] Supporting evidence for FCP and/or osteochondrosis associated with asynchronous growth was also provided in an unpublished study by Pool.[184-186] This study involved necropsy dissection of limbs from over 400 juvenile large-breed dogs. The radius and ulna were observed to lengthen independently of each other until about 5 months of age, at which time the interosseous membrane and ligament became mature and constrained longitudinal movement between the bones. Based on the gross and histological findings, Pool concluded that FCP is caused by an asynchronous growth mechanism that leads to displacement of the MCP 1-2 mm proximal to the radial head, and 'kissing lesions' are then mechanical erosions caused by interference between trochlea and the MCP.[184,185] Slightly older dogs with FCP and 'kissing lesions' were considered to have mature MCP and articular cartilage of the humeral condyle.[184,185] Pool found mature or near mature MCP are generally strong enough to initiate pressure necrosis and osteochondrosis-like lesions of the opposing articular surface of the trochlea humeri prior to MCP fragmentation. Following fragmentation of a proximally displaced MCP, Pool explained that there was a period of increased longitudinal growth of the radius, and the radioulnar and humeroradial congruity was restored in some dogs.[184,185] This may explain why JI appears normal in radiographs or CT in some dogs with FCP.[187,188] Elbow incongruity, common in

chondrodystrophic breeds such as the Bassett Hound, has been termed *distractio cubiti*. This manifests as a retardation of ulnar growth relative to the radius in the absence of distal physeal injury. This particular form of asynchronous growth predisposes dogs to UAP because of the sustained pressure on the developing anconeal process.[166]

2.2.4.4.2 Trochlear Notch Dysplasia

Trochlear notch dysplasia (decreased radius of curvature of the trochlear notch) and humeroulnar incongruity has been proposed to be one of the forms of elbow incongruity that leads to FCP. Previous radiographic studies have found the trochlear notch of Bernese Mountain Dogs (breed significantly predisposed to FCP) to be more elliptic than in Rhodesian Ridgebacks (a breed not predisposed to FCP).[189] In contrast, a similar study comparing the curvature of the trochlear notch in cadaveric specimens, failed to demonstrate a significant difference of the radius of curvature between Rottweilers (a breed predisposed to FCP) and Greyhounds (a breed not predisposed).[92] However, several other studies in humans and dogs have suggested that bicentric concave humeroulnar incongruity may be normal, and the cartilage atrophy in the center of the trochlear notch, and medial aspect of the AP may be a normal response to the absence of loading in these areas.[24,25,32,52,89-92,94,190] Greater degrees of HU incongruity, signified by cartilage atrophy at the center of the trochlear notch, correlates with body-weight and is a common finding in large- and giant breed dogs as well as humans. Eckstein claims this geometric incongruity in normal joints

serves to optimize stress distribution during loading.[89-91,190] In humans, the trochlear notch is deeper than necessary to accommodate the trochlea humeri. This conformation allows bicentric transmission of forces at low loads. As loading increases, incongruity decreases because of the elastic deformability of cartilage and subchondral bone. At maximal loading in humans, a state of true joint congruence is reached and the loading forces are distributed more homogeneously throughout the joint.[89] In addition to even distribution of stress, physiological incongruity provides normal, intermittent stimulation of cartilage, and maintains normal chondrocyte metabolism, nutrition, and lubrication during cyclic loading.[87,178,190] However, bicentric distribution of forces within the canine elbow could not be similarly replicated *in vitro.*[32,180,191] The fact that dogs ambulate with elbows extended may account for species differences in force distribution.

2.2.5 Treatment Options for Elbow Dysplasia

Treatment for elbow dysplasia consists of conservative medical therapy or surgery. Conservative therapy may include weight management, activity restriction or low-impact exercise (such as swimming), chondroprotective agents, and non-steroidal anti-inflammatory agents for pain. It is stressed that early diagnosis is essential to alleviate pain and slow the progression of osteoarthrosis.[7,8,11,144,167,168,192-194] Radiographic diagnosis of UAP is relatively straightforward after 5 months of age, and based on the presence of a radiolucent fissure through the anconeal process. Unfortunately, early radiographic diagnosis of OCD and FCP may be inconclusive in

dogs younger than 7 months of age,[194] and in many instances, the suspicion of a lesion is only supported by the presence of secondary osteoarthrosis that occurs approximately 7-9 months of age or later.[4,7,10,54,113,164,168,195] Osteochondritis dissecans may not be detected until discrete flattening of the trochlea occurs radiographically. A discrete fragment of the MCP is rarely seen on radiographs, and fragment visibility has been reported to be less than 10%.[59,164,196,197] Therefore, by the time radiographic changes are apparent, extensive cartilaginous damage may be present.[113,194,198-200]

Cartilage inherently has a limited healing response to injury.[147] Healing of osteochondral defects occurs by migration and metaplasia of nearby chondrocytes to produce fibrocartilage.[201] Methods to stimulate fibrocartilage production include superficial intracortical debridement or abrasion arthroplasty (abrasion of superficial layer of subchondral bone) and forage (drilling of multiple small holes into subchondral bone).[145] Both techniques disrupt subchondral blood vessels to induce bleeding and formation of fibrin clot formation over exposed subchondral bone. Undifferentiated mesenchymal cells from bone marrow migrate into the clot and differentiate into chondroblasts and chondrocytes and produce fibrocartilage.[202,203] However, irrespective of technique used to treat OCD lesions, the properties of fibrocartilage is not equivalent to the composition or mechanical properties of normal articular cartilage.[202,204] Institution of continuous passive motion post-operatively has been shown to stimulate differentiation of mesenchymal cells into hyaline-like articular cartilage, prevent adhesion formation, and increase range of motion of the

joint.[205,206] Unfortunately, the use of continuous passive motion is impractical in the dog, and this type of cartilage deteriorates quickly with resumption of weight bearing.[145,204]

Small OCD lesions may be treated successfully with medical management only. However, surgical exploration by means of arthrotomy or arthroscopy is recommended for young dogs (<1 year of age) with clinical signs of CED before the onset of severe osteoarthrosis.[6,58,144,176] Older dogs with radiographically visible lesions, extensive osteoarthrosis, and/or severe clinical signs may also improve with surgical exploration but their prognosis remains guarded. There remains some disagreement as to the proper therapy for older dogs or those with severe osteoarthrosis, as they have been considered by some to be poor surgical candidates and may be better managed with medical therapy.[113,207-211]

2.2.5.1 Ununited Anconeal Process

Surgery is recommended for dogs with UAP, as medical management alone results in rapid progression of osteoarthritis.[212] Surgical options include removal of the process, reattachment of the process, or corrective osteotomy or ostectomy of the ulna with or without fixation of the anconeal process.[26-28,212-215] Surgical excision of the anconeal process was originally the most common practice.[213] Excision of the process has resulted in good to excellent long-term function, and dogs treated by this procedure have a favorable prognosis.[214,216] Surgical reattachment of the AP via lag screw fixation was advocated to maintain elbow stability and congruity, and is best

performed before 24 weeks of age. Perfect anatomic reduction is essential, but becomes more difficult with age due to progressive osteoarthrosis and bony remodeling.[186,213] This procedure is also associated with complications of implant failure at the original fissure line. Ulnar osteotomy is often performed to reduce abnormal forces applied to the anconeal process. The pull from the triceps muscles dynamically lengthens the ulna to allow realignment of the olecranon and trochlear notch with the humeral condyle. This procedure alone has resulted in good limb function and reduction in lameness in long-term follow up examinations.[28,212] Turner *et al* also reported good results, but found inconsistent fusion of the anconeal process.[27] Ulnar osteotomy or ostectomy with surgical fixation of the UAP is preferred when the UAP is grossly unstable.[186,215] Ulnar osteotomy with lag screw fixation of the UAP has resulted in good to excellent clinical outcome with minimal progression of osteoarthritis.[212,215]

2.2.5.2 FCP and Osteochondrosis

The goals of surgical intervention for FCP and OCD are to remove cartilaginous or bone fragments, debridement of the remaining cartilage and bone edges, and stimulation of fibrocartilage formation by superficial curettage. A medial arthrotomy via muscle separation technique has been advocated over medial epicondyle osteotomy for fewer complications and faster recovery period.[4,167,211] Arthroscopy is recommended by some authors over arthrotomy for its minimal tissue damage, reduced surgical time, and shorter post-operative convalescence

period.[176,195,199,200,217-219] In a study of 421 dogs with confirmed FCP, 42% of dogs treated by arthrotomy did not show any lameness, but 28% had persistent, although slightly reduced lameness in a 6+ month follow up exam. By comparison, 60% of dogs treated by arthroscopy showed no lameness, whereas only 10% had persistent, although improved, lameness.[219] Other authors propose that post-operative morbidity should not be a factor when deciding which surgical procedure to perform. A study implementing the use of kinetic (force plate) gait analysis found no difference in post-operative pain, weight-bearing, or range of motion between dogs treated with arthrotomy or arthroscopy.[220]

Arthroscopy is considered advantageous over arthrotomy for its superior visualization of joint surfaces because of its magnified view of tissues, which facilitates direct observation of articular surfaces and differentiation of chondromalacia from cartilaginous fibrillation, fissures, fragments, OCD, or kissing lesions.[195,217] Close examination of joint mice and the synovial membrane can also be performed, and therapeutic treatment can be offered at the same time. Arthroscopy has been advocated as an early diagnostic tool for CED, particularly in the absence of significant radiographic changes.[113,114,195,200,218,221] It should be noted, however, that the absence of a visible lesion via arthrotomy or arthroscopy does not exclude elbow disease, and emphasizes the importance of CT to depict lesions in early cases.[221] Regardless of the technique utilized (arthrotomy or arthroscopy), removal of the MCP fragment, damaged cartilage, and/or osteophytes may provide some pain relief, but does little to alter the progression of osteoarthritis and long-term medical

management is required.[97,111,210,212,222] Unfortunately, the results of medial arthrotomy with fragment removal as a surgical treatment for FCP have been unrewarding. Veterinarians continue to debate whether surgery for FCP or OCD offers any benefit to the patient compared with conservative measures. In one study, dogs in the medically managed group demonstrated a more rapid return to normal weight-bearing than the surgically treated group, and there were no differences between groups at 9-month follow up.[223] However, the surgically treated group did not receive concurrent medical therapy, whereas the medically managed group required long-term medical therapy. Several other studies have also not been able to demonstrate significant differences in the degree of lameness or outcome between medically and surgically treated dogs.[8,97,118,134,208,209,224] Regardless of treatment option, the majority of dogs will develop progressive osteoarthrosis.[8,97,118,134,208,209,224] Randomized and controlled, long-term prospective studies have yet to be performed to address this question.

2.2.5.3 Joint Incongruity

This failure of treatment to noticeably alter the progression of osteoarthritis (assessed radiographically) implies a failure to address the primary cause of DJD in many FCP cases, i.e. joint incongruity.[24,25,210] In dogs with evidence of JI, it has been suggested that removal of the MCP fragment alone will not achieve a positive, post-operative outcome.[225] A study of 17 dogs with surgically confirmed humeroradial incongruity (radial shortening) without the presence of FCP, OCD, or

UAP investigated the feasibility of medial coronoidectomy as a treatment for lameness.[224] Post-operative follow up examinations (1 and 12 months) showed complete resolution of lameness in 100% of dogs, although 28% developed decreased range of motion, and 11% had persistent joint effusion. As seen in previous studies, all dogs in this study developed progressive radiographic evidence of osteoarthrosis.[224] Good clinical results were also reported in dogs receiving medial arthrotomy and corrective proximal ulnar osteotomy as a salvage procedure in mature dogs with advanced DJD caused by FCP.[210,226] The rationale for this procedure is to alleviate abnormal humeroulnar joint contact at the medial coronoid process by facilitating caudomedial rotation of the proximal ulna.[210] This allows restoration of congruity and alignment of joint surfaces, and may reduce osteoarthritis, particularly if performed before evidence of bony malformation. Another procedure, the proximal ulnar sliding osteotomy, in association with FCP removal, has also shown good to excellent results in dogs with refractory lameness due to FCP.[227,228] The sliding osteotomy is proposed to allow the proximal ulna to shift cranially, with slight forward rotation to realign articular surfaces of the radius and MCP, while simultaneously alleviating excess pressure on the MCP.[228] The most appropriate site, type (ostectomy or osteotomy), configuration (transverse or oblique), and with or without internal fixation of the ulna is unknown.[229] It is generally agreed that in cases with radial shortening and proximal displacement of the MCP, ulnar shortening (via corrective ostectomy) is required. Despite valiant efforts by investigators, a

significant difference in outcome between medically and surgically treated groups has failed to be demonstrated.[8,118,134,208,209]

2.2.6 Prognosis for CED

The prognosis for FCP and OCD is variable and depends on the severity of the clinical signs, radiographic changes, and treatment protocol. The prognosis for UAP is generally more favorable, particularly if corrected early. The greatest cause of long-term debilitation in cases of CED is the progressive osteoarthritis. The source of osteoarthritis in dogs with UAP is marked elbow instability. The extent of DJD from FCP is determined by the size of the fragment, the degree of attachment, and duration of its presence.[7] This is complicated by the lack of correlation between the severity of clinical signs and severity of radiographic findings. In many cases, the time lag between the onset of lameness and the radiographic diagnosis has a negative influence on prognosis.[7,9-11] Factors that also affect the prognosis include: breed, age at which dysplasia develops, age at first diagnosis, age at initiation of treatment, rate of progression of the disease, and the presence of joint incongruity.[4] Surgery remains highly recommended in dogs less than 12 months of age, or those with mild radiographic changes. Surgical removal of fragments is not believed to be rewarding in older dogs or those with substantial osteoarthrosis. Results of available studies suggest that surgical removal of fragments without proper medical management does not improve long-term function. Owners should also be advised that breeding of affected dogs is not recommended.

2.3 DIAGNOSTIC IMAGING OF CANINE ELBOW DYSPLASIA

2.3.1 Radiography

Initial imaging of the canine elbow is usually performed using conventional or digital radiography.[4,6,7,10,117,230] High quality, well-positioned radiographs remain the most cost-effective method of diagnosing elbow dysplasia. However, even ideal radiographs may not show all abnormalities, or may only be suggestive of pathology, particularly if arthrosis has not yet developed. Evaluation of the elbow requires accurate positioning and careful scrutiny of the radiograph. Because of the complex superimposition of joint surfaces, knowledge of normal anatomy is paramount in evaluation of the canine elbow. The MCP is difficult to evaluate because it is obscured by the superimposition with the radial head and shaft of the ulna. In addition, visualization of structures is quite susceptible to positioning errors, and true lateral positioning is vital. Imprecise positioning can lead to misinterpretation of joint incongruity.[171,231]

High radiographic detail is essential to evaluate pathology within the elbow. With conventional radiography, radiographs are typically obtained with a non-grid table-top technique, low kVp and high mAs exposure, with detailed film screen combination.[5,6] The primary beam should be centered on the medial epicondyle. Standard radiographic views of the elbow include the craniocaudal and flexed mediolateral projections. Supplemental views may also be obtained in order to highlight specific anatomic structures or lesions, particularly the MCP. Radiographs

of the contralateral elbow should also be obtained because of the high incidence of bilateral disease, or to serve as an internal control.[6]

The mediolateral view is the easiest to position and provides good overall visualization of the elbow.[5,6] However, there has been some confusion as to the optimal angle for evaluation of the elbow, and 45º (flexed), 90º (neutral), 110º (semi-flexed), and 135º (extended lateral) positions have all been recommended.[6,171,197,231] Obtaining a 'true' lateral radiograph is critical. If the primary beam is centered at the humeral condyle, the normal elbow appears as a set of concentric rings. The smallest circle in this view represents the smallest portion of the trochlea humeri as it articulates with the 'keel' (smallest diameter) of the trochlear notch.[5] The articular surfaces of the keel and trochlea should appear parallel. The articular surface of the trochlear notch should form a continuous arc with the articular surface of the radial head. Subluxation or incongruity of the humeroulnar joint (HU) can be recognized by lack of parallelism between the articular surfaces. It can be difficult to assess whether HU incongruity is abnormal, as recent literature suggests it may be normal in dogs as it is in humans.[32,91] However, in the presence of osteoarthrosis, JI may be a contributing factor to disease. Artifactual incongruity can also be induced in the flexed mediolateral projection, and simulated with patient malpositioning.[231] Humeroradial (HR) incongruity is recognized as widening of this joint space, and often coincides with proximal radioulnar (RU) incongruity. When both are present, this is recognized as a 'step' between the LCP and the radial head in mediolateral radiographs.[231]

The normal MCP summates with the caudal aspect of the radial head in lateral radiographic projections. It should be completely ossified by 6 months of age, and should be seen as a well-defined point as it meets the articular surface of the trochlea humeri. The tip of the MCP should be level with the physeal scar of the proximal radius. The margin of the MCP slopes cranially and proximally at approximately 45º from the cranial cortex of the ulna and should be slightly concave in contour.[230] Trabecular detail of the ulna at the trochlear notch and caudal to the MCP should be visible. Loss of visualization of the MCP apex, blunting or flattening of the MCP, and/or periarticular osteophyte formation are strong radiographic indicators of FCP.[230] Subtrochlear sclerosis of the trochlear notch is a combination of periarticular osteophyte formation, enthesiophyte formation at the joint capsule attachment sites, and sclerosis of underlying bone. Its appearance is subject to radiographic technique, therefore evaluation of this feature may be subjective.[5] When present, it is best seen caudal to the MCP on semiflexed or flexed lateral projections. The anconeal process should be a well-defined point within the olecranon fossa of the humeral condyle, although it may summate with the medial epicondyle of the humerus in neutral or semiflexed mediolateral projections. Periarticular osteophyte formation will be seen along the proximal aspect of the anconeal process with onset of osteoarthritis. Because the anconeal process is often obscured by the medial epicondyle, flexed mediolateral projections (45º inside angle) have the highest sensitivity for identification of osteophyte formation or UAP and is a standard view for elbow screening.[5,232] However, the flexed mediolateral view does not otherwise contribute

much to the evaluation of FCP or OCD when compared to other views. The craniocaudal view is useful for detection of OCD or kissing lesions of the trochlea humeri as well as for evaluation of degenerative changes of the medial aspect of the joint, but rarely demonstrates an FCP. Sesamoid bones within the tendon of origin of the supinator muscle may also be detected along the lateral aspect of the joint on craniocaudal views. These have been identified in approximately 31% of dogs, and can be unilateral, bilateral, and/or asymmetrical in size. The sesamoids are not considered a cause of lameness and should not be confused as an FCP or joint mouse.[233]

2.3.1.1 Humeral condyle

Survey radiography is less sensitive for diagnosing osteochondrosis or OCD of the humeral condyle than for the humeral head. This is especially true when subtle lesions are masked by extensive degenerative changes.[170,234] OCD or large kissing lesions will appear as a focal flattening, concave, or triangular shaped radiolucent subchondral defect of the trochlea humeri with or without surrounding sclerosis.[171,234] For optimal visualization of the medial aspect of the condyle, the 45º craniolateral-caudomedial oblique (Cr45ºL-CdMO) projection is considered superior to the craniocaudal projection because there is less superimposition of the ulna with the trochlea humeri.[171,234]

In dogs without condylar fracture, IOHC may be difficult to confirm with conventional craniocaudal projections. Because IOHC may exist concurrently with

FCP, the fissure may be obscured by advanced osteoarthrosis or simply overlooked due to inaccurate centering of the x-ray beam.[38,99] The vertically oriented, radiolucent intercondylar fissure is only visible when the x-ray beam lies parallel to the zone of incomplete ossification, and this occurs with mild supination of the elbow.[98-100] A recommended projection to best delineate the fibrous or fibrocartilaginous fissure in IOHC is the Cr15°M-CdLO (supinated craniocaudal) projection, but is not routinely included in survey radiographic evaluations of the elbow.[100,101]

2.3.1.2 Fragmented Coronoid Process

Survey radiography is very insensitive for the detection of FCP.[17,235] A discrete, mineralized fragment of the MCP cannot be visualized radiographically unless it is calcified and displaced.[5,17,167,168,197,230,232,236] Therefore, presumptive diagnosis of FCP is made on the basis of secondary osteoarthrosis and the exclusion of other forms of CED.[134,144,167,168,186,230,232] In the mediolateral view, radiographic changes consistent with FCP include loss of detail in the region of the MCP, a blunted and indistinct MCP, subchondral sclerosis of the trochlear notch, and periarticular osteophyte formation along the anconeal process, medial epicondyle, and cranioproximal radius. Osteophyte formation along the MCP and medial epicondyle are readily seen in the true craniocaudal view, although radioulnar step defects or humeroradial incongruity may also be seen.[6,170] Fragmented osteophytes, OCD flaps, or discrete fragments of the MCP are infrequently seen in this view.[117]

Additional oblique projections have been developed to enhance the evaluation of the MCP.[170,197] Two studies demonstrated the 15 º caudomedial-craniolateral oblique (Cd75ºM-CrLO, i.e. the extended and 15 º supinated mediolateral view) results in a true lateral view of the MCP.[170,197] Miyabayashi *et al* reported the extended and supinated view allowed visualization of the cranial border in 94% of elbows. By comparison, the cranial border of the MCP could only be seen in 56% of elbows in the maximally flexed projection, and 50% in the semiflexed projection.[197] Authors of a recent study reported the Cr45ºL-CdMO projection most useful to depict the MCP.[237] The 30º craniolateral-caudomedial oblique (Cr30ºL-CdMO, i.e. the pronated craniocaudal view) was found to be useful to assess osteophyte formation along the MCP and medial epicondyle, as well as osteochondral defects of the trochlea. However, the apex of the MCP is viewed *en face* in this projection and difficult for MCP fissures or fragments to be perceived.[197] Miyabayashi concluded that even though the extended and supinated mediolateral view resulted in the best visualization of the MCP, a fragment still may not be detected unless the x-ray beam is parallel to the plane of cleavage.[197] The medial aspect of the MCP is a common site for degenerative changes to appear, but fissuring and fragmentation tend to occur along the craniolateral aspect.[53,77] Visualization of a fragment in this plane would be unlikely unless the fragment is greatly displaced. Wosar *et al* determined the Cr15ºL-CdMO view had higher sensitivity (62% by consensus agreement) for detection of surgically confirmed FCP than 4 other radiographic projections, including the Cd75ºM-CrLO view (10-18% sensitivity).[232] The authors discovered that what was

radiographically diagnosed as FCP with the Cd75ºM-CrLO projection, were in fact only osteophytes. The authors concluded that in addition to having higher sensitivity of FCP detection, this projection also has the advantage of allowing evaluation of the trochlea for osteochondrosis. Some of the disadvantages of this study were the biased study population, and observers were aware of clinical status of the elbows and arthroscopic findings at the time of radiographic interpretation, and did not evaluate pre- and post-operative radiographs independently. Recently, a 35º mediodistal-lateroproximal oblique (MEDLAP) was developed to also enhance detection of MCP fragments.[238,239] This view was found to be more sensitive in detecting an abnormality of the MCP (non-FCP) than the craniocaudal, mediolateral, and Cr15ºL-CdMO projections when compared with arthroscopic findings.[238] However, there was no significant difference in accuracy between the MEDLAP and mediolateral views for detection of FCP. The advantage of this finding is clinicians will not need to have customized positioning sponges made for elbow radiography.

Many authors agree that secondary DJD will be radiographically apparent in most dogs with FCP or OCD by 7-12 months of age.[7,17,57,111,144] If a dog exhibits clinical elbow lameness but radiographic findings are equivocal for CED, follow-up radiography in 6 weeks has been recommended.[7] The rationale behind this recommendation is that pathology would progress to a degree that becomes radiographically evident to improve diagnostic certainty. However, the interim 'waiting period' may become detrimental to the dog.[7,167] If periarticular osteophyte formation is not radiographically evident in older dogs (>24 months of age) with

demonstrable elbow pain, FCP is usually not considered, or is completely excluded as a differential diagnosis.[240] In such cases, no further diagnostic imaging is pursued, and neither arthrotomy nor arthroscopy are performed.[240] This likely explains why CED has rarely been documented in older dogs with little or no osteoarthrosis.[222,241] However, this opinion is contested by Lang *et al* who suggest that normal radiographic findings alone cannot rule out elbow joint disease.[117]

There are a few case reports documenting FCP in dogs without evidence of osteoarthrosis.[222,241,242] Only one published study to date has investigated the prevalence of FCP in older dogs with elbow lameness. In that study, the boxer was one of the most frequently affected breeds in a group of dogs greater than 18 months of age in which arthrosis was absent or mild.[114] This study was the first to describe subchondral sclerosis caudal to the MCP as the sole radiographic finding in some older dogs with FCP.[114] Of dogs with IEWG grade 0 arthrosis (no osteophyte formation, but sclerosis is possible), there were 38 dogs (52%) greater than 12 months of age, 25 dogs (34%) were greater than 18 months of age, and 11 dogs (15%) were greater than 36 months of age. The most dramatic finding of the study was that 58 dogs (33%) greater than 18 months of age, with surgically confirmed FCP, had grade 0 or 1 arthrosis (osteophytes <2 mm) on survey radiographs. Everts *et al* claim there appears to be a second category of CED with an onset of signs at 4-5 years of age, which supports the findings of Meyer-Lindeberg *et al*.[115] Unfortunately, there was no histologic correlation in this population of older dogs. It is conceivable that in older dogs, these lesions may have been induced by subclinical incongruity as a result of

previous ligamentous strain or injury. Over time, concussive microtrauma during normal activity may result in clinically identical lesions of the MCP and trochlea humeri.

Diagnostic screening at 8-12 months of age is useful for identifying individuals that fit the typical presentation for CED and can be selectively eliminated from the breeding pool. The flexed lateral view is preferred for screening because it best displays the AP, which is the most common site for early osteophyte formation with FCP.[171,230] However, early radiographic screening will not effectively detect the subclinical joint incongruity. Therefore the subpopulation of dogs that develop the later onset form of CED may still remain in the breeding population.

2.3.1.3 Joint Incongruity

It has been suggested that radioulnar incongruity is a common denominator in dogs with FCP, OCD, and erosive kissing lesions.[3,4,15] Accurate assessment of genuine elbow incongruity is important in radiographs of dogs with suspected CED. Early detection of humeroradial joint incongruity may help facilitate corrective surgery before the development of degenerative changes.[24,181] However, humeroradial subluxation is not consistently present at the time of FCP diagnosis, and may be a transient finding in juvenile dogs with asynchronous growth of the radius and ulna.[57,185] Radiographic determination of humeroradial incongruity has relatively poor sensitivity and specificity, and is dependent on the severity of incongruence, positional obliquity, and interpreter experience.[243,244] Wind believed that a normal

congruent elbow could not be made to appear radiographically incongruent even with varying the positional obliquity, degree of flexion, or radiographic technique.[24] This, however, has been found to be untrue. Widening of the HR joint can be induced in flexed lateral views due to obliquity in positioning as joint surfaces are forced together.[231]

Joint incongruity can also be simulated with improper patient positioning or centering of the x-ray beam. Murphy *et al* tested inter-observer agreement for joint incongruity by varying the degree of elbow flexion in the mediolateral projection, in addition to altering the centering of the x-ray beam from the elbow to mid antebrachium.[231] Horizontal-beam craniocaudal views were also obtained level to the joint, and angled 30º proximal to and 30º distal to the bisecting angle of the elbow. The greatest observer agreement and level of certainty for humeroradial congruity was determined to be the mediolateral projection with 90º flexion of the elbow and x-ray beam centered at the elbow, or in the craniocaudal view with the beam angled slightly above the bisecting angle (30º toward the humerus).[231] The least agreement was observed with the 135º extended mediolateral view and x-ray beam centered at the elbow. Observer diagnostic certainty for joint incongruity was least (i.e. indeterminable congruity status) with 45º flexion of the elbow and mid-antebrachium centering of the x-ray beam. The authors concluded that there were significant effects of limb positioning and x-ray beam centering and angling on observer agreement and certainty in both projections. The study determined that artifact distortion of humeroradial joint width increased with elbow flexion in the mediolateral view, and

also increased as beam angle increased toward the humerus, rendering craniocaudal views non-diagnostic for subjective congruity assessment.[231]

The radiographic sensitivity and specificity for detection of manually induced radioulnar incongruence was tested in an *in vitro* study with cadaveric limbs.[243] Among 4 board-certified radiologists, the median specificity to correctly identify a congruent joint was 86% (range 67-100%) for the mediolateral view, and 82% (range 67-100%) for the craniocaudal view. The median sensitivity to correctly identify an incongruent joint was 87% (range 13-90%) on the mediolateral view. The median sensitivity to correctly identify a radioulnar step defect on the mediolateral view was 78% (range 9-88%) and 79% (range 9-90%) on the craniocaudal view. The magnitude of the step defect required to be radiographically detectable (with 90% sensitivity) ranged from 1.5-4 mm.[243] These findings suggest, that even under the best circumstances, radiologists are inconsistent in their ability to discriminate normal from incongruent elbows, as evidenced by high false positives and false negatives. This may result in unnecessary invasive surgical procedures to correct incongruence that may not be present. The results of a recent *in vitro* study investigating the effects of varying degrees of flexion and x-ray beam centering on observer performance, suggest that computerized radiography is a sensitive and specific screening test for moderate to severe radioulnar incongruence (>2 mm) for 90º flexion regardless of x-ray beam centering.[244,245] These findings support the previous study by Murphy *et al*.[231] Detection of incongruence ≥2 mm had 100% median sensitivity for 90º flexion and 80% for 135º flexion, with excellent observer agreement. However, for mild

incongruity (1 mm), sensitivity remained good at 80% for 135º flexion, but fell to 60% for 90º flexion. There was significant variation in sensitivity and specificity between observers for mild incongruity in both angles. Highest specificity was found consistently among the observer with the most experience. The lowest specificity was seen with the 135º angle (median 55%), and with the x-ray beam centered proximal to the medial epicondyle. This angle has been described as the angle of the elbow during the mid-stance phase of the gait cycle,[246] and may explain the presence of physiological humeroulnar incongruity.[32,247] Specificity improved only slightly (65%) and sensitivity dropped (50%) when simulated weight-bearing forces were applied to the elbow, which may not truly have simulated *in vivo* biomechanics, but did reduce the recognition of incongruity.[244] It was concluded that observer experience influences the recognition of normal elbows, but with moderate incongruity, radiography is sensitive enough to enable surgical planning.

2.3.2 Radiography – Surgery Correlation

The question remains, do radiographic changes correlate with clinical or surgical findings? The answer, surprisingly is no. As previously discussed, the development of osteoarthrosis is the basis for screening evaluations of the elbows.[119] However, Lang *et al* emphasized that normal radiographs do not rule out the presence of elbow disease. Ten percent of cases with surgically confirmed FCP had no evidence of osteoarthrosis on radiographs, even in the oldest dog of 4.5 years of age.[117] Of 332 elbows with arthroscopically confirmed FCP, 22% of dogs had grade 0 (no

osteophyte formation) on radiographs, and only 17% had positive identification of a fragment.[114] In this particular study, 11 elbows (grade 0) were from dogs greater than 3 years of age. Again, these findings contradict the conclusions of Walde and Tellhelm who reported CED does not occur in dogs >2 years of age without evidence of osteoarthrosis.[240] From a study of 335 dogs with surgically confirmed elbow 'osteochondrosis', Guthrie determined that it was not possible to predict the nature and extent of lesions from the radiographic score.[111] She also concluded there was no correlation between the radiographic score and the degree of lameness. This was supported by a prospective study of 55 Rottweiler puppies, in which radiographic findings were discordant with physical signs of elbow disease at 6 and 12 months of age.[194] Radiographic evidence of CED was present in 18% of puppies by 6 months and 57% of dogs by 12 months, although clinical lameness was observed in only 14% of puppies.[194] Osteophytes have been thought to form in response to joint laxity, stimulated by tension at the joint capsule attachment site on periosteum. As with hip dysplasia, this mechanism is thought to be an attempt at joint stabilization.[193] And also as with hip dysplasia, there is no evidence that radiographic severity of CED correlates with clinical severity.

2.3.3 Arthroscopic Findings of CED

Arthroscopic features reported to occur with joint incongruity include: distal displacement of the radial head (step defect) at the level of the medial coronoid process and lateral compartment of the joint; irregular cartilage between the radius

and ulna, and discolored, irregular, or softened cartilage on the radial head and trochlear notch.[248] Samoy *et al* state that incongruity was always accompanied by FCP in lame dogs.[248]

It was once believed that large, loose fragments would be associated with the most severe changes on radiographs. However a lack of correlation also exists between the degree of radiographic changes and type of arthroscopic lesions.[249] Large, loose, and clearly displaced fragments were seen in 20%[198] and 22%[114] of young and older dogs respectively, even when osteoarthrosis was not radiographically evident.[200] Alternatively, non-displaced FCP are also found via arthroscopy even when overlooked by advanced imaging techniques as linear tomography[170,236] and computed tomography.[17,249]

Both arthroscopy and CT reveal the variation in CED lesions. Nevertheless it is the experience of some surgeons that the absence of visible lesions with arthroscopy does not exclude the possibility of elbow disease.[221] In some cases, CT may demonstrate MCP fissures whereas arthroscopic findings may be normal.[221] It is possible MCP fragmentation may also be concealed underneath chondromalacia-like lesions which are described as soft and spongy cartilage without cleft formation, and may produce a false negative arthroscopic exam for FCP.[113] This indicates that alternative imaging techniques and modalities, such as scintigraphy, arthrography, linear tomography, computed tomography, and magnetic resonance imaging may also be appropriate screening tests for CED.

2.3.4 Linear Tomography

Linear tomography (LT) is 'layer radiography' that produces a detailed image of a selected, narrow plane within the body by blurring the images of the structures above and below the selected plane.[250] Images are achieved by the synchronous movements of the x-ray tube and film cassette about a central pivot point during radiographic exposure. The tube and film are connected via a rigid mechanical arm and move reciprocally about a pivot point, or fulcrum. The level of the fulcrum becomes the plane of focus, which can be manually set depending on the region of interest. Structures within the focus plane will appear relatively sharp, while structures above and below the plane will be very blurry. All methods of LT require a long exposure time (up to 3 seconds) therefore general anesthesia is required for all small animal imaging.[250] Other factors that need to be considered before imaging is the location and depth of the lesion of interest, which determines the direction of tube movement. Thinner desired plane thicknesses require larger tube swing angles. Tube swing movement is generally limited to 45º, which limits the thickness of the image plane to approximately 5 mm.[250] Therefore, before LT imaging is attempted, the lesion must be identified and localized on orthogonal survey radiographs. The use of LT in veterinary literature has been generally limited to the skull and axial skeleton.[250-255]

LT Sensitivity / Specificity

Reports of the sensitivity of FCP detection with linear tomography are limited. Voorhout and Hazewinkel compared radiographic and LT images with the findings

from medial arthrotomy in 14 dogs.[170] FCP was diagnosed in 5 dogs by radiography (extended and supinated projection) and LT. Linear tomography alone diagnosed 2 fragments and an MCP fissure that were radiographically undetected, but all were confirmed at surgery. The authors of this study concluded linear tomography was more accurate than conventional radiography for detecting FCP, but this claim was statistically unsubstantiated.[170] Carpenter *et al* compared the findings of conventional radiography, xeroradiography, arthrography, LT, and CT with those from arthrotomy.[17] Linear tomography alone was found to have low accuracy (60%) and sensitivity (41.2%) for detecting FCP, but had relatively good specificity (84.6%). No difference was found between the other modalities, although the combination of LT and radiography approached the accuracy of CT.[17] Although LT is no longer a commonly used or available imaging modality, it may be recommended when conventional radiographic techniques fail to demonstrate suspected CED lesions that are obscured by superimposed structures of the elbow.

2.3.5 Arthrography

Positive contrast arthrography has been used extensively for diagnosing OCD of the scapulohumeral joints in dogs,[256-262] however its utilization in the elbow has been quite limited in veterinary patients. In humans, both positive and double contrast arthrography have been used to diagnose developmental or trauma induced cartilage tears, defects, or intra-articular bodies.[263,264]

The radiographic anatomy and technique for use in dogs have been described in a single study in normal dogs.[265] Arthrography was performed under general anesthesia using a 1.5 inch, 20-22 gauge spinal needle inserted into the caudal and lateral aspect of the joint capsule between the trochlear notch and capitulum with the elbow in a moderately flexed position. Following injection, the joint was flexed and extended several times to ensure adequate distribution of contrast medium. Medial pouches of the joint capsule were identified under the tendon of insertion of the biceps brachii and tendons of origin of the carpal flexor muscles at the medial epicondyle. The lateral pouch was found in a similar location at the lateral epicondyle under the tendons of origin of the extensor carpi radialis and common digital extensor muscles. The cranial and caudal pouches of the joint capsule are more voluminous than the medial and lateral. The cranial aspect projects around the annular ligament, and the caudal extends laterally from the supratrochlear foramen and olecranon fossa. Optimal opacification was achieved with 2 ml of either 250 mg/ml or 370 mg/ml water soluble iodine containing contrast medium (sodium-meglumine diatrizoate) within 5-7 minutes of injection.[265] Image detail was reported to deteriorate quickly after 7 minutes and the diagnostic quality of the image was considered poor by 15 minutes post-injection. Larger volumes of intra-articular contrast media also resulted in poorer image quality regardless of radiographic position. The extended mediolateral view resulted in optimum visualization of articular margins of the radial head and trochlear notch in the majority of elbows. The extended and supinated mediolateral view provided the best visualization of the MCP, but could only be seen

in 24% of tested elbows. The craniocaudal and supinated craniocaudal projections resulted in excellent visualization of the articular surfaces of the trochlea humeri and capitulum, but not the MCP because it is projected *en face* in this view. The flexed mediolateral projection resulted in the poorest visualization of articular surfaces because it allowed contrast to accumulate in the cranial pouch thereby obscuring anatomic detail.[265]

The purported advantages of positive contrast arthrography are the technical ease of the procedure and the ability to visualize the surfaces of articular cartilage and synovial membrane. However, Lowry *et al* determined that clear visualization of the MCP could not be achieved with this technique in normal dogs, and the arthrographic anatomy of other joint surfaces was complex.[265] In a separate study, arthrography failed to detect any articular lesions in 25 elbows with surgically confirmed FCP and/or kissing lesions.[17] Although superficial scoring of articular cartilage has not been associated with clinically apparent synovitis, iatrogenic damage to articular cartilage is possible with this technique and was confirmed in 2 dogs at necropsy. If these cartilaginous defects had been seen with arthrography, it may be impossible to differentiate them from pathology due to dysplasia. Additional disadvantages of the procedure include iatrogenic introduction of air bubbles during the procedure which can be misinterpreted as lesions.[234] Adverse reactions to intra-articular ionic contrast media, such as meglumine-sodium diatrizoate, have been reported to induce synovitis.[257,259] Other disadvantages of this procedure include the rapid deterioration of image quality due to the dilution of contrast media from synovial fluid. This has

been minimized by the use of non-ionic contrast and the addition of epinephrine to prolong the crispness of the image.[256,257]

2.3.6 Ultrasonography

In veterinary medicine, sonography of orthopedic disease has been limited mainly to the examination of equine tendons and joints.[266-270] Small animal musculoskeletal ultrasonography has predominantly focused on the canine shoulder,[271-274] stifle,[272,275-277] or calcanean tendon.[278,279] Sonographic interrogation of periarticular soft tissues may be helpful in cases of known or suspected trauma but equivocal radiographic findings.

Potential advantages of ultrasonography include examination of ligaments and tendons that are not radiographically visible and real-time assessment of tendon and joint movement during direct manipulation.[280] Sonographic examination of the elbow may be easily performed without sedation if the animal is not painful, however, dynamic sonographic studies may necessitate patient sedation. Structures should be thoroughly examined in both longitudinal and transverse planes with adequate coupling gel and a high frequency linear probe (7.5-13 MHz) for best resolution and detail. Positioning the ultrasound beam perpendicular to the ligaments or tendons is important for visualization of fiber pattern and accurate assessment of echogenicity.[281] A flexible stand-off pad may enhance visualization of superficial ligamentous or tendinous structures.[280]

Normal Findings

The ultrasonographic appearance of the normal and dysplastic canine elbow has been recently described.[237,280,282] Normal structures of the elbow clearly visible with ultrasonography include: the medial and lateral epicondyles with associated tendons of origin for carpal extension and flexion, tendons of insertion of biceps brachii and triceps, medial and lateral collateral ligaments, humeroradial and humeroulnar joints, anconeal process, MCP, articular cartilage of the radius, and the supinator muscle with its associated sesamoid.[237,280] Articular cartilage appears as a thin hypoechoic to anechoic layer (approximately 1 mm thick) on the surface of subchondral bone plates. Subchondral bone appears as an intensely hyperechoic linear structure with strong acoustic shadowing. Joint spaces are identified as thin hypoechoic regions between subchondral bone layers of opposing bones.[237,280] In a recent study of normal canine elbows, the humeroulnar and humeroradial joints could be visualized, but the proximal radioulnar articulation could not.[237] The anconeal process in sagittal plane was best visualized in an oblique plane caudal to the epicondyles with the elbow in a flexed position of 80-90º,[237,280] but could also be seen in the transverse plane between the olecranon and distal humerus.[280] The outer margin of the MCP was best seen by following the medial epicondyle caudally toward the humeroulnar joint space. The apex of the MCP lies deep to the medial collateral ligament and biceps brachii tendon. It appeared as a sharp hyperechoic projection immediately distal to the HU joint surface on the medial aspect of the ulna.[237,280] The humeral condyle could not be seen sonographically. The sesamoid of the supinator muscle did not exhibit distal

acoustic shadowing, which was attributed to incomplete mineralization or small size. The sesamoid could be detected by its asynchronous movement against the radius during flexion and extension of the elbow.[237]

Abnormal Findings

Visualization of the MCP is enhanced with intra-articular injection of saline or with joint effusion.[237,282,283] The presence of synovial effusion is an abnormal finding in the elbow, and is an indication of underlying pathology.[237,282,283] Effusion provides a good acoustic window for evaluating intra-articular structures of the elbow and facilitates ultrasound-guided arthrocentesis.[282] FCP may sometimes be recognized if they are large and displaced. They appear as hyperechoic structures within or surrounded by joint effusion, and may have irregular margination due to bony remodeling or osteophyte formation.[283] Discrete fragments may be seen with dynamic sonographic examination as independent movement from the ulna as the elbow is manipulated through ROM.[283] Periarticular osteophytes can also be visualized as irregularities of cortical margins of the anconeal process, proximal radius, and epicondyles.[283] UAP appears as an interruption in the contour of the anconeal process, and sonographic examination during flexion and extension of the elbow may detect mobility of the process.[282,283] Prospective studies investigating the sensitivity and accuracy for detection of lesions associated with CED have yet to be reported. Ultrasound is a readily available, relatively simple tool for evaluation of periarticular soft tissues of the elbow, and may be useful as a complement to

radiography. However, as a screening tool for CED, this technique does not provide sufficient detail of articular surfaces and osseous structures to be useful.

2.3.7 Scintigraphy

Skeletal scintigraphy is one of the most commonly performed nuclear medicine procedures in veterinary medicine. Its use in small animal veterinary medicine has been primarily to evaluate the extent of primary skeletal neoplasms,[284] detection of distant metastasis,[285,286] loosening or infection of surgical implants,[287] or determine perfusion of extremities.[288,289] A problem commonly encountered in veterinary medicine when evaluating lameness is that radiographic changes often lag behind ongoing skeletal disease, and the magnitude of radiographic change may not correlate with the severity of clinical signs. Scintigraphy has very high sensitivity for detecting early changes in bone activity or metabolism associated with inflammation or lysis secondary to infection, trauma, or neoplasia.[290,291] Therefore it may be favored as a screening technique for occult or obscure lameness.

Bone scintigraphy involves intravenous injection of radioactive technetium-labeled methylene diphosphonate (^{99m}Tc-MDP) or hydroxymethylene diphosphonate (^{99m}Tc-HDP). Distribution of radiopharmaceutical (RP) is dependent on regional perfusion and osteoblastic activity. The diphosphonate RP binds to exposed hydroxyapatite crystals. Osteoblastic activity exposes more crystals and this usually results in increased RP uptake. Therefore bone uptake of diphosphonate-labeled RP is an indicator of osteoblastic activity at the time of injection. However, the final

scintigraphic image is dependent on other physiologic factors that affect RP distribution and localization after injection.[291]

Scintigraphic studies include 3 phases: vascular, soft tissue, and bone. Imaging during the different phases evaluates different physiologic processes. The vascular phase occurs immediately after injection and involves rapid dissemination of the RP to systemic capillary beds (i.e. blood pool). From the capillary bed, RP is rapidly distributed within the extracellular fluid (ECF) resulting in the soft tissue phase approximately 2-10 minutes after injection. Radiopharmaceutical in the ECF then binds to exposed hydroxyapatite crystals produced by metabolically active osteoblasts within 20-30 minutes of the injection. The RP that is not taken up by bone is cleared from soft tissues via renal glomerular filtration. The bone phase images are generally not obtained until adequate soft tissue clearance has been achieved (typically 2-3 hours after injection) to allow for the development of an optimal target to background ratio.[292]

All normal bone is constantly remodeling, therefore all bones that have adequate perfusion should have some RP uptake. This appears as low but uniform uptake at diaphyses, and slightly more at metaphyses and joints. Increased uptake will be seen at physes in younger animals. Abnormally increased osteoblastic activity will have significantly increased RP uptake and appears as a 'hot spot' on scintigraphic images. Pathological RP uptake may be seen 24-72 hours after injury, although radiographically visible lesions may not be detected for up to 2 weeks.[292]

In addition to early lesion detection, bone scintigraphy also offers the advantage of allowing side-by-side, time-matched comparison between limbs, and can quantitatively characterize the activity of radiographically identified lesions within bones, joints, or adjacent soft tissue with region of interest (ROI) count statistics.[293] Scintigraphy can also be used to monitor healing or therapeutic response.[292] Comparison of multiple views of joints, improves diagnostic confidence and localization of lesions. The major disadvantage of bone scintigraphy is lack of specificity, as increased RP uptake may be seen with infection, inflammation, and neoplasia. Lesions may also be overlooked if they are inactive. Because scintigraphy involves radioactive materials, these studies are limited to licensed institutions with trained personnel and imaging and radiation monitoring equipment. Strict radiation safety protocol must be followed which includes quarantine of the animal until the RP has decayed to a biologically safe level for patient handling. Image resolution with the gamma camera is also relatively low, even with a high resolution collimator, and requires precise patient positioning and restriction of movement. Image interpretation may be complicated with the presence of bilaterally symmetric disease. Altered attenuation of radiation may occur due to asymmetrical muscle atrophy, leading to false positive 'hot spots' on the scintigram. Normal physeal growth activity in young dogs may mimic or mask the detection of lesions, particularly in the elbow or stifle. Non-skeletal RP distribution, $^{99m}TcO_4$ labeling impurities, and/or cutaneous contamination with RP laden urine may also lead to false positive diagnoses.[293,294]

There are no reports in the literature that investigate the diagnostic accuracy or sensitivity of scintigraphy for FCP or other lesions within the elbow. However, a recent study investigated the usefulness of bone scintigraphy in the diagnostic workup of occult or obscure lameness in 12 dogs.[293] Focal increased activity was seen in the region of the elbow in two dogs with FCP, and in the humeral condyle in 2 dogs with IOHC. Three of these dogs had normal survey radiographs, and one dog had mild DJD. Although the authors concluded that scintigraphy localized or excluded bone pathology as a cause of lameness in most dogs, there was no follow-up gold standard procedure to confirm or refute the scintigraphic findings.[293] The presence of increased RP uptake in an elbow with minimal or no radiographic abnormalities, may provide some clinicians with more diagnostic confidence to pursue surgical exploration of the elbow. Alternatively, scintigraphy may detect abnormal foci of activity in adjacent soft tissues, representing a soft tissue injury, or other areas of the body that contribute to lameness. Scintigraphy may be a valuable diagnostic tool to localize or confirm the source lameness in dogs with normal to equivocal radiographic findings, but this procedure alone does not provide sufficient anatomic detail for thorough examination.

2.3.8 Magnetic Resonance Imaging

Magnetic resonance imaging (MRI) uses an external magnetic field to characterize the magnetic properties of hydrogen protons in the body. Proton density determines the signal characteristics of a tissue type. High soft tissue contrast is

produced by the difference in signal intensity from bone marrow, subchondral bone, cartilage, ligaments, tendons, joint capsule, synovial fluid, and fat. Other advantages of MRI for musculoskeletal imaging include: absence of ionizing radiation, direct multiplanar imaging of joints, and acquisition of tissue signal directly from intra- and juxta-articular structures.[295] Because of superior soft tissue resolution, MRI can detect pathological alteration of soft tissue via specific imaging sequences.[15,296] MRI is routinely used for evaluating elbow disease in humans,[297-301] and has been used for evaluation of FCP[15,235,295,302] and joint congruity in canine elbows.[303]

2.3.8.1 MRI Technique and Sequences for the Elbow

MR imaging of the canine elbow can be technically challenging. Because of its small size, and lateral decentering relative to the magnet isocenter, proper positioning of the elbow is critical. For 'off-axis' imaging of the elbow, Snaps *et al* recommend placing dogs in lateral recumbency, with the non-dependent elbow (joint of interest) secured in 90º flexion, and the proximal ulna placed within a surface or orbital coil, with the olecranon protruding through the coil.[295] Most MRI scanners permit 'off-axis' scanning, but for eccentrically located, small structures (such as the elbow), a surface coil is needed to optimize the signal-to-noise ratio (SNR).[295] Conventional spin-echo T1- or T2-weighted sequences limit slice thickness to 2 mm or SNR will be too low, and images becomes non-diagnostic.[15] However, ultra-thin slices can be acquired without compromising SNR with a three-dimensional Fourier transformation (3DFT) gradient echo (GE) fast imaging sequence, or volume acquisition imaging.[295]

It is termed 3D imaging because the RF pulse excites the entire volume of the voxel (pixel size x slice thickness). The data from the 3DFT may be reformatted into multiple planes that span the entire joint. This multiplanar function significantly reduces image acquisition time, and allows very thin (0.7 mm), contiguous slices without loss of data through inter-slice gaps, and has excellent SNR and resolution.[295]

GE 3DFT / FISP

The GE 3DFT sequence is also known as 'fast imaging with steady-state precession', (FISP) and has been recommended for scanning the canine elbow.[295] Gradient echo (GE) pulse sequences are created by reversing the magnetic field gradient to rephase the dephased protons instead of the 180º pulse used in standard spin-echo sequences. The GE pulse sequences use flip angles less than 90º therefore acquisition time is much faster because of shorter TR and TE times.

Proton signal from fat can dominate the MR image and obscure lesions of interest. Fat saturation sequences have been developed to selectively nullify the fat signal. Suppression of fat signal is achieved by applying a narrow bandwidth RF pulse that is centered at the resonance frequency for fat. This dephases only fat protons in the transverse plane (i.e. selective excitation, or spoiler gradient), y*et al*lows signal detection for all other tissue types. Fat saturation sequences suppress the signal from bone marrow and periarticular tissues so that the only structures exhibiting high signal intensity are those that demonstrate paramagnetic contrast enhancement on T1-weighted, and those that contain fluid or edema on T2-weighted images.[304] The GE

3DFT (FISP) sequence has been found to be superior to 2DFT for identifying small cartilaginous lesions (<2 mm), and when combined with a fat suppression technique, it demonstrates higher sensitivity for detection of articular defects than standard MR imaging sequences.[305-308] Fat saturated FISP sequences also increase the contrast between cartilage, joint fluid, and subchondral bone, where the cartilage appears as a thin band of high signal intensity.[308] However, fat saturation sequences cannot be used with 'off-axis' imaging. The region of interest to be fat saturated must be correctly centered within the magnetic field, therefore, this sequence is not suitable for use in live, large-breed dogs.[295]

STIR

Short T1 inversion recovery (STIR) sequences may be used in lieu of fat saturated T2-weighted sequences to enhance detection of subchondral edema associated with trabecular destruction. STIR sequence is often used for musculoskeletal imaging in veterinary patients.[304] STIR uses a 180º inversion RF pulse before the 90º signal pulse of the typical spin echo sequence to allow for additional T1 signal recovery. The time between the 180º and 90º pulses is defined as the inversion time (TI). The TI can be manipulated to selectively excite or suppress specific tissues, such as fat which has a short TI time. In these images, fat will have a low signal, and subchondral edema or synovial fluid will have increased signal.

A complete examination of the elbow should include transverse, sagittal, and dorsal plane images. The transverse (or axial) plane is most useful for detecting

abnormalities of the MCP and radial incisure.[15] The sagittal plane permits evaluation of humeroulnar, radioulnar, and humeroradial articulation. Abnormalities of the MCP and AP can also be seen in this plane. UAP has been described as a hyperintense linear signal between the proximal ulna and AP on T2 weighted spin echo images.[15] The dorsal plane allows clear visualization of the MCP and its articulation with the radial head. In T1 and T2 spin echo, and FISP sequences the normal MCP has uniform low signal intensity. Periarticular ligaments and joint capsule are also hypointense in all sequences. Relative to muscle, on FISP sequences, subchondral bone is hypointense, bone marrow is hyperintense, and articular cartilage is isointense.[295] Articular cartilage thickness is approximately 1 mm, however, when opposing surfaces are in contact, the separate layers cannot be distinguished.[295]

2.3.8.2 MRI appearance of FCP

Snaps *et al* have investigated the diagnostic uses of MRI for the canine elbow, and have recommended fast imaging gradient echo sequences for the canine elbow. The FISP sequence was found to provide precise depiction of the MCP and AP in multiple planes, as well as detection of pathology induced changes in signal intensity in dogs with confirmed FCP.[235] In that study, MRI findings were compared with surgical findings from arthroscopy or arthrotomy. Three types of MCP abnormalities were described: discrete (loose) mineralized FCP, non-displaced and unmineralized FCP, and non-displaced, mineralized FCP (*in situ* fragment). The fragmented, mineralized coronoid process had low signal intensity characteristic of dense

subchondral bone. The non-displaced, unmineralized FCP had high to iso-signal intensity compared with adjacent muscle. This type of FCP was associated with a sharp demarcation of signal intensity that correlated with a cartilaginous fissure within the coronoid process. Interestingly, fissure lines could not be visualized at arthroscopy until curettage of articular cartilage was performed.[235] *In situ* mineralized FCP were characterized by irregular margination of the MCP and low signal intensity. Kissing lesions of the trochlea humeri were described as focal, circular subchondral defects with hyperintense signal, consistent with seepage of synovial fluid into subchondral bone.[302]

MRI Sensitivity / Specificity

When compared to conventional radiography, MRI had higher accuracy and sensitivity for diagnosis of FCP, although radiography had higher specificity (100%) than MRI (93%). MRI demonstrated very high accuracy (95.5%) and sensitivity (100%) for discrete, mineralized fragments. MRI accuracy (91%) and sensitivity (87.5%) for non-displaced cartilaginous fragments was nearly the same for *in situ* mineralized fragments (accuracy 91%; sensitivity 83.3%). Radiography had an accuracy of 77.2%, and sensitivity of 28.6% for diagnosing FCP. MRI however, was not significantly more accurate (77.2%) than radiography (72.7%) for detecting subchondral lesions of the trochlea humeri.[235] As of yet, comparative studies between CT and MRI to determine diagnostic superiority for FCP have not been reported.

2.3.8.3 MRI and Joint Incongruity

Another advantage of MRI is the ability to assess joint congruity because of its ability to differentiate the bone-cartilage boundary of articular surfaces. MRI is also the only method that allows direct non-invasive examination of cartilage.[309,310] In humans, MRI has been found to be an accurate imaging method in the assessment of joint geometry.[309] However, when normal articular surfaces are in direct contact, the demarcation between opposing layers of cartilage cannot be distinguished as separate, and the cartilage signal appears as one.[295,303] A recent study utilized MRI to assess and quantify interosseous gaps (apparent joint space width) between the humeral condyle, radius, and trochlear notch in non-arthritic small-, large- and chondrodystrophic breed dogs.[303] There was significant correlation between body weight and interosseous gap of the humeroulnar joint at the midpoint of the trochlear notch in the sagittal plane of large breed dogs. Also in large breed dogs, there was a significantly narrower interosseous gap between the humeral condyle and anconeal process than seen in other breeds. Dissection of joints confirmed the presence of cartilage-free areas in the center of the trochlear notch in all large breed dogs. In other breeds, cartilage free areas were rarely seen, and only evident at the lateral coronoid process.[303] The findings of this study support histological evidence of non-inflammatory cartilage atrophy at these locations in breeds of dogs with physiological joint incongruity.[25,86,94] Findings are also supportive of monocentric humeroradial and bicentric concave humeroulnar incongruity in mature, large-breed dogs.[32,311] The decreased gap distance between the humeral condyle and anconeal process may

indicate predisposition for UAP, or decreased ability to compensate for intra-articular step defects when asynchronous growth between the radius and ulna (shortened ulna) occur.[303]

2.3.8.4 MR Arthrography

Intra-articular injection of dilute paramagnetic contrast medium, such as gadolinium chelates, has been attempted to enhance MRI sensitivity for detection of intra-articular lesions of the joint capsule or articular cartilage.[312-314] MR arthrography (MRAr) with intra-articular saline has been reported to be equally useful for detection of articular cartilage defects as gadolinium compounds in an in vitro study.[315] However, in a clinical study, saline arthrography was found to be inferior to dilute gadopentetate dimeglumine with GE studies as saline cannot differentiate between joint effusion and fluid within an adjacent bursa.[316] MR arthrography with gadopentetate dimeglumine obscured visualization of OCD lesions of the scapulohumeral joint in dogs.[312] Alternatively, intravenous gadolinium has also been shown to improve contrast in subchondral bone in canine shoulders with OCD lesions.[317] In human elbow arthrograms, intra-articular gadolinium (with fat saturation technique) is favored because it allows full distension of synovial recesses of the joint capsule and collateral ligaments and depicts synovial and articular cartilage defects. Injection can be performed by palpation, or guided by ultrasound or fluoroscopy. Although intra-articular gadolinium has a very good safety profile, it is not licensed for this route of administration in the U.S.A. or U.K.[313] In addition to

potential adverse reactions or iatrogenic synovitis, other diagnostic pitfalls that may occur include: joint overdistension, contrast extravasation (from overdistension) which may be mistaken with capsular disruption, air bubble artifacts which mimic loose bodies, and the presence of normal variants within the elbow (synovial fossae) that may create cartilaginous pseudolesions.[313]

A single study investigating the potential use of MR arthrography for FCP has been reported.[302] For the study, 6-8 ml of a 2 mmol/L solution of gadolinium-DOTA diluted with 0.9% NaCl (1:250) was used for injection into the cubital joint. Following injection, the elbows were manipulated to mix the solution with synovial fluid, and images were acquired immediately and compared with arthroscopic findings. Authors of this study reported the signal from intra-articular contrast masked visualization of articular cartilage. However, two types of FCP could be differentiated with arthrography on the basis of contrast infiltration around fragments. Discrete (loose) MCP fragments were associated with hyperintense signal (of contrast medium) infiltration along a fissure between the FCP and ulna. In two dogs, contrast was prevented from completely surrounding the FCP by a thin cartilage bridge between the ulna and fragment. Non-displaced fragments (mineralized and cartilaginous) did not exhibit dissection of contrast around the fragments. However, subchondral defects of the trochlea humeri demonstrated marked increase in signal with intra-articular contrast administration, indicating direct communication with synovial fluid.[302] Although arthrography permitted pre-operative differentiation between free and partially attached FCP, the procedure did not yield additional

information about FCP when compared to standard MR images, and was not conducive for diagnosing lesions involving only articular cartilage. Selective imaging the elbow with a strong T2-weighting may provide sufficient 'arthrogram-like' contrast of synovial fluid for detection of small cartilage defects.

Despite the superior soft tissue detail and image quality, there are several important limitations to MR imaging. Small animal studies require general anesthesia, and depending on the study, image acquisition times can be lengthy. Because of the strong external magnetic field, special anesthetic equipment must be used. Technologists experienced with MR sequences and patient positioning are essential. Magnets are expensive to house and maintain, and are generally limited to human hospitals, veterinary teaching hospitals, or large referral centers. Lastly, MRI examinations are expensive and are cost-prohibitive to many clients.

2.3.9 Computed Tomography

The structural complexity of the elbow joint has led to significant limitations in imaging of the MCP and articular surfaces affected by CED. Because of superimposition of the MCP with the radial head and narrow joint spaces, pathoanatomic information conveyed by conventional radiography, arthrography, and linear tomography is quite limited. Computed tomography (CT) has been shown to be extremely useful for evaluation of CED because it eliminates confusing anatomic superimposition seen with conventional radiography. Individual tomographic slices are acquired perpendicular to the long axis of the limb, and can be sequentially

reviewed. Collectively, the transverse images can be reformatted with computer reconstructive software into sagittal, dorsal, or oblique planes that are useful for visualizing site-specific lesions and surgical planning. For small joints like the elbow, it is critical to use thin slice thickness to minimize step-artifact that can mimic or mask lesions.[304] Computed tomographic images can also be used to create 3-D surface reconstructions of the elbow. Unfortunately, 3-D reconstruction techniques use a smoothing algorithm which averages the original data, and subtle cortical defects may be minimized or lost. Computed tomography is superior to radiography and MRI for cortical bone resolution, and has been reported as the modality of choice for evaluating the MCP.[318] Computed tomography has also been proven accurate and sensitive for the detection of FCP.[17,319] Although CT soft tissue detail is not as high as MRI, anatomic detail of periarticular tissues such as tendons, ligaments, vessels and some nerves is possible with soft tissue settings and is useful for evaluation of periarticular soft tissue structures.

Another advantage of CT imaging is that both elbows can be imaged simultaneously which significantly reduces scan time and anesthesia. Depending on the CT scanner, images can typically be acquired within 10 minutes, and newer scanner models have acquisition times of less than 1 minute. Short acquisition times permit surgical exploration under the same anesthetic episode without significant risk to the patient.[16] Also, with current reconstruction software, images can be reformatted and viewed side-by-side which allows comparison between elbows.

2.3.9.1 CT Technique and Image Display Parameters

There is great variation in the literature regarding optimal patient positioning, technique, and image display parameters. While under general anesthesia, dogs may be placed in sternal,[14,166,188] dorsal,[318] or lateral recumbency[16,101] with or without the head flexed toward the side out of the FOV. Ideally, forelimbs and joints should be positioned cranially and parallel to each other in extension, with elbows symmetrically positioned for optimal comparison of the elbows at the same level. Radiolucent wedge sponges or tape may be used to prevent rotation within the gantry, and limbs are positioned so the scan plane is perpendicular to the humeroradial joint or long axis of the ulna. A large FOV (22-28 cm^2) allows both elbows to be included in the same cross-sectional image. Individual elbows will appear small, but can be reconstructed separately for slightly magnified images, however, magnification >2x produces undesirable image quality.[318] A reconstruction algorithm for bone (high-frequency) and the thinnest (1-1.5 mm) contiguous transverse slices are recommended for best detail and to minimize step artifact on reformatted images.[15] For helical CT, image acquisition with a pitch of 1 has been reported.[166,320] Thinner slices will allow detection of smaller lesions and minimize partial volume averaging (PVA).[304]

Transverse images are typically obtained from the tip of the olecranon to the proximal diaphysis of the radius and ulna.[14,16] Image reconstruction may vary slightly between institutions and in the literature,[187,321] but several authors have attempted to standardize image reformatting protocols. Dorsal plane images are

obtained by reformatting the images approximately 90° to the long axis of the MCP, and sagittal plane images are obtained by reformatting the images approximately 45° to the long axis of the MCP.[187,188,320,321]

Currently, there is no consensus or recommendation for the ideal display parameters, although window settings reported in the literature fall into a 'bone' setting. Window widths (W) and window levels (L) available in the literature were either not described cover a large range; W1500 HU at L650 HU,[318] W2000 HU at L650 HU,[319] W2500 HU at L500 HU,[101] and W3500 HU at L500 HU.[16,188,321] A study describing the CT features of normal elbows also included soft tissue display parameters of W400 HU at L66 HU[16] for evaluation of periarticular soft tissues, however, soft tissue display settings are not typically used for evaluating intra-articular pathology.

A complete study of the elbow consists of dorsal, sagittal, and/or oblique (parallel to MCP) reformatted images. Transverse (axial) CT images allow visualization of the MCP, radial incisure, and trochlea humeri without superimposition of other bony structures. Discrete FCP is easy to recognize in this plane, but mineralized *in situ* fragments and osteophytes can also be visualized in transverse images, in addition to subchondral cyst-like lesions of the radial incisure.[14,16] Incomplete ossification of the humeral condyle (IOHC) is readily detected on transverse or dorsal images of the humeral condyle.[38,98-101,322] Sagittal and dorsal reconstructed planes allow evaluation of the entire humeroulnar and humeroradial joint and gross assessment of joint congruity[16,248] although the actual articular cartilage cannot be seen with CT.[295,321]

Displaced FCP, conspicuous MCP fissures, and large subchondral defects of the trochlea humeri may also be clearly seen on sagittal and parasagittal images. Although UAP is not an indication for CT it is depicted in this plane as a linear hypoattenuation of varying width that separates the anconeal process from the olecranon.[15] Subchondral sclerosis of the proximal ulna associated with panosteitis may also be detected on either sagittal or dorsal plane images.

Computed tomography shares some of the same disadvantages as MRI because most examinations require general anesthesia. However, with multislice helical CT scanners, rapid image data acquisition is possible with patient sedation only. Rapid imaging studies may become routine as these scanners become more available. Although overall bone detail is superior to that of MRI, CT may not accurately detect cartilaginous or partially mineralized *in situ* fragments. Like MRI, CT is still generally limited to veterinary teaching hospitals or referral and/or dedicated imaging centers. This modality requires knowledgeable technologists to perform the studies, and experienced clinicians for image reconstruction and interpretation. Computed tomography exams are more expensive than a conventional radiographic series, but are typically one-half the cost of MRI studies. Because image acquisition time is shorter, it significantly reduces anesthesia time over that of MRI.

2.3.9.2 CT Features of CED

The CT features attributed to CED have been recently described.[14,15] Only one study to date has defined the various CT characteristics in dysplastic canine elbows.[14]

Abnormalities of the MCP apart from fragmentation or fissure were most numerous and included: abnormal shape or remodeling, subchondral sclerosis or hypoattenuating defects, and osteophyte formation. Of particular interest was that blunting or thickening of the MCP, and medullary sclerosis adjacent to the MCP were present in >95% of elbows and were significantly associated with elbow lameness.[14] An abnormally shaped MCP has also been described as a sole feature of CED.[196] Abnormalities in shape and subchondral bone density likely reflect chronic remodeling as a result of altered weight-bearing. Sclerosis is an indicator of stiffened subchondral bone and often seen with osteoarthritis and may predispose overlying articular cartilage to damage and fibrillation.[30,60] Subchondral sclerosis caudal to the MCP and trochlear notch is seen early in elbow osteoarthrosis,[7,230] and has been reported in 94% of elbows with elbow pain.[14] Periarticular osteophytes are also a common manifestation of osteoarthritis, and the radiographic diagnosis of CED is based on the presence of secondary osteophyte formation.[7,167,230] However, the location of osteophytes is not specific or unique to a particular type of elbow disease. On CT, osteophytes appear as hyperattenuating protuberances or proliferations along or adjacent to the articular borders of the proximal radius, humeral epicondyles, and anconeal and medial coronoid processes. Osteophytes on the MCP generally cause it to become more pointed in appearance, or cause it to appear misshapen, blunted, or thickened.[15]

2.3.9.2.1 Fragmented Coronoid Process

The CT diagnosis of FCP is based on the visualization of a separate bone fragment or fragments adjacent to the MCP in transverse or sagittal images.[14,15] Medial coronoid process fissures or *in situ* fragments have also been characterized as a manifestation of CED.[14] These occur in the same location as FCP, but can appear as a dissection through articular cartilage or subchondral bone. In a CT study of 102 elbows, Reichle *et al*[14] identified a prevalence of discrete FCP (28%) and MCP fissures (27%) which was similar to a previous pathoanatomic study where fissures were detected in the cartilage or subchondral bone of 26% of young growing dogs.[10] Subchondral fissures may be overlooked if overlying cartilage has a normal appearance, and probing of articular cartilage is required to detect this type of fragment.[164,217,221]

Pre-operative identification of FCP is important in dogs with UAP because two separate surgical approaches may be necessary if both exist simultaneously.[101,112,207,219] Alternatively, pre-operative differentiation between OCD, FCP, and kissing lesions is not as critical because a medial approach is warranted in either situation.[207,217]

2.3.9.2.2 Radial Incisure

Abnormalities of the radial incisure (RI) have been described in a large percentage of dogs with elbow pain.[14,101] These abnormalities were characterized as irregularities of the RI contour (86% of elbows), or distinct 'lucencies' (46% of elbows) within subchondral bone. Irregularities of the RI appear as notches or

indentations along the cortical margin. The hypoattenuating defects have been described as circular, 1-2 mm cyst-like lesions deep within the cortical bone, and having variable communication with the radioulnar joint space.[101] Histologic examination of the radial incisure in dogs with FCP revealed proliferative synovitis and inflammation in this region.[196] Although histologic analysis was not performed in their study, Reichle *et al* conclude the RI abnormalities likely reflect chronic inflammatory changes associated with synovitis within the radioulnar joint. An alternative explanation for the nature of the hypoattenuating defects is extension of a fissure or fragment beyond the MCP into the incisure. This hypothesis is supported by histological evidence of varying patterns of MCP fragmentation, particularly those that occur in the sagittal plane.[53] It is this author's experience, planes of fragmentation have extended into areas of the hypoattenuating defects. However, it remains to be determined whether these RI hypoattenuating defects contribute to the fissuring or fragmentation of the MCP because of weakened subchondral architecture, or are a separate form of fragmentation.

2.3.9.2.3 Humeral Condyle and Trochlea Humeri

Lesions of the trochlea humeri are occasionally seen on CT images in dogs with CED, and appear as focal flattening and hypoattenuation of subchondral bone with or without surrounding sclerosis. Lesions are best identified on the dorsal plane, but may also be recognized in sagittal and transverse images if they are large and/or are

associated with sclerosis.[14,15] Although CT cannot differentiate between osteochondrosis, OCD, or erosive kissing lesions from FCP, if FCP and subchondral sclerosis of the trochlea are present, a kissing lesion should be suspected because they often occur simultaneously. Superficial erosive lesions or OCD cartilage flaps will not be conspicuous on CT images unless there is accompanying subchondral bone involvement. Articular cartilage is too thin to be resolved with CT and is obscured due to partial volume averaging with adjacent subchondral bone.[15]

Incomplete ossification of the humeral condyle (IOHC) has also been detected on CT images as a primary[100,322] or incidental lesion in combination with FCP.[38,98,101] Computed tomography image characteristics of IOHC include a linear or irregular hypoattenuating fissure between the capitulum and trochlea of the humeral condyle surrounded by hyperattenuating sclerosis. The fissure represents a retained cartilaginous plate from early condylar development or fibrous union of humeral condyles.[37,43] Lesions may vary from a faint fissure of the subchondral bone to a large, conspicuous fissure extending proximally to the supratrochlear foramen. The craniocaudal and vertical extent is also variable, but has been reported to extend from 1/3 to 1/2 the diameter of the humeral condyle.[38] Identification of this lesion is significant because it has been reported a primary source of lameness, is a heritable trait and often bilateral, and poses significant risk for condylar fracture.[38,99,100] It is important to note that persistent visualization of the fissure following lag-screw stabilization is common because intercondylar healing does not occur following transcondylar screw placement.[98-100] Although IOHC may be a primary cause of

elbow lameness, it may also occur concurrently with FCP, and may share a common pathogenesis. In one study of spaniels, there was high incidence of IOHC and FCP; radiographically visible discrete FCP was observed in 56% of dogs with intercondylar fractures, and 21% of dogs with intact condyles.[38]

2.3.9.2.4 Joint Incongruity

Because anatomic superimposition of the elbow joint is eliminated, joint incongruity is far more apparent on CT images than survey radiography. Gielen *et al* investigated the correlation of radiography, arthroscopy, and CT for detection of radioulnar step defects in 70 dogs with elbow lameness.[323] Incidence of RU incongruity was determined for each individual modality: radiography (44%), CT (55%) and arthroscopy (43%). Agreement between radiography and CT was only 36%, and 50% for all three modalities.[323] Recent *in vitro* studies have suggested CT is useful for pre-operative diagnosis of radioulnar incongruity, and has greater sensitivity and specificity than conventional radiography.[320,321] However, quantitative measurement methods are necessary to objectively measure distances between subchondral bone plates and exclude subjective observer assessment. A recent study used cadaveric limbs to manually induce radioulnar joint incongruity by reduction of radial length, and test differences in measurements between helical and incremental (axial) CT acquired images.[320] Authors of the study concluded there were no differences in accuracy between measurements obtained by incremental and helical CT scanned images, and highest direct and digital measurement correlation was found

in the oblique plane at mid-MCP. Although the manually created RU incongruities were known, this study avoided testing the most important question of CT accuracy and sensitivity for RU incongruity. Gemmill *et al* also tested the accuracy of reformatted CT measurements, intra- and inter-observer variability for normal radioulnar measurements, and the effect of limb positioning (inter-image variation) on measurement accuracy.[321] The authors reported good agreement between CT and anatomical specimens and good inter-image and intra-observer agreement, but only moderate inter-observer agreement due to imprecise resolution of joint surfaces.[321] However, authors concluded that despite moderate correlation, inter-observer estimation of joint space width is within a few 10^{ths} of a millimeter.[321] The major implication of this study is that minor positioning differences have minimal effect on image reformatting and joint space measurement.

In vivo estimation of joint incongruity has also been attempted in controlled studies of large breed dogs with known FCP and/or high grade cartilage damage of the MCP.[187,188] Gemmill *et al* measured single points at the humeroradial (HR) and humeroulnar (HU) joint spaces from sagittal and dorsal reformatted images in normal and dogs with FCP.[188] Dysplastic elbows were found to have significantly wider HR joints at the MCP apex when compared to controls, though HR incongruity was not found in all FCP cases. No differences were found between groups for HR measurements at the base of the MCP or HU joint space. However significant differences may have been minimized because the 'controls' used in this study consisted of the contralateral elbow of young dogs (median age 12 months) with

unilateral FCP, or elbows negative on IOHC screening, the entirety of all joint spaces were not included, and there was no surgical confirmation of the presence or absence of lesions.[188] Findings of a similar study do not support those of Gemmill *et al*, who found no significant differences in HR congruity at the MCP apex between disease-free and arthroscopically-confirmed dysplastic elbows at the time of diagnosis.[187] Furthermore, the only significant difference in HR congruity measurements between groups occurred at the base of the MCP.[187] Despite contradictory findings, both studies support Pool's hypothesis of transient asynchronous growth and temporary joint incongruity, as not all dogs with arthroscopically confirmed disease demonstrate joint incongruity at the time of diagnosis.[185] In such cases, the use of corrective osteotomy may be reconsidered.

CT Sensitivity / Specificity

Suspicion of FCP has become the most common indication for elbow CT examination. Early case reports heralded the potential value of CT for diagnosing FCP which could not visualized on radiographs.[319] Computed tomography has also been used to sequentially evaluate the progression of osteoarthritis in a Bassett hound puppy with bilaterally asymmetrical CED.[166] In this study, CT and arthroscopy were far more sensitive to subtle osteoarthritic changes over time when compared to radiography. There is only one study to date comparing CT and other diagnostic modalities for accuracy and sensitivity for FCP.[17] Carpenter *et al* found CT to have the highest accuracy (86.7%), sensitivity (88.2%), and negative-predictive value

(84.6%) for diagnosis of FCP when compared with other x-ray imaging modalities.[17] In this study, 11/17 (65%) of MCP fragments were unmineralized. CT provided false negative results in elbows with discrete cartilaginous fragments (1) and *in situ* cartilaginous fragment (1) and false positive result for an incompletely mineralized MCP osteophyte (1). Computed tomography accurately detected surgically confirmed OCD lesions in 2 elbows but also had 3 false positive results for OCD which were actually large kissing lesions.[17] Rovesti *et al* investigated the usefulness of pre-operative CT examination to determine if CT changed or better defined the radiographic diagnosis.[101] The CT diagnosis was different than, or more precisely defined radiographic lesions in 46% of elbows, which influenced the course of treatment. Surgical confirmation was not achieved in all cases, therefore accuracy and sensitivity were not determined, however, CT did not produce any false positive results, and there was excellent agreement between CT and surgery. Computed tomography was found to contribute to the radiographic diagnosis, and altered the surgical approach by the identification of FCP in dogs with UAP (2), FCP in dogs with normal radiographs (2) and mild subchondral sclerosis (2). Computed tomography was able to detect FCP as small as 1 x 2 mm, and confirmed RI irregularity and hypoattenuating defects that were not radiographically visible.[101]\

2.3.9.3 CT Arthrography

There are no reports in the veterinary literature employing CT arthrography (CTAr) to examine canine elbow joints. One study has described the CTAr

appearance of the cruciate ligaments and menisci in the normal canine stifle.[324] In humans, comparative studies of CT and MRI arthrography (MRAr) with arthroscopy have been used to evaluate articular cartilage defects, OCD, and intra-articular bodies in the elbow.[325,326] The technique used in previous CTAr studies included water-soluble iodinated contrast (300 mg I/ml) diluted 1:1 with saline under fluoroscopy-guided intracubital injection.[326] For mild (softening, fissuring) and severe defects (partial to full thickness lesion with possible subchondral bone exposure) there was no significant difference between CTAr and MRAr for detecting either grade of lesion, and both methods indicated limited diagnostic value for mild lesions when compared with arthroscopy. Overall sensitivity of CTAr and MRAr for mild lesions was 80% and 78% respectively, and 87% and 85% respectively for severe lesions. Specificity for both procedures and both grades of lesions ranged from 93-95%, and positive-predictive value ranged from 89-92%.[326] In a separate study, both procedures were compared with pre-operative radiographs and arthroscopy for detection of loose intra-articular bodies. Overall sensitivity of CTAr and MRAr was excellent (100% and 92% respectively) but specificity was low (77% and 15% respectively), compared to radiography (84%). The authors concluded that neither procedure was more reliable than survey radiography in detecting loose intra-articular ossified bodies.[325]

2.4 PRINCIPLES OF CT IMAGING

2.4.1 CT Scanner Components and Instrumentation

Computed tomography is an imaging process that produces cross-sectional or planar images of the body using x-rays and computer software. This requires three major components to acquire, process, and display the CT images: the imaging system, computer system, and image display, recording, storage, and communications system. Regardless of the manufacturer and model, CT scanners are all similar and have a scanning gantry, x-ray generator, computer system, operator's console, viewing console, and hard-copy printer or digital storage device. The CT gantry and patient couch are commonly referred to as the *scanner*. The gantry is the framework that surrounds the patient and houses the rotating x-ray tube, associated drive motor, slip rings, generator, pre-patient collimators, and detector array. Computed tomography scanners with slip rings (helical scanners) require highly stable 3-phase or constant potential generators to provide high, instantaneous power.[327-329] With modern CT scanners, the gantry can be tilted, within limits, to augment the scan plane that may be dictated by patient anatomy. The x-ray tube rotates and emits x-rays 360º around the patient positioned on the couch at the isocenter of the gantry aperture. The patient couch or table is cantilevered and supports and advances the patient into the CT gantry aperture at pre-selected increments that correspond to the slice (or image) interval of the study. With conventional CT scanning, the x-ray tube rotates around the patient to collect data from a single slice of tissue. Because the x-ray tube is connected to short power source cables, the tube has to 'unwind' and the couch

advanced before the next slice can be acquired. With helical CT scanners, image data is acquired as the couch is continuously advanced. The advent of the slip ring design allows for uninterrupted rotation of the x-ray tube within the gantry, and allows for a much faster acquisition time, minimizes motion artifact, and reduces patient radiation dose. Collimators are lead plates located between the x-ray tube and the patient at the inside margin of the gantry aperture. They physically widen or narrow, attenuating the primary beam, to determine CT slice thickness in 3rd and 4th generation scanners. X-ray photons are sensed by arrays of detectors within the gantry. Electrical signals generated by the detectors are amplified, mathematically converted and processed by complex computer software before a CT image can be generated. The operator console is where the imaging study parameters are set. Several variables are operator-dependent, such as mAs, kVp, FOV, slice thickness (collimation), image interval, pitch, reconstruction algorithm, and gantry tilt. Image post-processing can be performed at the operator console or at a separate viewer console. Modification of window width and level and multiplanar reformatting may be performed at the operator's console or other remote workstation to optimize the display image prior to data storage and image reproduction. Select images or the entire study may then be transferred to a film printer and/or stored on the computer hard drive, optical-disk, magnetic tape archival storage device, or in a picture archiving and computer system (PACS).

Detectors

The CT detectors record transmitted photons and convert them to a measurable electronic signal. They are positioned across from the x-ray tube and rotate simultaneously with the tube in 3rd generation CT scanners, or are placed in a stationary ring around the patient in 4th generation scanners.[330] There are 3 types of CT detectors: xenon gas ionization chambers, solid state scintillators, or multiple array. Xenon detectors are thin, elongated ionization chambers that contain high-pressure xenon gas within between metallic plates. Ionization of xenon produces an electronic signal that is amplified and digitized into a number proportional to the x-ray intensity detected. Because they are long and thin, they are highly directional with small, fixed detection angles, they are limited to 3rd generation scanners. Thin septae minimize inter-detetector dead space and improve geometric efficiency but conversion efficiency is only 50-60%. Solid-state detectors are $CdWO_4$, yttrium, or gadolinium ceramic scintillators coupled to photodiodes. Light is produced when the detector is struck by ionizing radiation. The light is collected by the photodiode, amplified proportional to incident photon intensity, and converted to an electrical signal. Solid-state detectors have higher absorption and conversion efficiency than xenon detectors (90%). Because of this, small gaps between detectors are necessary to avoid cross-talk, and this reduces geometric efficiency. The surfaces are flat, with a wide detection angle and are used mostly for 4th generation scanners. Multiple detector array CT scanners have an assembly of solid-state detector modules in series. With this type of scanner, slice thickness is determined by the width of grouped

detectors, not by collimation, and can be manipulated following image acquisition without needing to rescan.

Pixel, Voxel, and Matrix

Tomography is creation of an image that represents a single slice or section of anatomy. A complete CT scan consists of numerous, usually contiguous slices through the area of interest. Each slice has a defined thickness, and appears as 2-dimensional image of a three-dimensional structure. The basic 2D unit of the digital image visible on the computer monitor is the pixel, (short for picture elements). Each pixel represents a three-dimensional slice (volume) of tissue (or volume element) which is the voxel. Pixels of the CT image therefore display the average x-ray attenuation properties of the tissue within the corresponding voxel. Voxels are arranged in a series of rows and columns to make up the matrix. An increase in the number of pixels requires a reduction in pixel size, which results in improved spatial resolution.[331] Spatial resolution also improves with reduction of voxel size, i.e. reduction of tomographic slice thickness. Reduction of slice thickness minimizes partial volume averaging, but at the expense of decreased SNR. The matrix size depends on the CT scanner and is generally fixed. Larger matrices provide the best spatial resolution, but significantly increase image reconstruction time because the reconstruction algorithm must make more calculations.[332] With a 256 x 256 matrix, object margins are still distinct within a given image slice. As the matrix decreases to 128 x 128 the pixels become larger and the image becomes ‘coarse’ and at 64 x 64,

the image becomes non-diagnostic.[330] With a large matrix, selection of a small field of view (FOV) prior to image acquisition will improve spatial resolution because the same number of pixels (512 x 512) are assigned to a much smaller area. This is known as 'targeting'.[304,332] When the image is then magnified by the operator, the image quality remains good. With a smaller matrix, fewer pixels are assigned to a given FOV, and image magnification will accentuate the pixels and degrade image quality because of the loss of smooth transition between adjacent structures.[330]

Pitch

With helical scanners, pitch is a unitless parameter to describe couch advancement relative to slice thickness, and directly influences scan time, image quality, and radiation dose to the patient. For single detector array helical scanners, pitch is defined as the distance of couch advances (mm) per each 360º tube rotation ÷ slice thickness (mm).[330] A pitch of 1 implies that when averaged over the longitudinal axis of the body, the number of acquired helical CT images is comparable to the number acquired by contiguous axial scanning. A pitch <1 indicates overscanning of tissue sections and only increases patient dose without significant improvement in image quality. A pitch >1 indicates partial scanning with the advantage of faster scan time and reduced motion artifact. At a pitch of 1.5, 66% of data remains contiguous which is the minimum requirement to produce an adequate CT image with a 60° fan angle. A pitch of 1.5 has been determined as the upper limit without significant loss of information.

2.4.2 CT Data Processing

2.4.2.1 Pre-processing and Image Formation

The concept behind CT image formation is the internal structure of a complex structure can be reconstructed if the object is 'viewed' from many different angles. A ray is the measurement of a single, patient-attenuated x-ray beam by the CT detector. A projection is a series of rays emitted from the x-ray in a fan beam configuration that pass through the patient. Each ray within the projection has a different 'perspective' of the patient because it originates at a slightly different angle during tube rotation. As the tube rotates 360º around the patient within the gantry, x-rays penetrate the patient with variable attenuation along narrow paths generated by the beam. The emitted x-ray energy is absorbed by the CT detectors. The computer measures the difference in signal intensity between the reference detector (that measures unattenuated x-ray intensity), and the gantry detector (that measures attenutated x-ray intensity). The raw analog data can be displayed before reconstruction as a sinogram (analog signal graph); the vertical axis represents each projection angle and the horizontal axis corresponds to the data acquired in one instant along the length of the detector array.[330] The raw signal data then enter a pre-processing algorithm to determine the average linear attenuation coefficient (LAC) for a given voxel. A reconstruction algorithm (simple backprojection) is applied to the preprocessed sinogram to produce the CT image.[330] The 2D image is created by emulating the acquisition process in reverse by applying the LAC value from each ray from every projection onto the image matrix. With the compilation of data from a

large number of rays, areas of high and low attenuation reinforce each other to build up an image.[330] The simple backprojection produces a blurry image, so the sinogram is mathematically filtered before data is backprojected onto the image matrix. This involves application of mathematical filters or 'convolution kernels' in hundreds of thousands of simultaneous computations to enhance desired characteristics, resulting in an accurate CT representation of the object imaged. The kernel is a group of pixels with values that vary with the desired data modification which is applied along the rows and columns within the matrix. It involves integral calculus functions that multiply or divide the pixel value of the kernel with the pixel value of the matrix to produce a weighted average between neighboring pixels. This process shapes the data by selective reduction of high or low frequencies.[330] This serves to optimize desired signal to noise ratio (SNR) for the type of study performed.[330] Smoothing filters selectively minimize differences between adjacent pixels, thereby resulting in blurred edges. Sharp or edge enhancement filters accentuate differences between adjacent pixels to enhance edges.

2.4.2.2 Display Window and Level

The CT image is composed of a spectrum of black, white, and varying shades of gray, known as the gray scale or window. The shade of gray for a particular pixel is determined by the x-ray attenuation properties of the tissue within the associated voxel. Tissues of differing density, thickness, and/or atomic number will have different x-ray attenuation properties, or linear attenuation coefficient.[329,331] The

LAC reflects the amount of the primary x-ray beam that is absorbed or scattered by a volume of tissue. The shade of gray assigned to a particular pixel is determined by the average LAC value of the tissue within the voxel. The numerical LAC value of the tissue within the voxel is compared to that of water to generate a Hounsfield Unit, or CT number.[304] The gray scale is then distributed onto the image matrix. The final CT image results from a normalization of the HU of various tissues relative to the LAC value of water (0.195 for CT). With an electronic cursor, a region of interest (ROI) technique can be used to determine the HU value for any structure in the image. The HU spectrum is typically -1000 (darkest black) for air, -90 to -10 for fat, 0 (central gray) for water, +30 to +55 for brain and soft tissue, +50 to +80 for clotted blood, and +1000 to + 3000 (brightest white) for bone, iodinated contrast medium and metal.[304,330] The HU assigned to a given tissue varies between scanners and between manufacturers, and is highly dependent on calibration.[328]

CT images typically contain 12 bits of gray scale (4,096 shades) and computer display monitors are capable of displaying 8 bits (256 shades) of gray, but the human eye can only differentiate 20-30 shades of gray.[304,330,331] The CT data (12 bit) must be condensed to 8 bits in order to be accommodated by image display equipment, and this is achieved by windowing and leveling of the CT display. This is a post-processing method used by the operator to manipulate contrast and brightness without permanent loss of data. The operator can readily alter the window settings while scrutinizing the image in order to adequately assess and optimally display all tissue types. The display window maps the stored pixel HU into sets of discrete shades of

gray within the visual image. The window width is the range of HU values (i.e. shades of gray) above and below the central gray color (level) of the window. The selected window width determines the number of shades to be used, and HU values within the range will then be scaled to a spectrum of gray, whereas HU values lying outside the upper and lower window threshold will be truncated, or 'lost' from the display.[20] Hounsfield unit values beyond the upper threshold will appear white and those below the threshold will appear black. The HU value at the center of the window is the window level (central gray). The window width controls image contrast, and the window level controls image brightness, both of which are determined by the operator. Ideally, the window level should be set at the HU of the tissue of interest, and the window width should reflect the range of tissues on either side of the level that need to be discriminated.[304] Selection of the proper window level for the tissue of interest is crucial; otherwise the image will be too light or too dark and information will be lost.[318] With a narrow display window, tissues are represented by fewer shades of gray, which accentuates differences of HU values between adjacent tissues. Narrow widths are preferred for evaluation of soft tissue, where there is poor inherent contrast. Alternatively, with a wide window display, tissues are represented by many shades of gray. Because the local differences between tissues have been minimized, wide display windows provide a flat, low-contrast image.[20] Wide window displays are generally recommended for evaluating tissues that have a high degree of inherent contrast or for displaying a wide range of tissues (lung, nasal cavity, or bone).[20,304]

2.4.2.3 Multiplanar Image Reconstruction

Another significant advantage of CT is the ability to depict the plane of interest without superimposition of other structures. Certain structures may be better displayed planes other than transverse, and the extent of lesions can be ascertained if viewed from multiple planes. Reformatted images are created with existing data obtained from the transverse plane to reproduce images in alternative planes. Image reformatting requires special multiplanar reconstruction (MPR) software that allows the operator to display an image in the sagittal or dorsal (or coronal) plane. The advantage of reformatted images is the improved perception of anatomic relationships or lesions that may not be best displayed in the transverse plane. However, spatial resolution is somewhat compromised with reformatted images.[330,333] Spatial resolution is best in the *x*- and *y*- axes, but resolution is limited in the *z*-, or longitudinal axis which is determined by slice thickness.[330,333] Multiplanar reconstruction (MPR) combines the data from the *x, y*, and *z* dimensions, which creates some degree of mismatch in spatial sampling.[333] To compensate for missing or mismatched data, MPR software interpolation is required in order to maintain proper planar ratios. Interpolation is often used for helical scanning methods to 'fill in the gaps' inherent with helical image acquisition. The interpolated data is essentially a weighted average of data acquired from slices on each side of the reconstruction plane, which accounts for the slightly reduced spatial resolution in the MPR plane.[330] Spatial resolution in the MPR plane can be improved by using a smaller slice thickness and small interspace interval, or overlapping slices during

acquisition of the transverse images.[333] Three-dimensional reconstruction may be particularly helpful to provide a panoramic view of a bone lesion. This requires operator-dependent identification of specific landmarks on sequential 2D images (segmentation) in order to reconstruct a 3D image. The simplest segmentation algorithms allow the operator to select a threshold HU, and only those values above the threshold will be displayed. It is commonly used to eliminate overlying soft tissues to reveal only bony structures, and provide a global view of regional anatomy. Use of small slice thickness and interspace interval provide the most satisfactory 3D reconstructed images.[333]

2.4.3 CT Image Quality

2.4.3.1 Image Noise and Resolution

Apart from inherent limitations of the imaging system, image quality is determined by the ratio of the amount of useful information (signal) versus the amount of random or useless information (noise, or quantum mottle) received by the detectors. The signal-to-noise ratio (SNR) is fundamentally tied to contrast and spatial resolution, and should be considered when selecting CT study parameters. The SNR reflects the number of detected signals (x-ray photons) used per pixel within the digital image, which is ultimately dependent on pixel dimension, slice thickness, and radiation dose (detected x-rays).[330] A large proportion of noise in CT images is quantum related. Results of phantom studies have demonstrated that image noise is

decreased (increased SNR) by increasing the kVp and mA, and is most noticeable with larger patients.[334]

The resolution of an imaging system is the ability of that system to faithfully reproduce and display information about the object being imaged. For CT, spatial resolution and contrast resolution play important roles in image quality, and are inversely proportional to each other.[328,330] Spatial resolution is the ability to discriminate closely opposed objects as being separate, and affects sharpness and detail of an image. This is dependent on the geometry of the data collecting system (detectors) and the frequency of data sampling, which in turn is dependent on the reconstruction algorithm, matrix size, and FOV.[334] Contrast resolution is the ability to differentiate subtle differences in contrast (i.e. x-ray attenuation properties) against a homogeneous background, which reflects the nature of its composition.[304,332] Computed tomography has superior contrast resolution to any other x-ray imaging modality. Conventional radiography requires a 5-10% difference in tissue x-ray attenuation in order to be detected, whereas CT only requires a difference of 0.25 to 0.5%.[328,330] The improved contrast resolution with CT is due to reduction of scatter by tight collimation, removal of anatomic superimposition, wide dynamic range of detector array, reconstruction algorithms, and post-processing image modification.[328]

2.4.3.2 Reconstruction Algorithms

The resolving capabilities for CT vary with individual scanner quality and software. Reconstruction algorithms are applied to data to improve the spatial

resolution for small or closely spaced objects. Typically, there are high or low spatial frequency algorithms, depending on the frequency of information needed to be reproduced in the image. Low spatial frequency algorithms are also known as 'soft tissue' or 'standard' algorithms. These produce more smoothing to the image and result in reduced visible noise and improved contrast resolution, but at the expense of reduced spatial resolution.[334] High spatial frequency algorithms are also known as 'bone', 'edge enhancement', or 'sharp' algorithms. Bone algorithms have much less smoothing and sharpen the resolution of small structures. This algorithm enhances any existing background noise and accentuates aliasing, therefore increased spatial resolution occurs at the expense of increased image noise.[334]

2.4.3.3 Field of View

The image field of view (FOV) is the proportion of the sampled gantry diameter from which the image will be calculated and displayed.[304,330] Pixel size is inversely proportional to matrix size, and spatial resolution is inversely proportional to FOV. The FOV also determines the pixel size; with a small FOV, the matrix is assigned to a smaller area and results in very small pixel dimensions and results in better spatial resolution. Therefore narrowing the FOV to closely approximate the region of interest (targeting) will improve spatial resolution.[304,334] Spatial resolution does not improve with magnification, where both image and pixel size are increased.[334] A large FOV with a fixed matrix size results in larger pixel dimension and reduced spatial resolution. However, larger pixels (and voxels) will contain more detected

signal than smaller ones which results in improved SNR (i.e. contrast resolution). Therefore, as FOV increases, contrast resolution increases (high SNR), but spatial resolution decreases. As FOV decreases, contrast resolution decreases (low SNR), but spatial resolution increases.[330]

2.4.3.4 Slice Thickness

In 3rd and 4th generation CT scanners, slice thickness is determined by the collimator. The slice thickness determines the volume of the voxel. Slice thickness and SNR are also inversely proportional and will affect contrast and spatial resolution. With a decrease in slice thickness, there is a decrease in SNR and contrast resolution, but an increase in spatial resolution. Therefore, small slice thickness provides better spatial detail, but result in a 'noisier' image, particularly in larger patients.[328] To combat this, a higher mA can be used to improve SNR for thin slices. However, if contiguous thin slices are required, a larger number of total slices are needed to completely include the region of interest. This results in increased scan time, tube loading, and patient dose. Alternatively, an increase in slice thickness (larger voxel size) is associated with increased SNR and contrast resolution, but at the expense of decreased spatial resolution. Additional disadvantages of thicker slices include the possibility of 'missing' lesions that are smaller than the slice thickness, and partial volume averaging. Partial volume averaging (PVA) is a phenomenon that occurs when tissues with different attenuation properties are contained (and averaged) within the same slice plane, and alters the actual HU of the tissue. The probability of

PVA is decreased when thinner slices are used, and small lesions are more likely to be detected.

2.4.4 CT Artifacts and Imaging Pitfalls

An image artifact can be defined as any discrepancy between the reconstructed values in the image and the true attenuation coefficient of the object.[328] Artifacts are caused by erroneous measurement of x-rays received by the detectors and result in degradation of image quality.[331,332] The complex nature of CT imaging makes it susceptible to image artifacts. Artifacts arise because of geometric inconsistencies in received data that manifest as spurious information in the digital image. CT artifacts differ in their etiology and degree of image degradation, but most commonly appear as bright or dark streaks across the image.[331,332] They are caused by inconsistencies in x-ray or projection measurements and include: motion, aliasing, beam hardening, edge gradient or high density, and out of FOV artifacts. Artifacts may also arise from faulty detectors. It is important to recognize the common sources of artifacts so images are not misinterpreted.

2.4.4.1 Partial Volume Averaging

Each image is a 2D representation of a 3D slice of tissue, created by averaging the attenuation properties for the volume of that slice.[318,330,331] When objects of widely different attenuation values (LAC) occupy the same voxel, the calculated HU value is

proportional to the average LAC of contributing tissues, therefore the final HU value is not representative of either tissue. Partial volume averaging is present in all images, but becomes more pronounced as slice thickness increases. This is most pronounced with rounded structures that lie nearly parallel to the scan plane, resulting in reduced margin 'crispness' or blurriness at the margins. It can be corrected by using thinner slices, but mA must be increased to improve SNR. Partial volume averaging is commonly recognized and infrequently leads to misdiagnosis because the operator can 'scroll' through adjacent images to confirm its presence. However, this artifact can lead to misdiagnoses when adjacent structures are unexpectedly present.[330]

2.4.4.2 Motion Artifact

Errors occur in data acquisition and image reconstruction occurs when structures change position between slices during the scan. The reconstruction algorithm cannot compensate for data inconsistencies. Small motions (cardiac contractions or intestinal peristalsis) cause blurring of the image, whereas larger movements (respiration or voluntary motion) may produce prominent streaks or image duplication ('ghosting').[330] Highly attenuating objects will create prominent parallel light streaks in the direction of movement. Correction of motion artifact depends on its cause. Most veterinary patients are under general anesthesia as part of CT scan protocol which minimizes voluntary motion. However, physiological motion,

particularly respiratory movement, is more difficult to control, so using breath-hold techniques with rapid acquisition times are recommended.

2.4.4.3 Aliasing

Aliasing artifact results from insufficient sampling of x-ray projection data, and appear as fine, curved black streaks that emanate from higher frequency objects, such as a bone-air interface.[331] Objects with sharp edges require a higher sampling to depict crisp margins, and data sampling must be at least twice the spatial frequency of the object scanned. Modern CT scanners that acquire more than 1000 samples per projection have minimal aliasing. For helical CT scans, aliasing can be minimized by using a pitch less than 1.5.

2.4.4.4 Beam Hardening

Beam hardening occurs when the polyenergetic spectrum of the x-ray beam is transmitted through dense or very thick tissue and low-energy photons are selectively attenutated by the patient to a greater extent than high-energy photons. As the x-ray beam penetrates the patient, the spectrum of energy becomes skewed toward the higher energy range and the average energy of the beam progressively increases. The CT reconstruction algorithm interprets the increase in photon intensity is due to decreased tissue attenuation, therefore assigns that area a low HU. Intense beam hardening artifacts appear as blurry dark streaks emanating from interfaces of high

attenuation and low attenuation. This occurs most often with bone, particularly the caudal fossa of the skull, because of the high bone attenuation and irregular contours of petrous temporal bones. Most CT scanners have beam-hardening correction algorithms that help minimize the artifact, but do not eliminate it completely.[330]

2.4.4.5 Edge Gradient / High Density

Edge gradient artifact is the result of sampling the x-ray attenuation profile from different perspectives and projections around an irregularly shaped object with high density. This creates inconsistencies in the sampled attenuation information and causes variation in calculated HU values during image reconstruction. Edge gradient or high density artifacts appear as light streaks that emanate or radiate from high density objects that have sharp or abrupt margins and large attenuation differences with surrounding tissue.[331] This artifact is difficult to eliminate, but can be minimized with high sampling rates.

2.4.4.6 Field of View

The scan FOV is the field size within the gantry aperture from which attenuation data is collected for image reconstruction. Objects lying outside the scan FOV, such as extremities, ECG leads, IV tubing, or other anesthetic monitoring devices can inadvertently attenuate the x-ray beam outside the scan FOV. This creates erroneous attenuation data at the reference detector because the space beyond the scan FOV is

assumed to have a LAC equal to air.[331] This artifact results in parallel (corduroy-like) light streaks across the entire image. Highly attenuating structures or those located asymmetrically about the patient produce more pronounced artifacts. This artifact is easy to correct by correct patient positioning and removing or securing extraneous monitoring devices.

2.5 LESION DETECTION AND OBSERVER PERFORMANCE

The ability to detect a lesion by CT is dependent on the physical limitations of the imaging system (quantum mottle, modulation transfer function, and x-ray spectrum), the physical characteristics of the lesion, and psychophysical characteristics of human vision.[335] High-contrast structures are limited by image resolution, whereas low-contrast structures are limited by image noise.[336] The visible characteristics of a lesion is dependent on the attenuation gradient between the lesion and background (i.e. contrast). Small or low contrast lesions, however, must also be differentiated from background noise that exists in the normal surrounding tissue. Lesion detectability is therefore related to the inherent contrast of the lesion and the amount of background noise (SNR).[18] Image noise is partly determined by the applied reconstruction algorithm.[20,21] Manipulation of the image data via the reconstruction algorithm will in turn affect the lesion SNR, and such data manipulation has been shown to predict changes in observer performance.[18,21,335] For this reason, wide display windows (which compress HU variation, and decrease image noise) have been reported to decrease observer performance in lesion detection.[18,23,335]

The detectability index is a measure of SNR as detected by an observer.[336] Variations in window width should not have an effect with an 'ideal' observer because the image signal and noise are scaled at the same rate.[337] However, it has been shown that observers will introduce 'noise' into the system that is affected by spatial frequency of the object and other 'human' variables. Warren defined this 'observer noise' as the physiological or psychological effects of decision making, and found that it contributes to an overall reduction of SNR.[336] In this study, marked differences were found between observers for individual measurement points, although overall detectability trends were similar. Warren also found that noise detection varies with viewing distance from the image.[336,338] At short distances (<1 m) image noise is detected more than lesion signal, resulting in low SNR, whereas lesion signal is detected more efficiently than image noise at larger viewing distance (>1 m). However, at large viewing distance (3 m) lesion detectability is markedly reduced as a result of observer noise due to exceeding the spatial resolution limits of human vision.[336,338] Warren found the optimum reading distance to be approximately 2 m, which is unpractical in a clinical setting. An alternative to this was to reduce CT image size to 9 image frames per film sheet. The distance at which maximum detectability occurs depends on image noise, which is determined by window width but is independent of window level.[338] The level of observer noise is insignificant in images with a narrow window, whereas it becomes significant for wide display window. At narrow windows, original image noise is high and dominates observer

noise until viewing distance is increased. Conversely, for wide windows with low image noise, observer noise is dominant at short viewing distances.[336,338]

Many human studies have demonstrated the effects of CT display parameters and reconstruction algorithms on image quality and sensitivity of lesion detection *in vitro*.[20,21,23,334,335] Most in vivo studies focus on the effect of algorithms in the evaluation of parenchymal lung disease in which lesions in question (hyperattenuating) are projected against a fairly uniform hypoattenuating background of aerated lung.[334,339-341] Detectability of *in vitro* or *in vivo* osseous lesions has not been tested, and few studies have studied the effect of image display in musculoskeletal CT exams. In one of those few studies, Fishman *et al* investigated the effect of edge-enhancement algorithms on the appearance of multiplanar reformatted images in human skeletal trauma.[342] Images were obtained in transverse plane with small slice thickness and interscan interval with a standard (smooth) algorithm and edge-enhancement (sharp) algorithm then reformatted into coronal and sagittal images. When compared to smoothed images, the edge-enhanced images were deemed of superior quality for assessment of fractures of the acetabulum and tarsus regardless of planar reconstruction.

Wagner's theoretical analysis predicts the SNR of a lesion would be most affected by the reconstruction filter for small lesions (2-3 pixels), but would have no effect for larger lesions.[18,343] Results of a phantom study suggest smooth reconstruction filters may enhance lesion detection because of increased lesion SNR, however, this may only be true for small, high-contrast lesions.[18] Judy *et al* tested four reconstruction

algorithms of varying degrees of smoothness and sharpness, and six different window widths on image noise and detection of small, high-contrast phantom lesions. Results of this study showed that smoother filters increased lesion SNR which resulted in increased lesion detectability.[18,23] Unfortunately, all of these studies employed biased observers; some of the researchers who constructed the phantoms also served as the observers, and knew the 'lesions' were present within each image. Nonetheless, for smoother filters, detection of small, high-contrast lesions was found to be relatively insensitive to manipulations of CT window width between 100 to 1000 HU, but observer performance falls at the widest window widths (2800) where noise is minimal.[20,23] For larger, low-contrast lesions, it has been suggested that visualization may be more dependent on lesion contrast than SNR.[18]

Wagner's theory has been refuted by other studies that found the detectability of lesions was strongly influenced by window width.[336,338,344] According to Twible *et al*, the magnitude of the effect of a wide window is greater for larger, low-contrast lesions than for smaller, high-contrast lesions.[335] That study found that manipulation of the display window does not affect the data contained within the image based on SNR calculations for a 'lesion-matched' filter, i.e. the display window has no effect on the value of lesion SNR. Because signal and noise are equally scaled during window manipulation, the change in display should not affect the physical SNR for a lesion.[335] Results of contrast threshold experiments from this study demonstrated that for small, high-contrast lesions, detectability was dependent on the resolution of the imaging system; but for larger, low-contrast lesions, detectability is dependent on the

inherent contrast relative to normal background tissue. Larger lesions need a relatively greater increase in contrast to be detected with a wide display window.[335] Window width determines contrast threshold limits, and the effect of threshold limits on lesion detection varies with lesion size. However lesion detectability decreases rapidly with increasing window width regardless of lesion size.[335] The authors concluded that the effects of window on observer performance was attributed to psychophysical properties of the human visual system, or 'observer noise'.[335] It is this source of variability in detection decision-making that compromises accurate measurement of observer performance. Cross-correlation models of observer's decision variable have been found to be linearly related to the value of SNR regardless of image size, contrast, and overall image noise levels. The cross-correlation model was useful to predict observers' ability for lesion detection.[18,20]

There are varying opinions as to the effect of image contrast on lesion detectability. Several investigatiors have reported that a wide CT display window negatively affects the detectability of both small and large lesions within CT images.[23,336,338] One *in vitro* study investigated the effects of contrast and display window on observer performance in the detection and size discrimination between circular disks superimposed on CT images of water phantoms. Seltzer *et al* found observers' ability to detect lesions improved with increasing CT contrast (90-1440 HU) but dramatically worsened at the widest display window (2880 HU).[23] However, observers' ability to discriminate between small changes in object size was unaffected by window width.[23] Window width was found not to affect discrimination between

objects with features that are easily visible (e.g. small vs. medium disk size). These results suggest that the effect of altering CT display window may depend on the spatial frequency of the object needing to be discriminated.[23,338]

According to Hanson, perceptual tasks are divided into lower order and higher order tasks.[22] Feature detection and brightness discrimination are lower order tasks that use low spatial frequency information to determine signal intensity. Size discrimination is a higher order task and requires broad range of spatial frequency to precisely locate margins of structures. He concluded that changing the CT window had a greater effect on lesion detection than lesion margin discrimination.[22] Another in vitro study investigated the effects of a narrow display window and smooth and sharp reconstruction algorithms on observer performance for detection of dark (hypoattenuating) lesions.[20] Observer performance was calculated using a ROC curve, with the premise that the lesion's detectability in the displayed image would depend on noise variations within the display window.[20] The area below the ROC curve provided a non-parametric measurement of observer accuracy. In that study, images of circular lesions within phantoms were reconstructed using both high and low frequency reconstruction algorithms, displayed with a narrow window (100 HU) with varying window level (95 to 230 HU). Results of that study showed the window level affected lesion detection most with smooth CE reconstructions at the very high and very low window level settings. For smooth CT images, there was an abrupt difference in detection performance for a very narrow range of levels because the majority of critical lesion and/or non-lesion pixels were at threshold. For sharp CT

images, there was a more gradual effect on detection performance as the fraction of pixels critical for lesion detection reached threshold at the window level boundaries were reached gradually.[20]

Radiologists' perception and interpretation of images is influenced by the spatial frequency of the data and individual interpretation experience.[345] Comparative studies between radiologists of varying levels of experience have shown that experience seems to attune the visual system to spatial frequency information that contributes to better lesion detection and decision making.[345] However, it remains incompletely understood as to what specifically in the image (region of the lesion) that attracts visual attention. It is also not completely understood how radiologists extract pertinent information from the image and convert it into the identification of a normal or abnormal feature.[345]

CHAPTER 3

THE EFFECT OF CT DISPLAY WINDOW AND IMAGE PLANE ON DIAGNOSTIC CERTAINTY FOR CHARACTERISTICS OF CANINE ELBOW DYSPLASIA

3.1 INTRODUCTION

Elbow dysplasia is the most common cause of forelimb osteoarthritis in popular large and giant-breed dogs. The etiology of CED is multifactorial and is believed to shares a similar pathogenesis to OCD of the human elbow.[143,156] Canine elbow dysplasia (CED) also exhibits polygenic inheritance with a reported incidence of up to 17-25% in the Labrador Retriever,[104,115,160,161] 30-50% in the Rottweiler and Newfoundland,[102,103,108] and 36-72% in Bernese Mountain Dogs.[115,162,163] Canine elbow dysplasia (CED) is typified by four primary lesions: ununited anconeal process (UAP), fragmented medial coronoid process (FCP), osteochondrosis and/or osteochondritis dissecans (OCD), and joint incongruity.[3,4,346] Radiographic detection of lesions within the elbow, particularly of the medial coronoid process, is greatly limited by the complex joint anatomy,[15,16] and sensitivity for diagnosing FCP is reported to be as low as 9 percent.[235] There is no correlation between clinical signs and the severity of surgical or radiographic findings, and the absence of radiographic abnormalities does not rule out elbow disease.[111,113,117,200]

Computed tomography has become one of the preferred diagnostic modalities for investigating FCP because it allows detailed evaluation of the medial coronoid

process (MCP) and articular surfaces without superimposition of adjacent bony structures.[221,347] Multiplanar image reformatting (MPR) is one of the primary advantages of CT which allows the reader to evaluate anatomic relationships in alternative planes.[321,332] Sagittal, dorsal, or oblique planes may reveal the extent of complex lesions that may be underestimated in transverse images. Computed tomography may also provide information about changes to subchondral bone that may not be arthroscopically evident.[164,217,221] Additionally, CT is helpful for identifying additional lesions that may significantly alter surgical planning, such as incomplete ossification of the humeral condyle and joint incongruity.[98,100,112,172] Computed tomography has recently been used to assess joint congruity in normal and dysplastic elbows.[14,187,188,320,321] Even though CT may accurately depict humeroulnar incongruity, the clinical significance of this finding remains uncertain as some degree of incongruity has been demonstrated in normal elbows in dogs[24,25,32,180] and humans.[90,91]

The CT characteristics attributed to elbow dysplasia have been described.[14,15] Abnormalities involving the MCP include abnormal shape, subchondral sclerosis, hypoattenuating defects, and subchondral fissures (*in situ* fragment) in addition to discrete fragmentation. Focal hypoattenuating subchondral defects of the trochlea humeri with or without surrounding sclerosis on dorsal plane images are believed to represent primary OCD or 'kissing lesions'.[14] Hypoattenuating defects and irregular contour of the radial incisure have also been found in transverse images of dogs with elbow disease,[14,101] and may represent radioulnar synovitis.[196] Humeroradial and

humeroulnar incongruity has been documented on sagittal and dorsal reformatted images, however none of the previous studies used these planes to evaluate abnormalities of the MCP or trochlea humeri.

The diagnostic sensitivity for abnormalities in the elbow may be affected by variations in CT image quality. CT image quality is inherently related to the signal to noise ratio (SNR) and contrast to noise ratio (CNR).[348] Both ratios are dependent on: slice thickness, display window width and level, matrix size, FOV, mA and kVp, reconstruction algorithm (convolution filter), and pitch. Other variables that affect image quality are imaging artifacts, patient positioning, and precision of planar reconstruction.[318,328,330] Lesion detectability is a factor of the inherent contrast of the lesion and level of background noise (SNR).[18,21,349] Detectability of high-contrast structures is limited by spatial resolution, whereas detectability of low-contrast structures is limited by image noise.[336,348] Studies have found that observers' ability to detect low-contrast lesions improves with increasing image contrast (narrower window) but worsens with wide window settings.[18,19,336,348] The magnitude of this effect (diminished detectability) of a wide window is greater for larger, low-contrast lesions than for smaller, high-contrast lesions.[335]

Understanding how CT image display influences diagnostic certainty for characteristics of elbow dysplasia is important because this information will help establish standardized image display guidelines. Currently, there are no published guidelines for optimal elbow CT image display. The authors are also unaware of any study in the veterinary literature that investigates the effects of CT window display or

planar reconstruction on observer performance for lesion detection. Based on the authors' experience and review of the literature, we hypothesize that diagnostic certainty for the presence or absence of an elbow lesion will be affected by the CT display window and/or reformatted image plane.

3.2 METHODS

3.2.1 Patient Selection

Medical records at Texas A&M University Veterinary Medical Teaching Hospital (TAMU) were reviewed for dogs with a diagnosis of elbow dysplasia from 1999 to 2003. Inclusion criteria for this study were: large breed dogs (weight >20 kg) with clinical history of lameness isolated to at least one elbow joint, elicitation of pain in the elbow during lameness examination, original CT image data of the elbows available on archival storage media, and recorded arthroscopic or surgical findings from at least one elbow joint. Seventy-two dogs were found to satisfy the clinical criteria, however 23 dogs were eliminated because of insufficient surgical records. From this group of dogs, 50 surgically explored elbows from 49 dogs were randomly selected for the study. For dogs with bilateral disease, the right or left limb was selected at random to be evaluated.

Five clinically sound, large breed dogs were selected from a purpose bred colony of dogs at TAMU to serve as negative controls for the experiment. These dogs belonged to a colony with sex-linked protein losing nephropathy, and the average

weight, conformation, and size of the dogs were comparable to the dysplastic sample population. Selected control dogs were examined by a board-certified veterinary surgeon (SCK) and determined to be clinically free of elbow disease. CT studies of the elbows were considered to be normal by the author.

3.2.2 Computed Tomography

Following orthopedic examination, the elbows of clinically normal dogs were scanned using a similar protocol as that used for elbow dysplasia dogs. Dogs were premedicated with intramuscular acepromazine[a] (0.025 mg/kg), glycopyrrolate[b] (0.011 mg/kg), and hydromorphone[c] (0.1 mg/kg). Anesthesia was induced with propofol[d] (4-6 mg/kg IV) and maintained with isoflurane[e] (2-2.5%) and oxygen. Dogs were positioned in sternal recumbency within a plexiglass and foam trough, with forelimbs secured parallel to each other in forward extension. Images were obtained using a 3rd generation CT scanner[f] with 25 cm FOV, 130 mA and 120 kV, with a bone algorithm. Transverse images were obtained as contiguous 1.0 mm slices from the point of the olecranon to 2 cm distal to the radial head. Sagittal plane reformatted images were created as 1.5 mm contiguous slices and oriented parallel to the long axis of the medial coronoid process (MCP) and between the epicondyles to include lateral and medial coronoid processes of the ulna, trochlear notch, and entire articular surfaces of the radial head and humeral condyle. Dorsal plane reformatted 1.5 mm contiguous slices were also created perpendicular to the long axis of the MCP

to include the entire articular surface of the humeral condyle and trochlear notch of the ulna.

Original CT image data from the 50 dysplastic elbows were reloaded onto the CT workstation at TAMU from archival magnetic optical discs.[g] Computed tomographic images of normal and dysplastic elbows were filmed using 12 frames per sheet of transparent laser printed film. Each elbow was filmed in transverse, and reformatted sagittal and dorsal planes. Transverse images were acquired perpendicular to the long axis of the ulna; sagittal images were acquired in a plane parallel to the long axis of the MCP; dorsal plane images were acquired perpendicular to the long axis of the MCP. For each plane, images were filmed in three different display window widths: 1500, 2500, and 3500 HU to serve as high contrast, intermediate contrast, and low contrast images. The 1500 and 2500 HU windowed images were set at a level of 300, and the 3500 HU images set at a level of 500. Selected window width and levels were chosen based on those reported in recent literature.[14,17,188] A total of nine film sets were generated for each elbow, i.e. 540 films for all 60 elbows. Film sets were composed of images from one elbow filmed in one plane and one window. Each film set was assigned a random identification number to prevent patient recognition by observers, then film sets were randomized to window and plane. The film sets were divided into two batches; each batch consisting of one-half of all studies. Film batches were sent to two readers, with batches exchanged after readers completed the first.

3.2.3 CT Evaluation and Visual Analog Scale

Two board-certified veterinary radiologists with similar CT reading expertise independently evaluated all film sets. Evaluators were unaware of the clinical and surgical findings for each dog. Evaluators were asked to evaluate each film set for seven characteristics reported to be possible indicators of elbow dysplasia.[14] These included: 1) hypoattenuating subchondral MCP defects, 2) MCP fissure (*in situ* fragment), 3) discrete MCP fragment, 4) irregular margination and/or hypoattenuating defects of the radial incisure of the ulna, 5) subchondral sclerosis of the trochlea humeri, 6) hypoattenuating subchondral defect, erosion, or flattening of the trochlea humeri (representing a 'kissing lesion' or OC/OCD-like lesion), and 7) incongruity of the humeroradial, humeroulnar, and/or radioulnar joints. Visual analog scales (VAS) were employed to record the level of observer diagnostic certainty for the presence or absence of each CT characteristic.[350] Visual analog scales consisted of 15 cm horizontal lines with vertical bars at each extremity with 0.5 cm line extension beyond the vertical bar (Fig. 3.1). The left extremity of the scale was labeled 'definitely absent' (0 cm), the right extremity labeled 'definitely present' (15 cm), and the center was labeled 'unable to determine' (7.5 cm). Evaluators were asked to place a vertical mark along the scale line that reflected their level of certainty for the presence of each CT characteristic for each film. The 'unable to determine' category was to be used for characteristics that were considered equivocal due to inappropriate windowing, plane, filming artifacts, or other technical factors. The VAS scores were created by measuring the distance of the observers' mark from 0 (left extremity) in

centimeters to the nearest millimeter using a ruler. Additional space on the VAS data sheets was provided to allow for observer comments. Observers were provided with CT images of normal elbows in transverse, sagittal, and dorsal planes, as well as representative examples of the seven CT characteristics for reference use during the evaluation period. Voluntary comments from evaluators regarding specific CT characteristics were noted. Surgical reports were reviewed, and notable abnormalities, particularly those of the medial coronoid process, articular cartilage, joint congruity, and synovium were also recorded.

3.2.4 Definition of CT Characteristics

For purposes of this study, CT characteristics were defined as the following: *MCP hypoattenuating subchondral defects*- focal, irregular hypoattenuating areas (presumed osteomalacia) within subchondral bone of MCP that may be individual or coalescing, but do not form a cleavage line or fragment (Fig. 3.2, A); MCP may be abnormally shaped, but is still intact; *MCP fissure / in situ fragment*- a linear or curvilinear hypoattenuating structure that likely indicates a subchondral fissure or a non-displaced or partially attached osteochondral fragment (Fig. 3.2, B); fragments may remain partially attached by cartilage and usually seen along the lateral margin or apex of the MCP; *Discrete MCP fragment (FCP)*- a clearly identifiable mineralized fragment that is separate from the MCP (Fig. 3.2, C); often variable in size, number, margination, opacity, and degree of displacement, and a fracture bed may be visible; *Radial incisure irregularity*- loss of normal smooth cortical margin,

often see irregular contour and/or focal indentations; may also have focal, hypoattenuating subchondral cyst-like lesions that may be well- or poorly-circumscribed (Fig. 3.3); *Subchondral sclerosis of the trochlea humeri*- increased attenuation of subchondral bone of the humeral condyle opposing the MCP that may vary in extent and depth (Fig. 3.4, B); *Subchondral flattening or hypoattenuating defects of the trochlea humeri (i.e. kissing lesion or OCD)*- focal concave defect or flattening of the trochlea; usually associated with focal hypoattenuating lesion with or without a surrounding zone of sclerosis (Fig. 3.4, D) and may also be associated with FCP or calcified cartilage flap; *Joint incongruity*- normal congruity should have parallelism between articular surfaces of the humerus, radius, and ulna; incongruity is recognized as widening or loss of parallelism between joint surfaces, with/or without step defects between the proximal radius and ulna (Fig. 3.5).

3.2.5 Statistical Analysis

Statistical analyses were performed using SAS proc mixed software program.[h] Least squares means (LSM) was used to estimate combined observer certainty for a given CT characteristic, and the differences of the LSM were used to detect whether combined observer certainty differed between certainty levels of status, window, or plane. VAS scores obtained from the two observers were transformed using an arcsin square root tranformation[i] to represent the degree of diagnostic certainty for the presence or absence of a given CT characteristic on a 15 point scale, where 0 represented complete uncertainty and 15 represented absolute certainty for presence

or absence of a given CT characteristic. The effects of elbow status (normal or dysplastic), display window, and image plane on diagnostic certainty were analyzed using split-plot analysis of variance, starting from a full model. Single-, 2- and 3-way interactions of these effects were also tested. Those interaction effects that were significant at $\geq$ 20% level were kept in the reduced model. The level of statistical significance was set at 0.05 for all other tests.

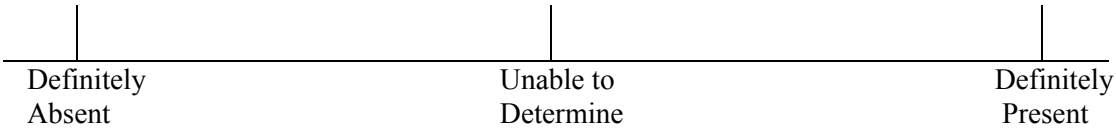

Figure 3.1. Visual analog scale used by radiologists to assess individual CT characteristics. 'Definitely absent' = 0 cm, 'unable to determine' = 7.5 cm, and 'definitely present' = 15 cm. The VAS scores were created by measuring the distance of the observers' mark from 0 in centimeters to the nearest millimeter using a ruler.

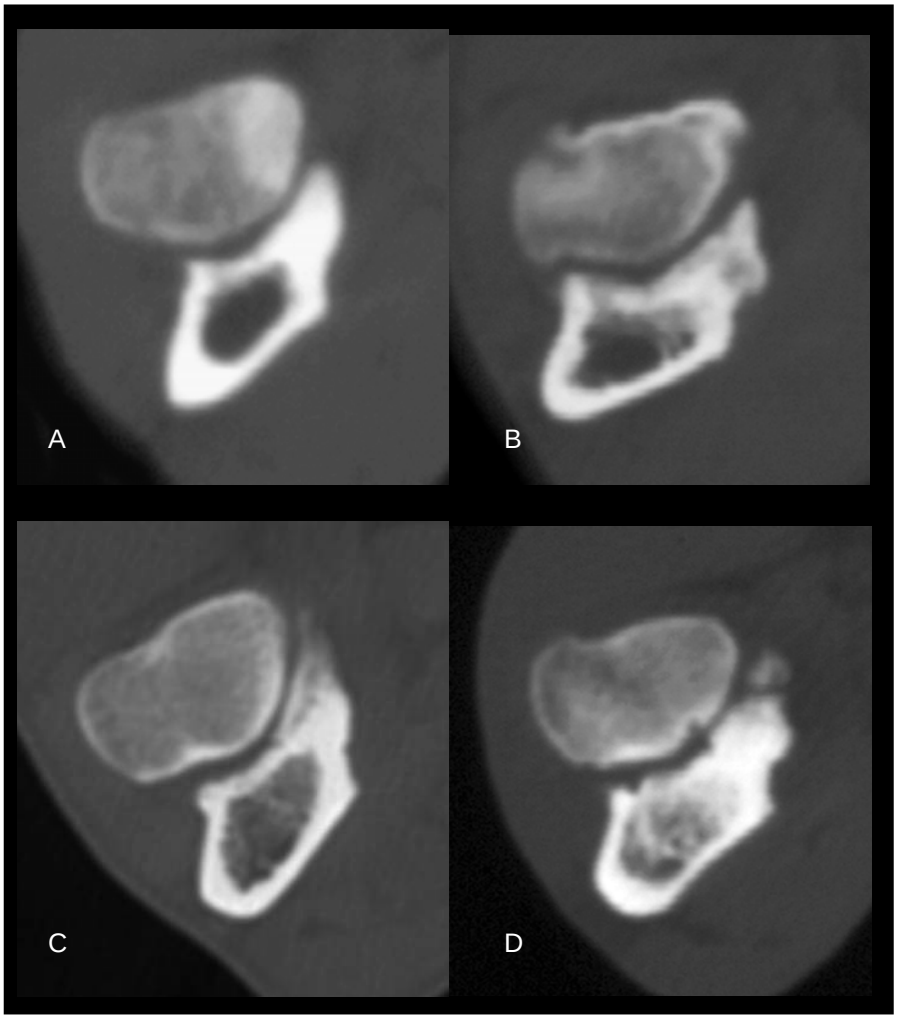

Figure 3.2 Transverse CT images of a normal elbow (A), and elbows with a hypoattenuating subchondral defect (B), in situ fissure (C), and discrete fragment (D) of the MCP.

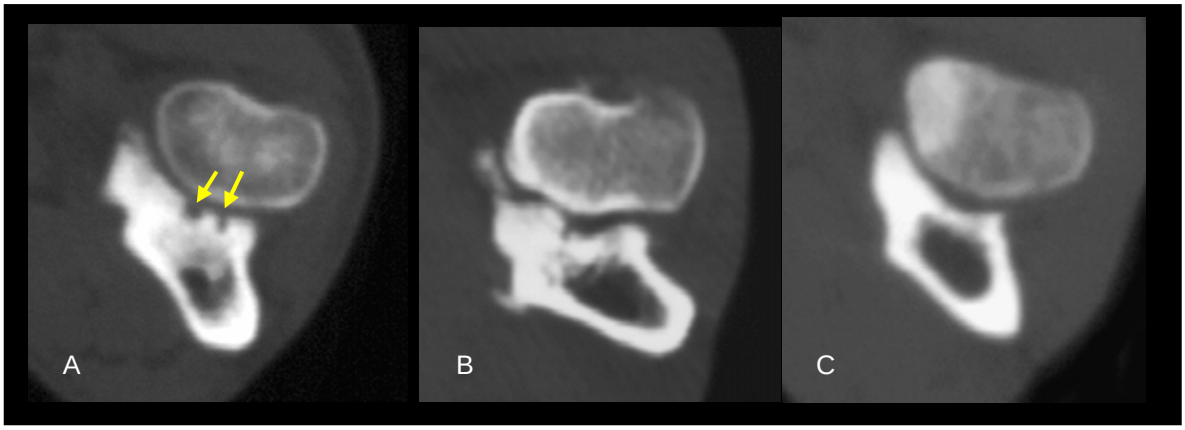

Figure 3.3 Transverse CT images of the elbow illustrating hypoattenuating subchondral defects (A, arrows), and marked irregularity of the radial incisure (B) compared to the appearance of a normal radial incisure (C).

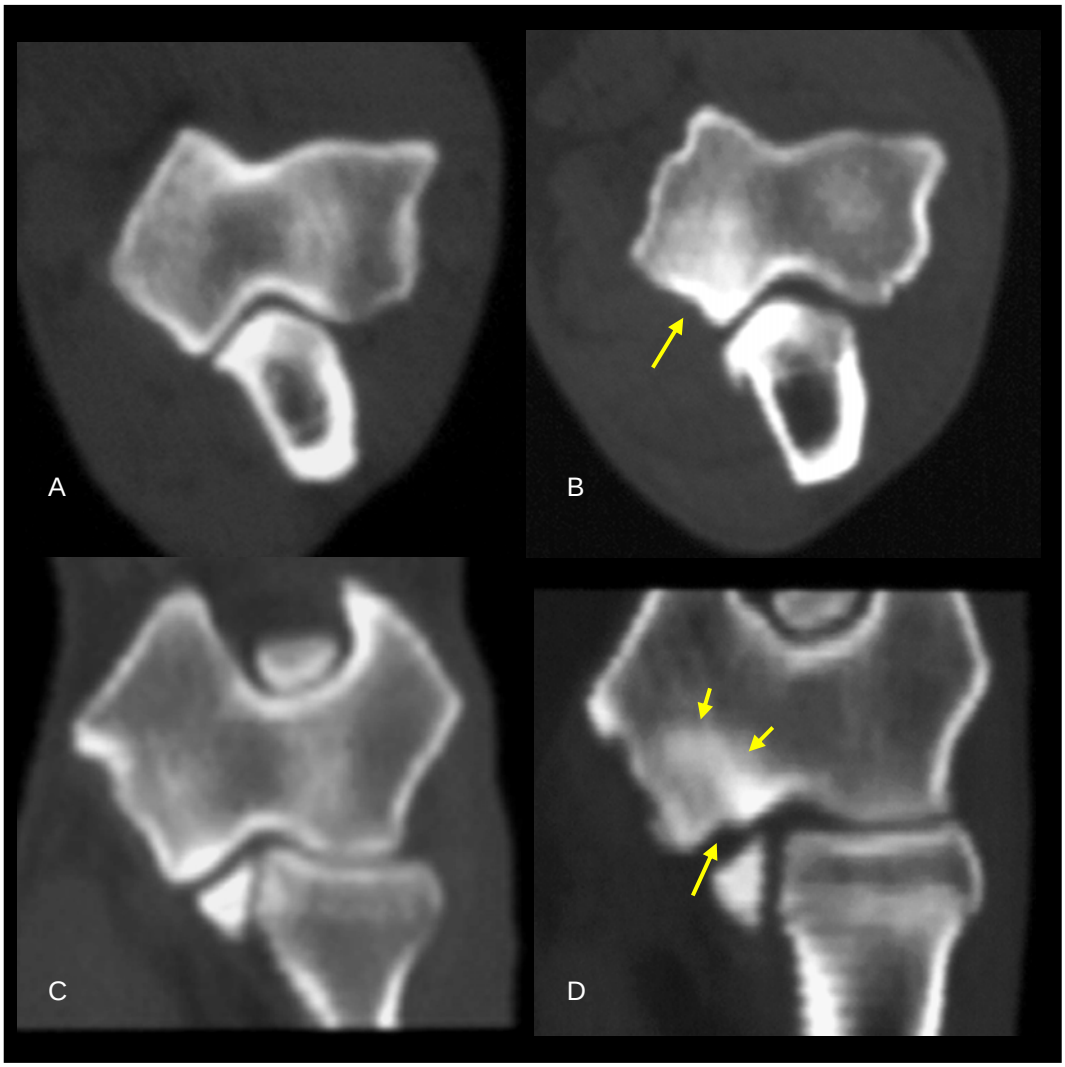

Figure 3.4 Transverse (A and B) and dorsal plane (C and D) CT images of the elbow at the level of the trochlea humeri. Note the appearance of subchondral sclerosis (B, arrow) compared to the normal elbow (A) and a hypoattenuating subchondral defect (D) with surrounding sclerosis (short arrows) and articular flattening (arrow) compared to the normal elbow (C).

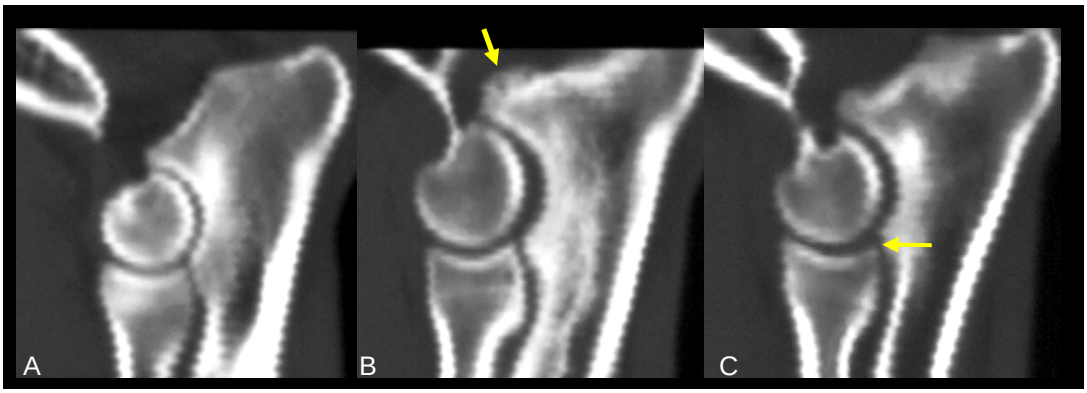

Figure 3.5 Sagittal CT images of the elbow illustrating normal joint congruity (A), humeroulnar incongruity (B), and humeroradial incongruity (C). Humeroradial joint incongruity and radioulnar incongruity are indicated by the presence of a 'step defect'. Note periarticular osteophyte formation along the anconeal process (arrow) and subchondral sclerosis caudal to the MCP.

3.3 RESULTS

3.3.1 Study Population

CT images of 50 elbows from 49 affected dogs, and 10 elbows from 5 clinically normal dogs were included in the study. The group of normal dogs included 3 intact males, and 2 intact females. All normal dogs were 9 months of age, with a median body weight of 23.9 kg (range 20.7-28.6 kg). The group of affected dogs included 25 males (14 intact) and 25 females (7 intact). Median age of affected dogs was 23 months (range 7-120 months); median age for males was 18 months (range 7-104 months) and females was 26 months (range 9-120 months). Median body weight of affected dogs was 34.1 kg (range 21.8-65 kg); median weight for males was 36.4 kg (range 22.7-65 kg), and females was 32.3 (range 21.8-40.7 kg). Affected breeds included: Labrador Retriever (14), Rottweiler (11), Golden Retriever (6), mixed breed (6), Chow Chow (2), German Shepherd (2), and Newfoundland (2). Other breeds included Black and Tan Coonhound, Blue Heeler, Bouvier des Flandres, Boxer, Flat-coated Retriever, and St. Bernard (1 each).

Arthroscopic exploration of both elbows was performed in 19 dogs, the left elbow only in 19 dogs, and the right elbow only in 12 dogs. Retrospective evaluation of arthroscopy reports confirmed the presence of discrete (loose) FCP (29), partially attached FCP (5), absence of FCP (16), abnormal MCP shape (2), kissing lesion or OCD (3), UAP (2), unspecified joint incongruity (10; 6 of which required corrective ulnar osteotomy or ostectomy), severe cartilage fibrillation (12), osteomalacia and/or

chondromalacia (7), moderate to severe degenerative joint disease (9), and synovial proliferation and/or pronounced synovitis (6).

CT Imaging and VAS Analysis

CT images used in this study included 28 left and 22 right elbows from affected dogs, and included both elbows from one dog. Regarding the VAS scoring method, there was a distinct observer effect on VAS scores. This was unexpected, and presumed to be a result of the way in which observers utilized the VAS scale. Observer 1 demonstrated a categorical style for scoring diagnostic certainty, i.e. marks were made at the extremities (denoting absolute absence or presence) or at the center (denoting uncertainty), with few marks in between. In contrast, observer 2 demonstrated a continuous style, with very few categorical or polarized marks. Despite these differences in scoring style, inter-observer variance was relatively low for most CT characteristics.

3.3.2 MCP Hypoattenuating Subchondral Defect

As expected, observer diagnostic certainty for the presence or absence of subchondral defects of the MCP was greatest in the transverse plane (Fig. 3.7 A and B). Of the main effects, image plane had the greatest effect on certainty ($F= 14.8$; $p<0.0001$), followed by status (normal or dysplastic) ($F=6.73$; $p=0.012$). Alone, display window had no effect on certainty ($F=2.79$; $p=0.063$), but did when combined with status and plane ($F=3.87$; $p=0.004$). For normal elbows, the certainty for the

presence or absence of this characteristic was significantly greater in the transverse plane at 1500 HU when compared to other plane and window combinations ($p=0.0032$), whereas there was no difference between 2500 HU and 3500 HU. In contrast, for dysplastic elbows, certainty for the presence or absence of the characteristic was greater at 3500 HU ($p<0.0001$) and 2500 HU ($p<0.0001$) than at 1500 HU. This was expected because hypoattenuating defects are better visualized in the low contrast images (Fig. 3.8.)

3.3.3 MCP Fissure (*in situ* fragment)

In general, observer diagnostic certainty for the presence or absence of MCP fissures was affected mostly by elbow status, where certainty was significantly greater in normal elbows than those with dysplastic characteristics. Certainty for the presence of MCP fissures was affected most by elbow status ($F=72.5$; $p<0.0001$) than any other single effects. Status and plane had a high combined effect ($F=17.55$; $p<0.0001$), whereas window ($F=8.81$; $p=0.0002$) and plane ($F=8.12$; $p=0.0003$) has moderate individual effect. For a given plane and window, the transverse plane at 2500 HU and 3500 HU was associated with greater certainty ($p<0.0001$) over other planes for the presence or absence of the characteristic, particularly in normal elbows. An unexpectedly low certainty for the presence or absence of MCP fissures may have been caused by a high inter-observer variance effect (Fig 3.9). For a given plane, diagnostic certainty in normal elbows was greatest in the transverse plane ($p=0.0002$), but this was not true in dogs with dysplasia ($p=0.0822$). For a given window, both

the 2500 HU ($p=0.0007$) and 3500 HU ($p=0.0012$) windows were different than the 1500 HU window, but there was no difference between the 2500 HU and 3500 HU window (Fig. 3.10).

3.3.4 Discrete MCP Fragment (FCP)

Observers demonstrated higher diagnostic certainty for the presence or absence of FCP in normal elbows than dysplastic elbows, and this was regardless of image plane or window (Fig. 3.11). The combined effect of status and plane ($F=33.56$; $p<0.0001$) on certainty was greater than the effect of status ($F=17.99$; $p<0.0001$) or plane ($F=11.24$; $p<0.0001$) alone. Window, as expected, had no effect on certainty (i.e., fragments, when present, were visible in all windows). For a given plane in normal elbows, certainty for the presence or absence of FCP was greatest in the transverse plane ($p<0.0001$). In dysplastic elbows, certainty was unexpectedly the least in the transverse plane and greatest in the sagittal plane ($p<0.0001$; Fig. 3.12). This finding may have been due to partial volume averaging (PVA) between the trochlea humeri and the MCP (Fig. 3.6). For observer 2, PVA may have affected certainty for FCP in the transverse plane, but not for observer 1. For observer 2, certainty for FCP was higher in the sagittal plane where PVA was not a factor.

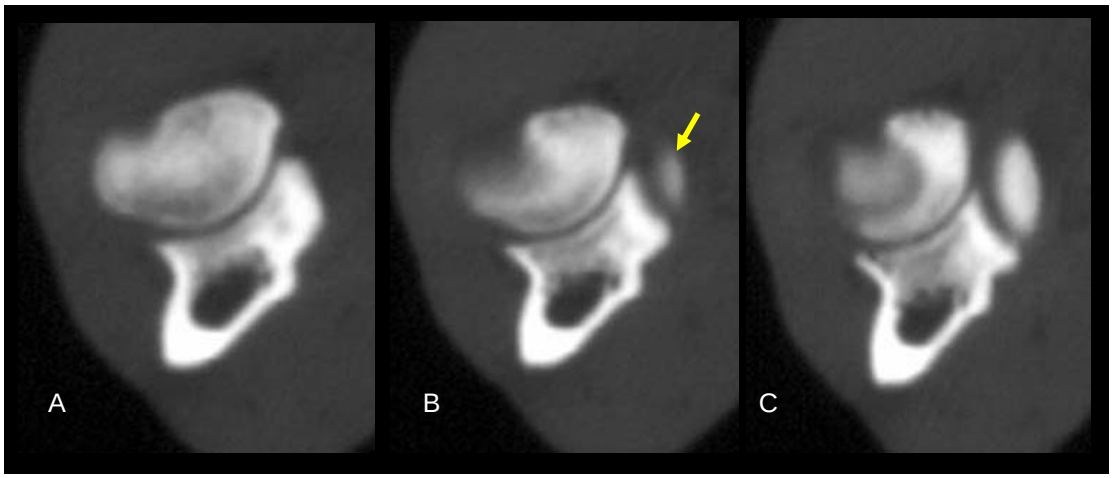

Figure 3.6 Transverse CT images of a normal elbow at the level of the MCP (A). Notice the partial volume averaging that occurs in the first slice of the articular surface of the trochlea humeri (B, arrow) which could be mistaken as a displaced FCP. As the sequence of images progress proximally, the structure becomes continuous with the humeral condyle (C).

3.3.5 Radial Incisure Irregularity and Hypoattenuating Subchondral Defect

Observers demonstrated near absolute diagnostic certainty for the presence or absence of RI irregularities in the transverse plane regardless of window (Figs. 3.13 and 3.14). Image plane demonstrated the strongest effect ($F=198.6$; $p<0.0001$) on certainty followed by status ($F=13.25$; $p=0.0006$). As expected, certainty was greater in the transverse plane ($p<0.0001$) than any other plane because the RI is seen more clearly in this plane. Display window, as expected had no effect on certainty ($F=2.51$; $p=0.0824$).

3.3.6 Subchondral Sclerosis of the Trochlea Humeri

The display window setting affected diagnostic certainty for the presence or absence of subchondral sclerosis more than any other CT characteristic of the study. Combined, the effects of status and window (1500 and 3500 HU) had the strongest effect on certainty ($F=33.28$, $p<0.0001$), whereas the combination of status, plane, and window ($F=5.10$; $p=0.0005$) had only moderate effect. Single variables had no effect on certainty. In normal elbows, certainty for the presence or absence of subchondral sclerosis was greater at 3500 HU in all planes, but was only significantly different from other windows in the dorsal plane ($p=0.008$; Fig. 3.15 A and B). This was expected because the dorsal plane best depicts the articulation between the trochlea humeri and MCP. The 3500 HU window does not mimic the presence of sclerosis when it is not present. Also, as expected, certainty for the presence or absence of subchondral sclerosis in normal elbows was least at 1500 HU because this

window may mimic the appearance of sclerosis even if it is not present ($p=0.0008$; Fig. 3.16). For dysplastic elbows, there was an opposite trend. In dysplastic elbows, certainty was significantly greater at 1500 HU ($p=0.0002$) in both the dorsal and transverse planes, and least at 3500 HU ($p<0.0001$). This also was expected because, if sclerosis is present, it will be accentuated at 1500 HU whereas it will be minimized in the wide window of 3500 HU. The 2500 HU window had no effect on certainty ($p=0.59$).

3.3.7 Subchondral Defects of the Trochlea Humeri

Observers demonstrated greater diagnostic certainty for the presence or absence of subchondral defects of the trochlea humeri in normal elbows, whereas in dysplastic elbows, the diagnostic certainty was unexpectedly low (Fig. 3.17). The combined effect of status and plane had the strongest effect on observer certainty ($F=34.16$; $p<0.0001$), followed by individual effects of status ($F=33.35$; $p<0.0001$) and plane ($F=5.67$; $p=0.0037$). Window had no effect on certainty. As expected, the certainty in normal elbows was significantly different in the dorsal plane ($p<0.0001$) than other planes, regardless of window. This is because it best displays the articulation between the trochlea humeri and MCP (Fig. 3.18). However, an unexpected finding was that the dorsal plane was associated with the least certainty for a trochlear lesion in dysplastic elbows. This finding was also due to an inter-observer effect. When VAS scores were analyzed for individual observers, differences in certainty were discovered. For observer 1, status and plane had the greatest combined effect on

diagnostic certainty ($F=124.22$; $p<0.0001$), although status ($F=27.42$; $p<0.0001$) and plane ($F=13.69$; $p<0.0001$) alone also had moderate affect on certainty. Observer 1 demonstrated the greatest certainty for the presence or absence of trochlear defects in the dorsal plane ($p<0.0001$). Diagnostic certainty for observer 2 was only affected by elbow status ($F=31.45$; $p<0.0001$). For observer 2, diagnostic certainty was reduced in some dysplastic elbows by the presence of subchondral hypoattenuating defects or cyst-like lesions adjacent to the olecranon fossa.

3.3.8 Joint Incongruity

As expected, image plane had the strongest effect on observer certainty for the presence or absence of joint incongruity ($F=31.63$; $p<0.0001$), followed by elbow status ($F= 14.5$; $p=0.0003$). The window, as expected, had no effect (Fig. 3.19). For a given status, there was greater certainty in normal elbows than incongruent elbows ($p=0.0003$). As expected, observers demonstrated the greatest certainty in the sagittal plane ($p<0.0001$; Fig. 3.20) because this plane best displays the articulations between radius, ulna, and humerus.

3.3.9 Temporal Effects

Temporal analysis was performed on all variables to determine the effects of time (period) or sequential evaluation of CT characteristics on diagnostic certainty. The certainty for subchondral defects of the trochlea humeri was the only variable to

demonstrate temporal effects, which were mild, and only when period and image plane were combined; observer 1 (F=4.22; p=0.0152); observer 2 (F=3.32; p=0.0370). For a given plane and period, there were no significant effects on diagnostic certainty for either observer. Period effects were not observed for any other CT variables.

Additional Observer Findings

Other findings voluntarily recorded by observers included: moderate to severe osteophyte formation (41), incomplete ossification of the humeral condyle (3), ununited anconeal process (3), suspect panosteitis (3), condylar fracture (1), and calliopsis circumscription (1).

3.3.10 Observer Disagreement and Possible Confounding Factors

For the following CT characteristics the number of film sets (out of 540) in which there was complete observer disagreement were: MCP hypoattenuating subchondral defects (34), MCP fissure (45), discrete MCP fragment (15), RI irregularity (28), sclerosis of the trochlea humeri (51), kissing lesion or OCD (21), and joint incongruity (40). For MCP subchondral defects and discrete MCP fragments (FCP), observer differences were equal for positive and negative certainty, i.e. there was no observer bias. When there were observer differences, observer 1 had greater diagnostic certainty for the presence of an MCP fissure whereas observer 2 was more equivocal. Comments provided by observers to explain equivocal responses for abnormalities of the MCP (subchondral defects, fissures, and fragments) included off-

axis reformatted image plane and/or the MCP was not completely included in the sagittal reformatted images. For RI irregularity and/or hypoattenuating subchondral defects there was no observer bias. The variable, as defined for the study included both hypoattenuating defects and margin irregularity. If a given elbow had one condition but not the other, observers may have been unsure how to respond. In most cases, if only one of the conditions existed, the observer made note as to which was present. For subchondral sclerosis of the trochlea humeri, subchondral defects of the trochlea humeri, and joint incongruity observer differences tended to be biased. Observer 1 had greater certainty for the presence of trochlear sclerosis, whereas for these cases, observer 2 felt the characteristic was absent. Observer 2 diagnosed the presence of subchondral defects of the trochlea humeri in more than twice as many film sets as observer 1. For differences in agreement for joint incongruity, observer 2 diagnosed humeroulnar and humeroradial incongruity far more often than observer 1. Observers did not indicate significant interpretation difficulties for these characteristics. Overall, the most common technical artifacts noted in the images included off-axis planar imaging or incomplete MCP evaluation (21), and partial volume averaging (4).

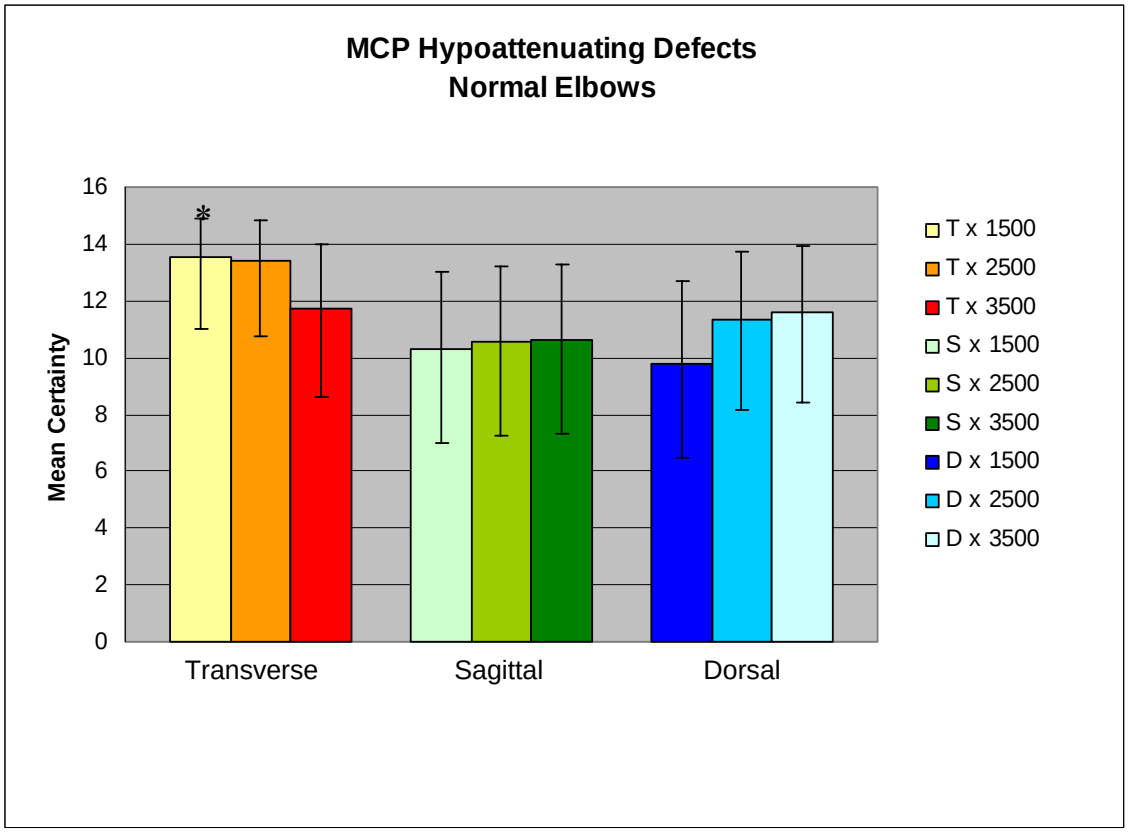

Figure 3.7A The combined effect of status, plane, and window on diagnostic certainty for the presence or absence of hypoattenuating subchondral defects of the MCP in normal elbows. Statistically significant factors are indicated with (*).

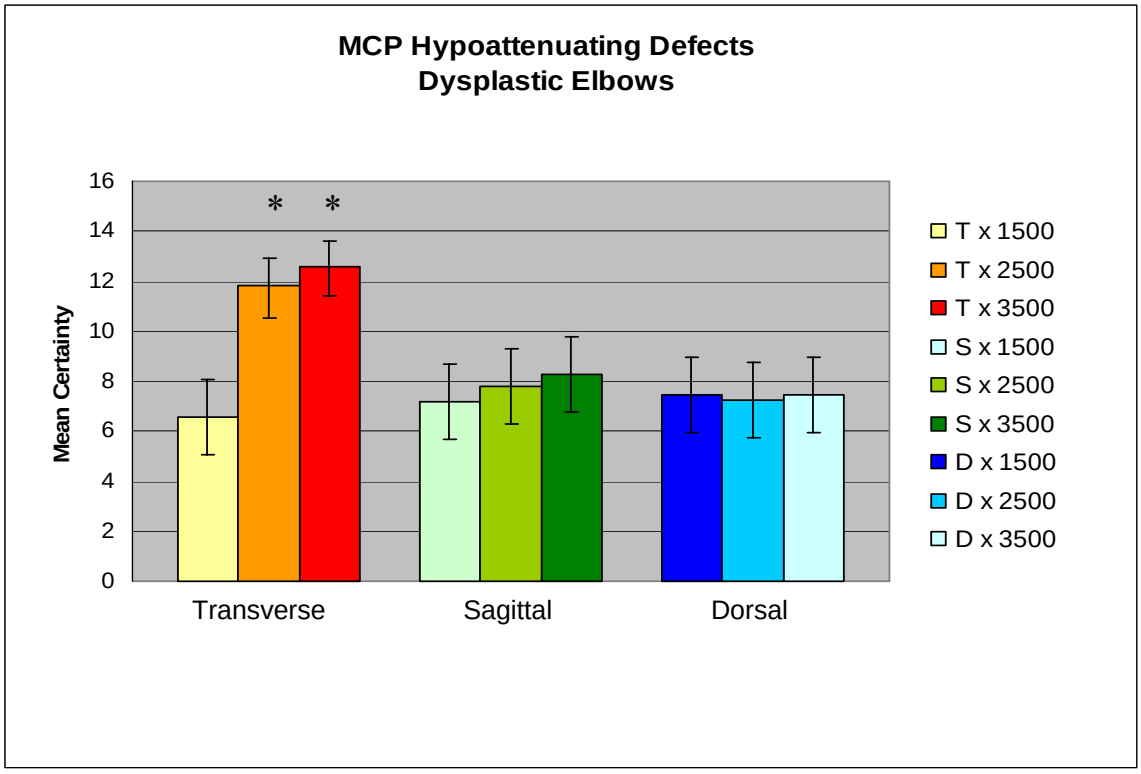

Figure 3.7B The combined effect of status, plane, and window on diagnostic certainty for the presence or absence of hypoattenuating subchondral defects of the MCP in dysplastic elbows. Statistically significant factors are indicated with (*).

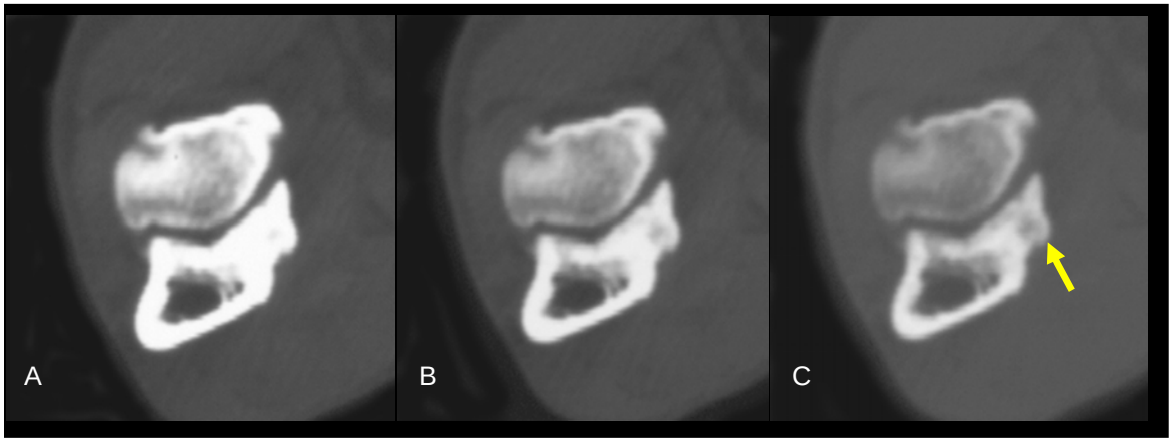

Figure 3.8 Transverse images (A-C) of a hypoattenuating subchondral defect of the MCP. Image A is displayed in a window width of 1500 HU, B in 2500 HU, and C in 3500 HU. Note the lesion becomes more conspicuous as the image contrast is decreased (C; arrow).

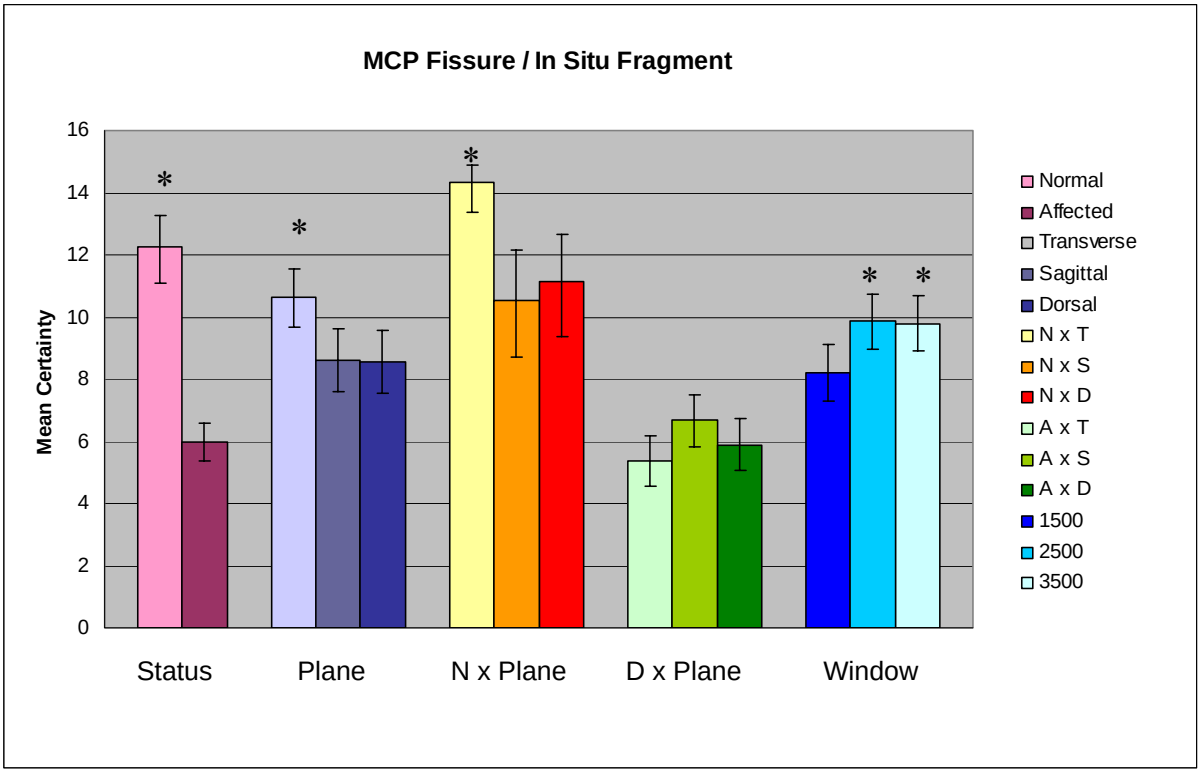

Figure 3.9 The effect of status, plane, interaction of status and plane, and window on diagnostic certainty for the presence or absence of MCP fissures. Statistically significant factors are indicated with (*). N x Plane= normal elbow; D x Plane= dysplastic elbow

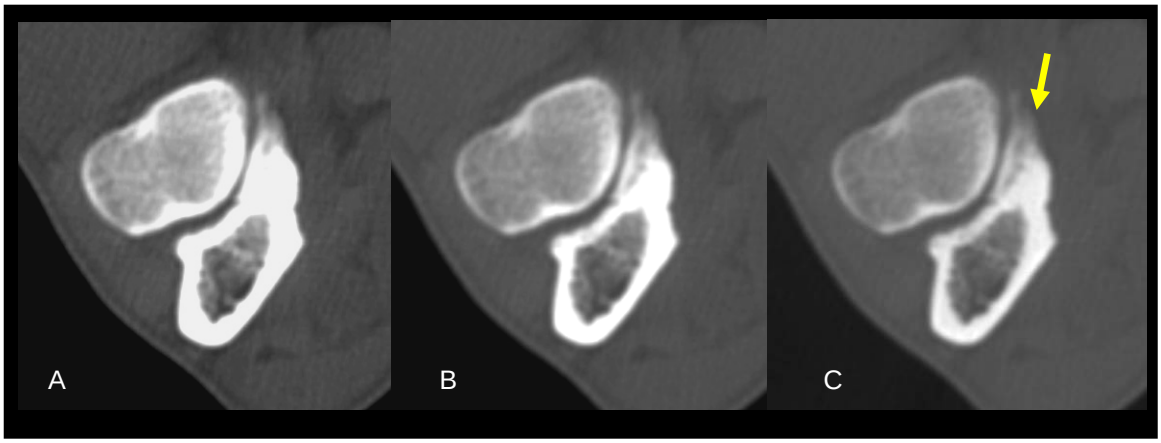

Figure 3.10 Transverse images of the elbow at the level of the MCP to demonstrate a sagittal fissure of the MCP (arrow). Image A is displayed in window width of 1500 HU, B in 2500 HU, and C in 3500 HU. Note the fissure becomes more conspicuous as the image contrast is decreased.

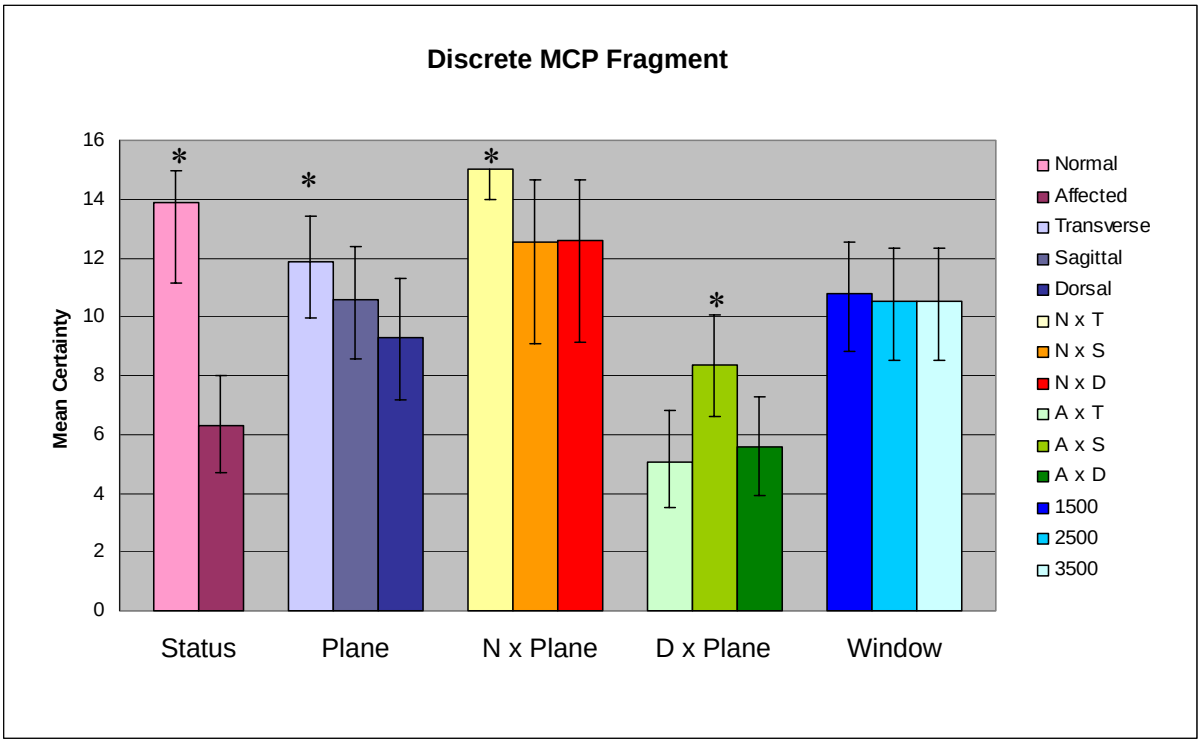

Figure 3.11 The effect of status, plane, interaction of status and plane, and window on diagnostic certainty for the presence or absence of discrete MCP fragments (FCP). Statistically significant factors are indicated with (*). N x Plane= normal elbow; D x Plane= dysplastic elbow

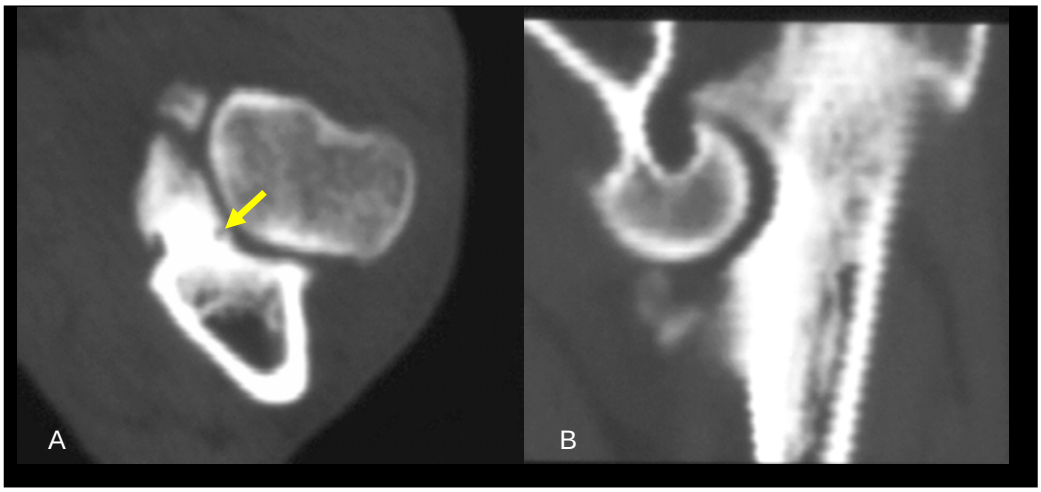

Figure 3.12 Transverse (A) and midsagittal (B) images of a large, discrete fragment of the medial coronoid process. Large, displaced fragments such as this could be seen in both planes regardless of window setting. Note the hypoattenuating subchondral defect and abnormal shape of the MCP, in addition to the hypoattenuating defect within the radial incisure (A; arrow). RI abnormalities are not well visualized on sagittal plane images (B). Humeroulnar joint incongruity is also noted (B).

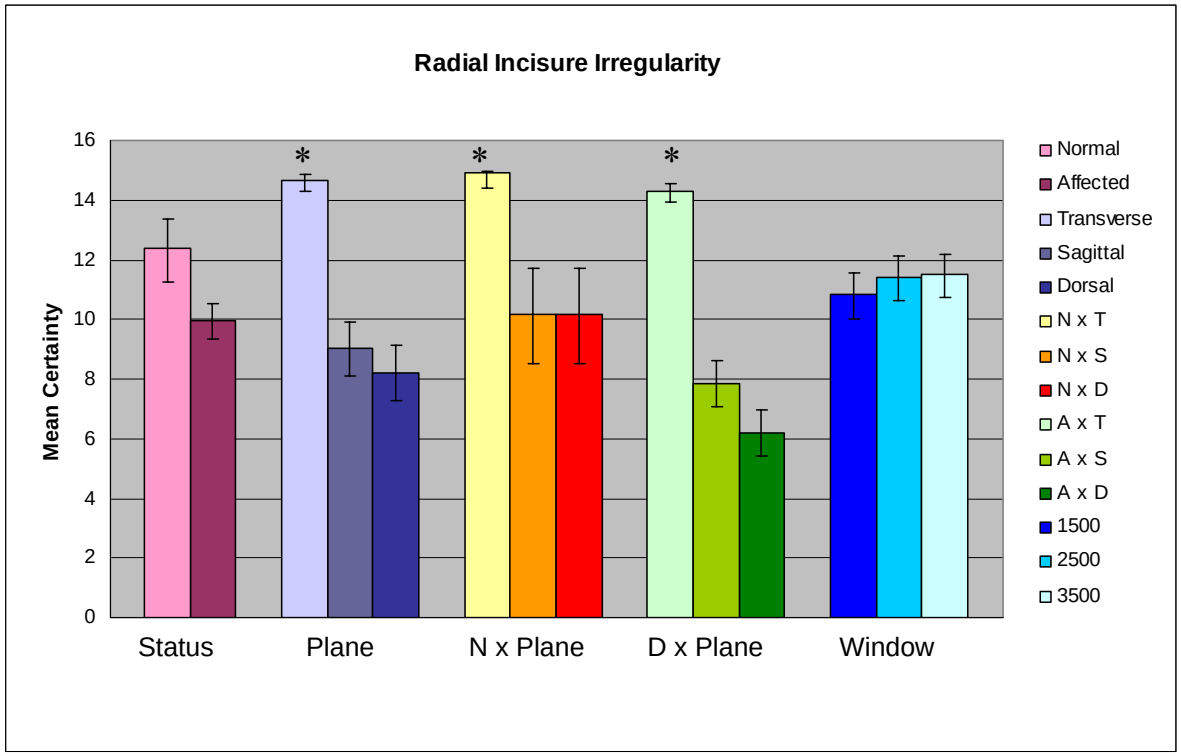

Figure 3.13 The effect of status, plane, interaction of status and plane, and window on diagnostic certainty for the presence or absence of radial incisure irregularity. Statistically significant factors are indicated with (*). N x Plane= normal elbow; D x Plane= dysplastic elbow

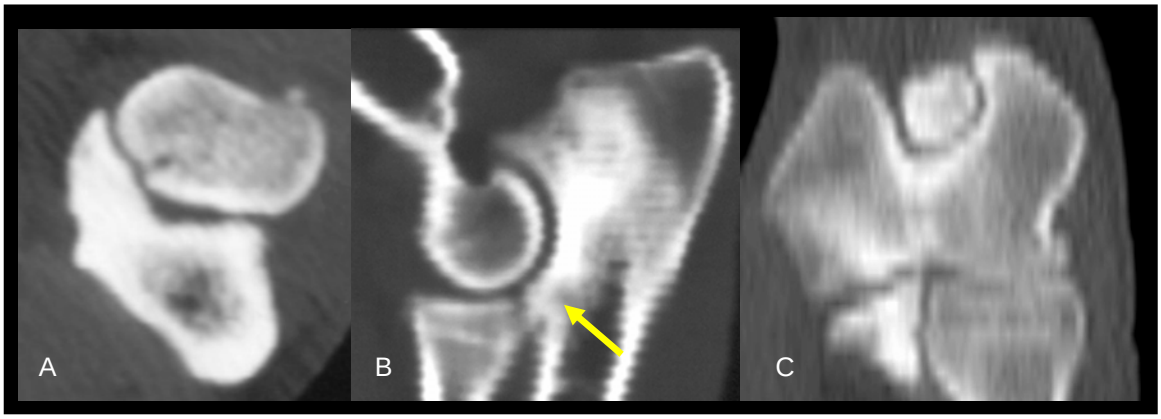

Figure 3.14 Transverse (A), sagittal (B), and dorsal plane (C) images of the elbow to illustrate the effect of image on the ability to assess the radial incisure of the ulna. Note that this structure is optimally displayed in the transverse plane, whereas it is only partially visible in sagittal images (arrow), and cannot be seen in the dorsal plane.

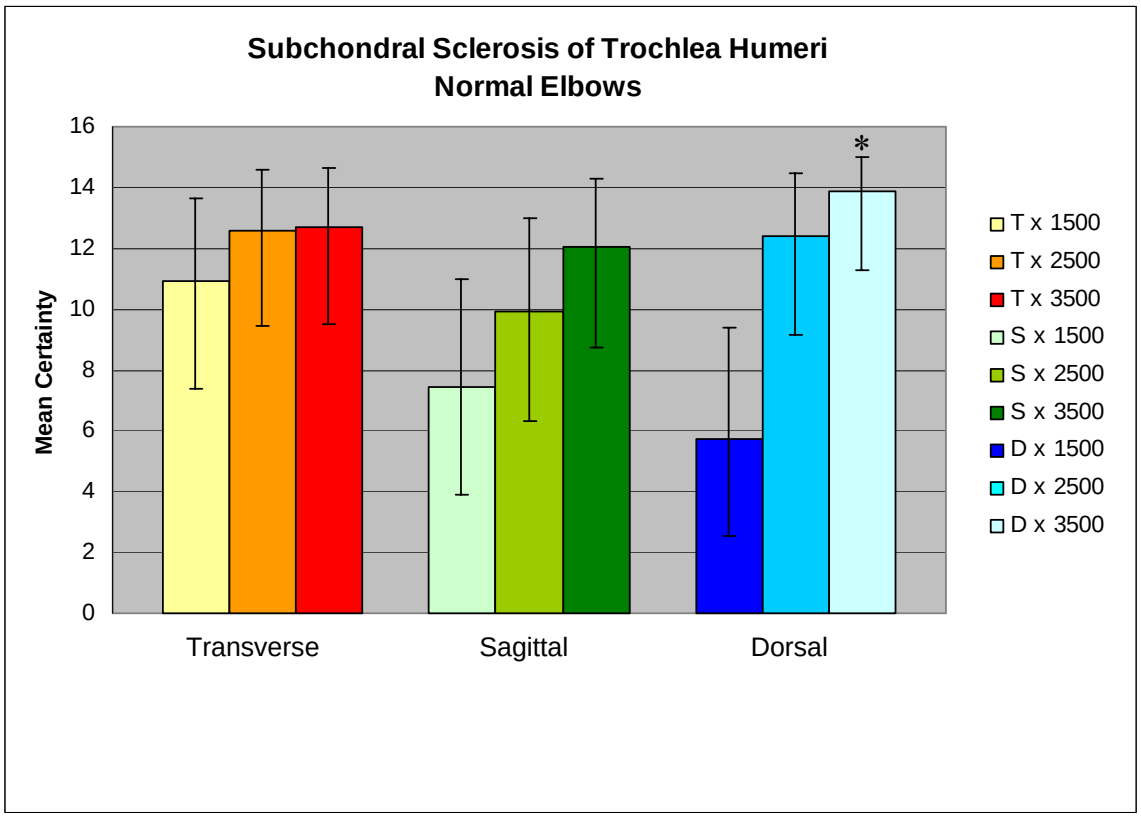

Figure 3.15A The combined effect of plane and window on diagnostic certainty for the presence or absence of subchondral sclerosis within the trochlea humeri in normal elbows. Statistically significant factors are indicated with (*).

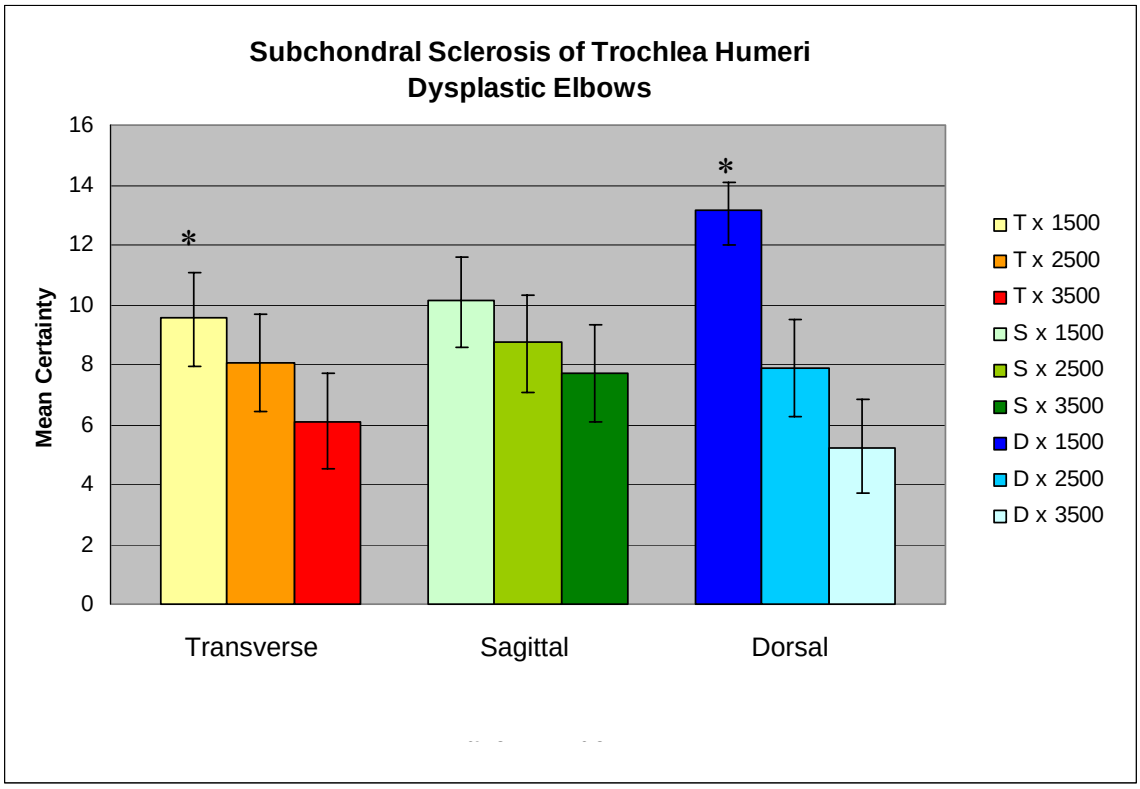

Figure 3.15B The combined effect of plane and window on diagnostic certainty for the presence or absence of subchondral sclerosis within the trochlea humeri in dysplastic elbows. Statistically significant factors are indicated with (*).

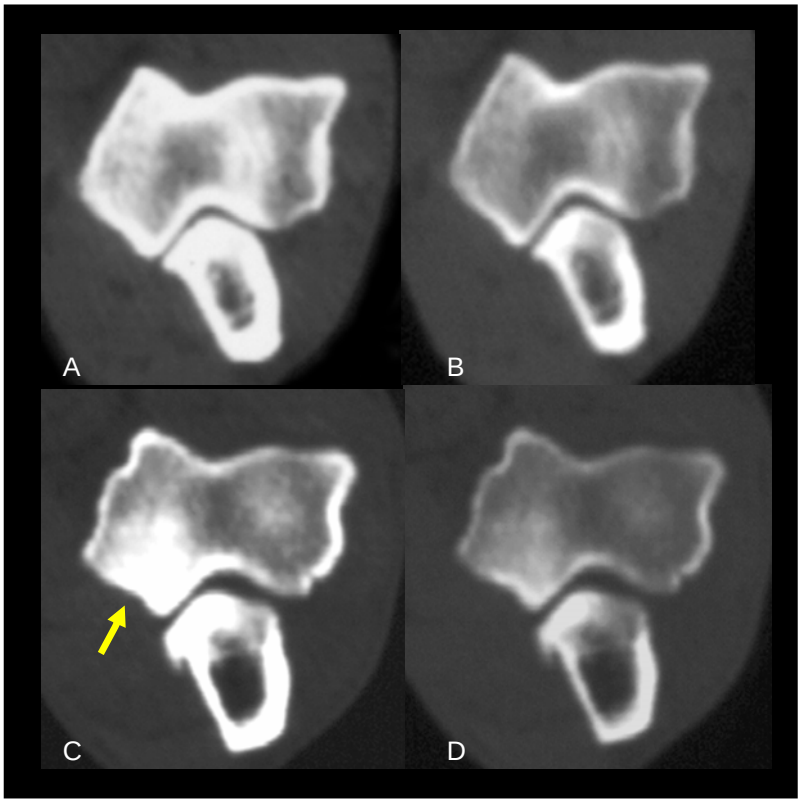

Figure 3.16 The effect of display window on the appearance of subchondral bone in a normal elbow (A, B) and elbow with subchondral sclerosis of the trochlea humeri (C, D). The left column is displayed in a window of 1500 HU (high contrast) and the right column is displayed in a window of 3500 HU (low contrast). Sclerosis is accentuated in the high contrast image (C, arrow) and minimized in the low contrast image (D). Note the high contrast window accentuates subchondral bone in the normal elbow and may be mistaken for subchondral sclerosis, whereas the appearance in sclerosis is reduced in the low contrast window affected elbows may be mistaken for normal.

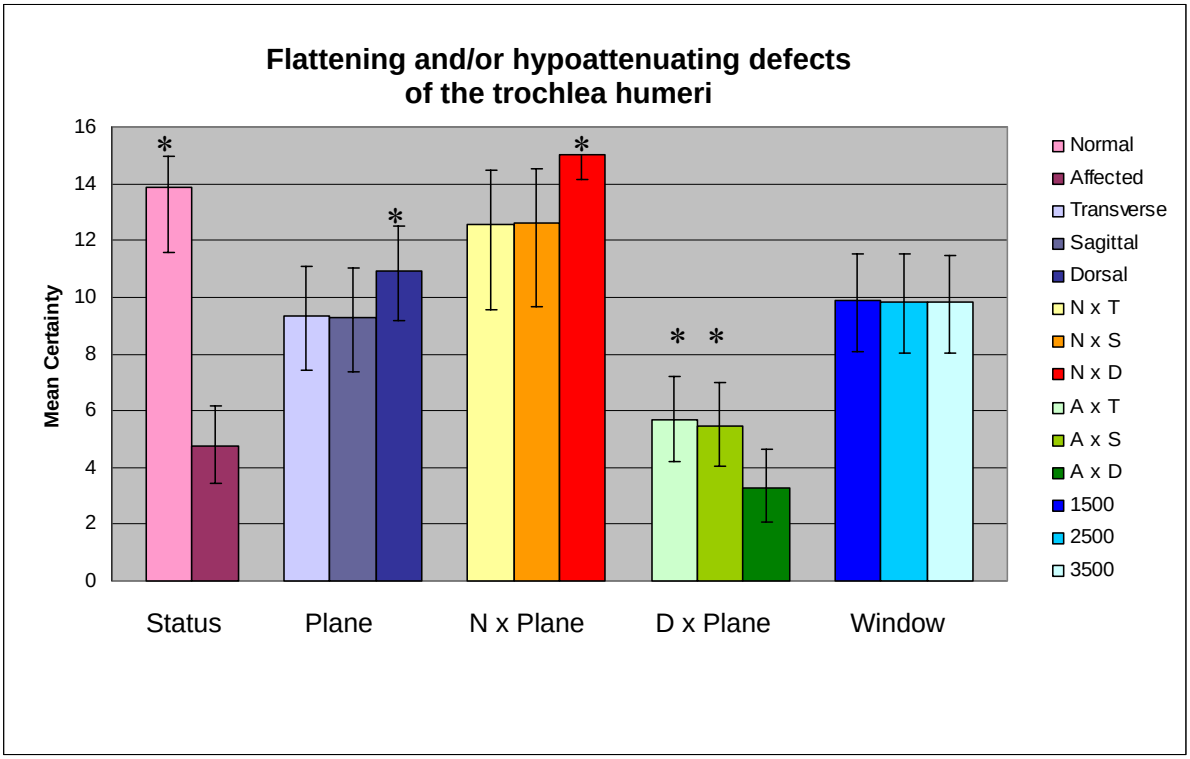

Figure 3.17 The effect of status, plane, interaction of status and plane, and window on diagnostic certainty for the presence or absence of flattening and/or hypoattenuating subchondral defects of the trochlea humeri (kissing lesion or OCD). Statistically significant factors are indicated with (*). N x Plane= normal elbow; D x Plane= dysplastic elbow

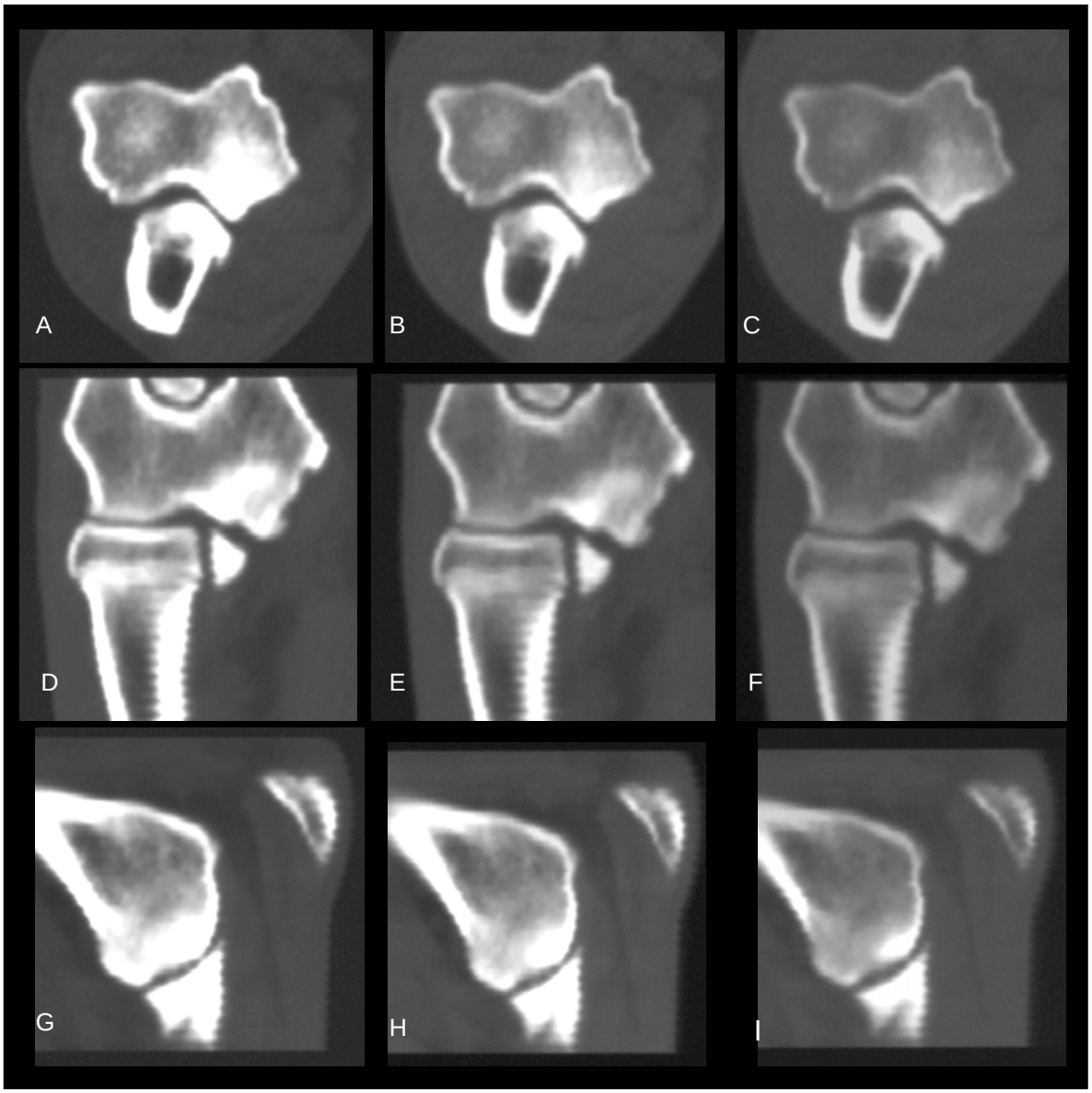
A
B
C
D
E
F
G
H
I
1
2
3

Figure 3.18 (opposing page) Transverse images of the humeral condyle (A-C), dorsal plane images of the elbow (D-F), and medial parasagittal plane images of the elbow at the level of the MCP and trochlea humeri (G-I) of an elbow with a surgically confirmed kissing lesion. Images in column 1 are displayed in window width of 1500 HU; column 2 in 2500 HU; and column 3 in 3500 HU. Subchondral sclerosis of the trochlea humeri is best demonstrated with high contrast window settings, and the articular defect is optimally displayed in the dorsal plane.

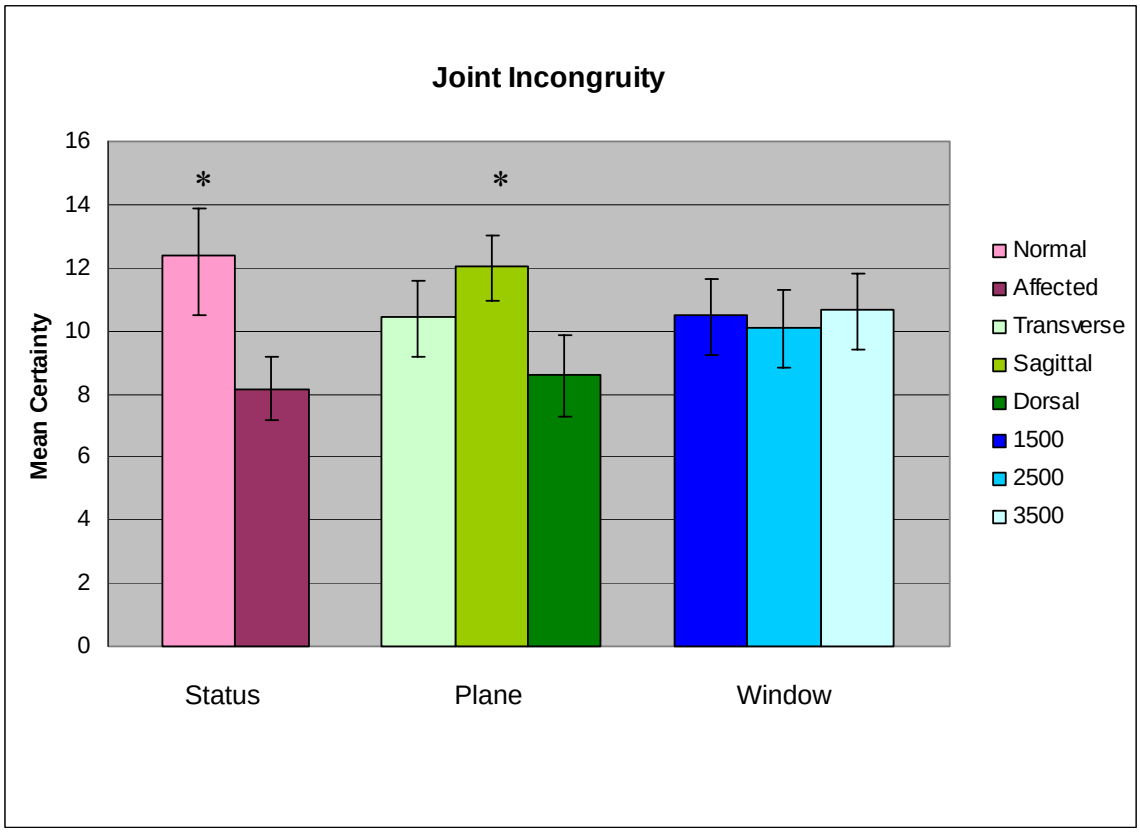

Figure 3.19 The effect of status, plane, and window on diagnostic certainty for the presence or absence of joint incongruity. Statistically significant factors are indicated with (*).

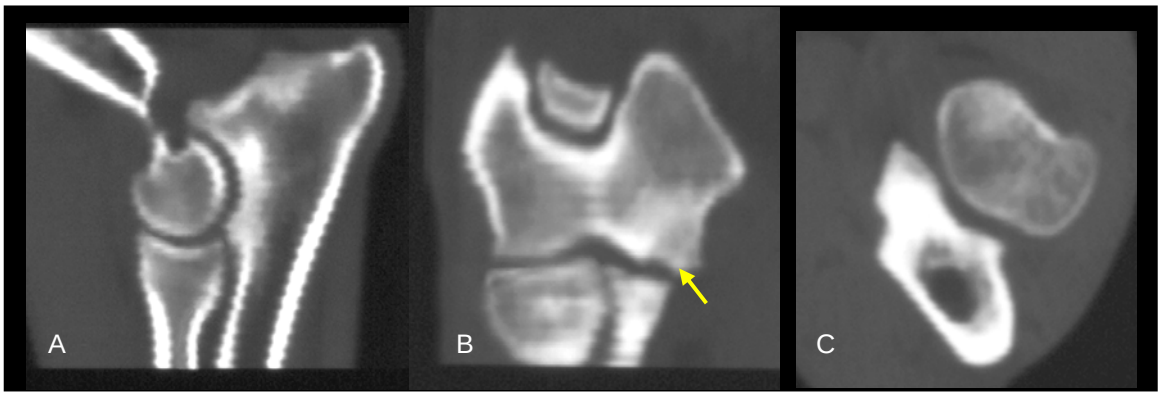

Figure 3.20 Sagittal (A), dorsal (B), and transverse (C) images of elbows with moderate humeroradial, humeroulnar, and radioulnar joint incongruity. Note the incongruity is best demonstrated in sagittal plane images, but can also be detected in dorsal plane images. Humeroradial joint incongruity is not demonstrated in the transverse plane at the level of the MCP (C). Note the articular defect with surrounding sclerosis of the trochlea humeri (B; arrow).

Table 3.1 CT image display parameters found to have a statistically significant effect on observer diagnostic certainty for the presence or absence of CT characteristics in normal and dysplastic elbows.

CT Characteristic	Elbow Status	Image Display Parameter
MCP hypoattenuating subchondral defect	Normal Dysplasia	Transverse plane at 1500 W Transverse plane at 2500 or 3500 W
MCP fissure	Both	Transverse plane at 2500 or 3500 W
Discrete fragment (FCP)	Both	Transverse and Sagittal planes
Radial incisure irregularity	Both	Transverse plane
Sclerosis of trochlea humeri	Normal Dysplasia	Dorsal plane at 3500 W Dorsal and Transverse at 1500 W
Subchondral defect of trochlea humeri	Both	Dorsal plane (1 observer only)
Joint incongruity	Both	Sagittal plane

3.4 DISCUSSION

Diagnostic certainty is the confidence of an observer that a lesion does or does not exist. Because it is a subjective phenomenon, the use of a visual analog scale (VAS) was considered appropriate for quantifying observer diagnostic certainty for this study. Visual analog scales have been proven useful in human and veterinary studies to assess the quality of sleep, severity of pain, and measure observer diagnostic certainty.[350-354] A major advantage of the VAS is that it provides measurement on a continuous scale, and eliminates categorical constraints placed on observers that occur with numerical rating scales. The VAS also permits the use of parametric statistical analyses, which have a higher power than non-parametric analyses.[350,351,354] One disadvantage is that use of this method requires an experienced observer. In addition, it can be difficult to determine if small incremental changes in VAS scores are statistically or clinically significant.[350,354]

In our study, differences in inter-observer VAS scoring style had an unexpected effect on diagnostic certainty scores. This likely contributed to the unexpected results for some CT characteristics. Previous studies have also reported this effect.[116,243] Despite the observer variation, there was good overall accord for differentiating normal from dysplastic elbows. We also determined that image plane and window did have significant effects on diagnostic certainty. In a clinical setting, CT images may be interpreted by readers of varying experience or training, and style. The final interpretation may vary even among radiologists. The selection of two observers for the study was to simulate image interpretation in a 'real world' clinical scenario

rather than a strictly controlled experiment. We accepted there would be some individual observer bias.

There was no attempt to randomize the interpretation sequence of CT characteristics in the data sheets, so it is possible that sequence could have affected individual observer decision-making. However, no significant temporal effects were discovered between batches of films in our analysis. The authors feel that, regardless of the actual sequence, most radiologists would evaluate elbow CT images in a systematic fashion as they would for any other imaging study.

Although arthroscopic findings served as inclusion criteria for this study, details available in the surgery reports varied widely. Most reports were based on a template and stated a final diagnosis, but descriptive findings regarding the appearance of articular cartilage, osteophytes, and size, number, and location of MCP fragments or fissures was inconsistent. Financial constraints for the study prohibited arthroscopic exploration of the elbows, which was another limitation of the study. Nonetheless, because clinical and CT examinations of these dogs were found to be normal, surgery was not ethically justifiable. Ideally, a prospective study requiring completion of a questionnaire during surgical exploration of dysplastic elbows would have provided more precise detail for use in diagnostic sensitivity analysis. Alternatively, observer consensus could have served as the gold standard for this study, but we felt it was more important to investigate the effect of inter-observer variation. Reviewing video obtained during arthroscopic exploration could have been used to determine

sensitivity and specificity for variables other than FCP, but this was considered to be beyond the scope of the study.

We chose to have reviewers evaluate film sets independently in order to minimize internal observer bias. In reality, most radiologists interpreting such cases typically have access to a computer workstation with multiplanar capability and would evaluate all images collectively to arrive at a final diagnosis rather than from a single plane or window. At the computer workstation, radiologists can manipulate the images as needed to maximize their diagnostic certainty for lesions. Whereas, surgeons or primary care clinicians may only have access to hard copy printouts that provided to them by external medical imaging facilities. The findings from this study can be used as a guide for such users.

Our results showed that observers demonstrated significantly greater diagnostic certainty for normal elbows than for dysplastic elbows. The large effect of elbow status was unexpected, as it was anticipated that most CT characteristics, if present, would be detected with a high degree of certainty. It is possible that observers formed an overall opinion that an elbow was normal or dysplastic from available images. If the elbow was judged to be normal, then the diagnostic certainty for the absence of all CT characteristics was high. However, if the elbow was judged to be dysplastic, then diagnostic certainty for certain CT characteristics became more variable.

In general, diagnostic certainty for defects of the MCP and RI was greatest in the transverse plane because this best displays the anatomy of those structures.[15]

However, diagnostic certainty for FCP was greatest in the sagittal plane rather than the transverse plane. Partial volume averaging (PVA) between the trochlea humeri and MCP can be mistaken for FCP on transverse CT images. This may especially be true for small fragments that are only visible on one transverse image. Because there is no anatomic superimposition between the trochlea humeri and the MCP in the sagittal plane, small FCP may be more clearly discernable.

Diagnostic certainty for *in situ* fragments (MCP fissures) in the transverse plane was lower than expected. Fissures of the MCP, like hypoattenuating subchondral defects, were diagnosed with greatest certainty in the wide window setting. Diagnostic certainty for somewhat high-contrast lesions, such as MCP hypoattenuating defects and fissures, was anticipated to be greatest in the widest window because image noise would be minimized. One could assume that if a subchondral defect or fissure was best identified in the 3500 HU window, the inability to identify a lesion in this window would be associated with greater certainty for a normal MCP. This is because small, ill-defined lesions may be obscured in a narrow window (high contrast image) that has increased image noise.[336] We found that some subchondral bone defects became obscured in the 1500 HU window setting, which resulted in a normal appearing MCP. This scenario emphasizes the caution that should be applied when using a narrow window setting because small and potentially relevant subchondral defects may be overlooked, leading to a false negative diagnosis. However, we also found that CT may be too sensitive for detecting slight alterations of subchondral bone. For example, subtle changes in bone

attenuation became more visible in the wide display window setting, casting doubt as to whether the elbow was normal or not. Therefore, we also found that the 3500 HU window may be overinterpreted, leading to a false positive diagnosis. These findings contradict *in vitro* phantom studies that reported the detectability of low-contrast lesions diminished as window width was increased.[23,335,338] However, some authors reported this effect of decreasing lesion detectability was less pronounced for small high-contrast lesions than for larger, low-contrast lesions,[335] as well as for those obtained with a sharp reconstruction algorithm than a smooth algorithm.[18,20,344] Because our images were obtained with a sharp algorithm, image noise, particularly in the high contrast display window may account for the decreased conspicuity of subchondral defects. To the authors' knowledge, observer performance for *in vivo* osseous lesion detection has not been reported prior to this study, therefore it is difficult to draw comparisons between ours and the *in vitro* phantom studies.

In this study, the observers had difficulty discriminating focal subchondral defects from fissures of the MCP. Based on the assumption that any hypoattenuating alteration of subchondral bone signifies osteomalacia, the presence of cartilage fibrillation and/or chondromalacia may also be assumed and surgical exploration may be indicated. The clinical relevance of differentiating between focal subchondral defects and MCP fissures has yet to be determined as the decision for surgical exploration may be based solely on the presence of abnormal subchondral bone of the MCP.

Diagnostic certainty for the presence of subchondral sclerosis of the trochlea humeri was strongly affected by both window and plane. Where hypoattenuating defects of subchondral bone were best visualized at the 3500 HU window, certainty for subchondral sclerosis was greatest at the 1500 HU window setting. This agrees with previous phantom studies that have shown the detectability of lower-contrast lesions is improved when displayed in a narrow CT window.[20,335,336] The dorsal plane permits evaluation of the articulation between the trochlea humeri and MCP so it was expected that abnormalities of the trochlea would be best displayed in this plane. It was assumed that certainty for subchondral defects of the trochlea humeri would also be highest in the dorsal plane, however certainty was unexpectedly low. Inter-observer variation in the way the humeral condyle was evaluated was thought to account for this disparity. Certainty for this CT characteristic in the dorsal plane was lower than expected for observer 2. This was probably due to the presence of additional subchondral defects or cyst-like lesions within the caudal portion of the condyle or epicondyle in some elbows. When these changes were present, the diagnostic certainty for the characteristic was reduced. Specifically, when evaluating elbows for 'kissing lesions' or OC/OCD lesions the authors consider the dorsal plane the most ideal.

Our finding that joint incongruity was diagnosed with the greatest confidence in the sagittal plane supports other recent CT studies in both normal and dysplastic elbows.[14,187,188,320,321] In actuality, CT can only provide a gross estimation of congruity because articular cartilage is not visible in CT images.[295,310,320]

Measurements of elbow joint spaces on dorsal and sagittal reformatted images have been found to be accurate, and minor differences in limb positioning have minimal effect on image reformatting or joint space measurement.[321] Interestingly, authors reported only moderate inter-observer agreement for measurements due to imprecise resolution of joint surfaces.

Multiplanar image reformatting (MPR) is one of the primary advantages of CT which allows the reader to evaluate anatomic relationships in alternative planes.[321,332] Sagittal, dorsal, or oblique planes may reveal the extent of complex lesions that may be underestimated in transverse images. Images in the sagittal and dorsal plane allow evaluation of the entire humeroulnar and humeroradial joint.[16] To the authors' knowledge, this is the first report in the veterinary literature to describe the effect of CT image display on diagnostic certainty.

CHAPTER 4

CONCLUSIONS

Observer effects were greater than expected. In spite of this, some display parameter effects were found to be statistically significant. This study therefore provides an accurate representation of likely 'real world' scenarios. For most CT abnormalities of the canine elbow, diagnostic certainty was more dependent on image plane or combined effects, than window level alone. Detection of gross structural abnormalities of the MCP, radial incisure, and joint incongruity were most influenced by image plane. However, window width affected the perceived alteration in subchondral bone attenuation for the MCP and trochlea humeri. To maximize diagnostic certainty for detection of CT characteristics of canine elbow dysplasia, the authors make the following recommendations:

1) transverse images in 3500 HU are recommended for hypoattenuating subchondral defects and *in situ* fissures of the MCP
2) dorsal and transverse images in 1500 HU to diagnose subchondral sclerosis associated with subchondral defects of the trochlea humeri.
3) the transverse plane in any window for diagnosing radial incisure irregularity
4) transverse and sagittal plane in any window to diagnose MCP fragments
5) sagittal plane in any window to diagnose humeroulnar or humeroradial joint incongruity

FOOTNOTES

[a] acepromazine maleate, Vedco, Inc., St. Joseph, MO, USA.

[b] glycopyrrolate, Baxter Healthcare Corporation, Deerfield, IL, USA.

[c] hydromorphone, Baxter Healthcare Corporation, Deerfield, IL, USA.

[d] Rapinovet™, Gensia Sicor Pharmaceuticals, Inc., Irvine, CA, USA.

[e] IsoFlo™, Abbott Laboratories, North Chicago, IL, USA.

[f] GE Sytec 4000, GE Medical Systems, Milwaukee, WI. USA

[g] DEC-702 optical disk, Pioneer Electronic Corp., Keetberglaan, Beveren, Belgium.

[h] SAS Institute v. 9.2, Cary, NC. USA

[i] transformed X=arsin (sqrt(X/15))

REFERENCES CITED

1. Zontine WJ, Weitkamp RA, Lippincott CL. Redefined type of elbow dysplasia involving calcified flexor tendons attached to the medial humeral epicondyle in three dogs. *J Am Vet Med Assoc* 1989;194:1082-1085.

2. Walker TM. A redefined type of elbow dysplasia in the dog--2 cases. *Can Vet J* 1998;39:573-575.

3. Wind AP. Elbow Dysplasia. In: Slatter D, ed. *Textbook of Small Animal Surgery*. 2 ed. Philadelphia: W. B. Saunders, 1993;1966-1977.

4. Boulay JP. Fragmented medial coronoid process of the ulna in the dog. *Vet Clin North Am Small Anim Pract* 1998;28:51-74.

5. Hornof WJ, Wind AP, Wallack ST, et al. Canine elbow dysplasia. The early radiographic detection of fragmentation of the coronoid process. *Vet Clin North Am Small Anim Pract* 2000;30:257-266, v.

6. Kirberger RM, Fourie SL. Elbow dysplasia in the dog: pathophysiology, diagnosis and control. *J S Afr Vet Assoc* 1998;69:43-54.

7. Olsson SE. The early diagnosis of fragmented coronoid process and osteochondritis dissecans of the canine elbow joint. *J Am Anim Hosp Assoc* 1983;19:616-626.

8. Read RA, Armstrong SJ, O'Keefe JD, et al. Fragmentation of the medial coronoid process of the ulna in dogs: A study of 109 cases. *J Small Anim Pract* 1990;31:330-334.

9. Berzon JL. Osteochondritis dissecans in the dog: diagnosis and therapy. *J Am Vet Med Assoc* 1979;175:796-799.

10. Grondalen J, Grondalen T. Arthrosis in the elbow joint of young rapidly growing dogs. V. A pathoanatomical investigation. *Nord Vet Med* 1981;33:1-16.

11. Fox SM, Walker AM. Identifying and treating the primary manifestations of osteochondrosis of the elbow. *Vet Med* 1993;88:132-146.

12. Burmester E, Mendoza AS, Gmelin E. [Computerized tomography of the elbow joint]. *Rofo* 1985;143:671-676.

13. Zwaan M, Borgis KJ, Weiss HD, et al. [CT diagnosis of the elbow joint]. *Radiologe* 1990;30:106-112.

14. Reichle JK, Park RD, Bahr AM. Computed tomographic findings of dogs with cubital joint lameness. *Vet Radiol Ultrasound* 2000;41:125-130.

15. Reichle JK, Snaps F. The elbow. *Clin Tech Small Anim Pract* 1999;14:177-186.

16. De Rycke LM, Gielen IM, van Bree H, et al. Computed tomography of the elbow joint in clinically normal dogs. *Am J Vet Res* 2002;63:1400-1407.

17. Carpenter LG, Schwarz PD, Lowry JE, et al. Comparison of radiologic imaging techniques for diagnosis of fragmented medial coronoid process of the cubital joint in dogs. *J Am Vet Med Assoc* 1993;203:78-83.

18. Judy PF, Swensson RG. Detection of small focal lesions in CT images: effects of reconstruction filters and visual display windows. *Br J Radiol* 1985;58:137-145.

19. Judy PF, Swensson RG. Detectability of lesions of various sizes on CT images., in *Applications of Optical Instrumentation in Medicine XIII*. Society of Photo-Optical Instrumentation and Engineering 1985;38-42.

20. Judy PF, Swensson RG. Display thresholding of images and observer detection performance. *J Opt Soc Am A* 1987;4:954-965.

21. Judy PF, Swensson RG, Szulc M. Lesion detection and signal-to-noise ratio in CT images. *Med Phys* 1981;8:13-23.

22. Hanson KM. Variations in task and the ideal observer. *Society of Photo-Optical Instrumentation Engineers* 1983;419:60-67.

23. Seltzer SE, Swensson RG, Judy PF, et al. Size discrimination in computed tomographic images. Effects of feature contrast and display window. *Invest Radiol* 1988;23:455-462.

24. Wind AP. Elbow incongruity and developmental elbow diseas in the dog: Part I. *J Am Anim Hosp Assoc* 1986;22:711-730.

25. Wind AP. Elbow incongruity and developmental elbow disease in the dog: Part II. *J Am Anim Hosp Assoc* 1986;22:725-730.

26. Fox SM, Burbidge HM, Bray JC, et al. Ununited anconeal process: lag-screw fixation. *J Am Anim Hosp Assoc* 1996;32:52-56.

27. Turner BM, Abercromby RH, Innes J, et al. Dynamic proximal ulnar osteotomy for the treatment of ununited anconeal process in 17 dogs. *Vet Comp Orthop Trauma* 1998;11:76-79.

28. Sjostrom L, Kasstrom H, Kallberg M. Ununited anconeal process in the dog. Pathogenesis and treatment by osteotomy of the ulna. *Vet Comp Orthop Trauma* 1995;8:170-176.

29. Sjostrom L. Ununited anconeal process in the dog. *Vet Clin North Am Small Anim Pract* 1998;28:75-86.

30. Breit S, Kunzel W, Seiler S. Postnatal modelling of the humeroantebrachial contact areas of radius and ulna in dogs. *Anat Histol Embryol* 2005;34:258-264.

31. Fox SM, Bloomberg MS, Bright RM. Developmental anomalies of the canine elbow. *J Am Anim Hosp Assoc* 1983;19:605-615.

32. Preston CA, Schulz KS, Kass PH. In vitro determination of contact areas in the normal elbow joint of dogs. *Am J Vet Res* 2000;61:1315-1321.

33. Olsson SE. Osteochondrosis in domestic animals. Introduction. *Acta Radiol Suppl* 1978;358:9-14.

34. Olsson SE. General and local [corrected] aetiologic factors in canine osteochondrosis. *Vet Q* 1987;9:268-278.

35. Guthrie S, Plummer JM, Vaughan LC. Post natal development of the canine elbow joint: a light and electron microscopical study. *Res Vet Sci* 1992;52:67-71.

36. Hare WC. Radiographic anatomy of the canine pectoral limb. Part II: Developing limb. *J Am Vet Med Assoc* 1959;135:305.

37. Hare WC. The ages at which centers of ossification appear roentgenographically in the limb bones of the dog. *Am J Vet Res* 1961;22:825.

38. Marcellin-Little DJ, DeYoung DJ, Ferris KK, et al. Incomplete ossification of the humeral condyle in spaniels. *Vet Surg* 1994;23:475-487.

39. Smith RN, Allcock J. Epiphyseal fusion in the greyhound. *Vet Rec* 1960;72:75-79.

40. Riser WH, Shirer JF. Normal and abnormal growth of the distal foreleg in large and giant dogs. *JAVRS* 1965;6:50-64.

41. Hanlon GF. Normal and abnormal bone growth in the dog. *J Amer Vet Radiol Society* 1962;3:13-16.

42. Chapman WL, Jr. Appearance of ossification centers and epiphysial closures as determined by radiographic techniques. *J Am Vet Med Assoc* 1965;147:138-141.

43. Ticer JW. Radiographic interpretation. Common diseases of elbow and shoulder joints in dogs. *Mod Vet Pract* 1973;54:73-78.

44. Salmeri KR, Bloomberg MS, Scruggs SL, et al. Gonadectomy in immature dogs: effects on skeletal, physical, and behavioral development. *J Am Vet Med Assoc* 1991;198:1193-1203.

45. Carrig CB, Morgan JP. Asynchronous growth of the canine radius and ulna- Early radiographic changes following retardation of growth of the ulna. *JAVRS* 1975;16:495.

46. Skaggs S, DeAngelis MP, Rosen H. Deformities due to premature closure of the distal ulna in fourteen dogs. *J Am Anim Hosp Assoc* 1973;9:496-500.

47. Hanlon GF. Additional radiographic observations on elbow dysplasia in the dog. *J Am Vet Med Assoc* 1969;155:2045-2046.

48. Cawley AJ, Archibald J. Ununited anconeal process of the dog. *J Am Vet Med Assoc* 1959;134:454.

49. Van Sickle DC. The relationship of ossification to canine elbow dysplasia. *Animal Hospital* 1966;2:24-31.

50. Breit S, Kunzel W, Seiler S. Variation in the ossification process of the anconeal and medial coronoid processes of the canine ulna. *Res Vet Sci* 2004;77:9-16.

51. Ljunggren G, Cawley AJ, Archibald J. The elbow dysplasias in the dog. *J Am Vet Med Assoc* 1966;148:887-891.

52. Maierl J, Bottche P, Liebich HG. Biomechanics of the fractured medial coronoid process and the isolated anconeal process in the canine elbow joint. [abstract] in 25th Congress of the European Association of Veterinary Anatomists (EAVA), Oslo, July 2004. *Anatomia, Histologia, Embroylogia* 2005;34:31-32.

53. Kunzel W, Breit S, Probst A. The subchondral split line patterns of the medial coronoid process in canine ulnae. *Anat Histol Embryol* 2004;33:339-343.

54. Hazewinkel HA, Kantor A, Meij B, et al. Fragmented coronoid process and osteochondritis dissecans of the medial humeral condyle. *Tijdschr Diergeneeskd* 1988;113 Suppl 1:41S-46S.

55. Wolschrijn CF, Weijs WA. Development of the trabecular structure within the ulnar medial coronoid process of young dogs. *Anat Rec A Discov Mol Cell Evol Biol* 2004;278:514-519.

56. Wolschrijn CF, Weijs WA. Development of the subchondral bone layer of the medial coronoid process of the canine ulna. *Anat Rec A Discov Mol Cell Evol Biol* 2005;284:439-445.

57. Wind AP. Incidence and radiographic appearance of fragmented coronoid process in the Bernese mountain dog. *Calif Vet* 1982;6:19-26.

58. Grondalen J. Arthrosis with special reference to the elbow joint of young rapidly growing dogs. I A review of the literature. *Nord Vet Med* 1979;31:62-68.

59. Grondalen J. Arthrosis in the elbow joint of young rapidly growing dogs. VI. Interrelation between clinical, radiographical and pathoanatomical findings. *Nord Vet Med* 1982;34:65-75.

60. Eckstein F, Jacobs CR, Merz BR. Mechanobiological adaptation of subchondral bone as a function of joint incongruity and loading. *Med Eng Phys* 1997;19:720-728.

61. Eckstein F, Muller-Gerbl M, Steinlechner M, et al. Subchondral bone density in the human elbow assessed by computed tomography osteoabsorptiometry: a reflection of the loading history of the joint surfaces. *J Orthop Res* 1995;13:268-278.

62. Muller-Gerbl M. The subchondral bone plate. *Adv Anat Embryol Cell Biol* 1998;141:III-XI, 1-134.

63. Schön M, Eckstein F, Vogt S, et al. Subchondrale spaltlinien des menschlichen ellbogen- und kniegelenks- Ausdruck der biegung und zugbeanspruchung des subchondralen knochens? *Osteologie* 1998;7:77-87.

64. Carter DR. Mechanical loading history and skeletal biology. *J Biomech* 1987;20:1095-1109.

65. Cadet ER, Gafni RI, McCarthy EF, et al. Mechanisms responsible for longitudinal growth of the cortex: coalescence of trabecular bone into cortical bone. *J Bone Joint Surg Am* 2003;85-A:1739-1748.

66. Burr DB, Schaffler MB, Yang KH, et al. The effects of altered strain environments on bone tissue kinetics. *Bone* 1989;10:215-221.

67. Farkas T, Boyd RD, Schaffler MB, et al. Early vascular changes in rabbit subchondral bone after repetitive impulsive loading. *Clin Orthop Relat Res* 1987:259-267.

68. Eckstein F, Merz B, Schon M, et al. Tension and bending, but not compression alone determine the functional adaptation of subchondral bone in incongruous joints. *Anat Embryol (Berl)* 1999;199:85-97.

69. Behrens JC, Walker PS, Shoji H. Variations in strength and structure of cancellous bone at the knee. *J Biomech* 1974;7:201-207.

70. Vesterby A, Mosekilde L, Gundersen HJ, et al. Biologically meaningful determinants of the in vitro strength of lumbar vertebrae. *Bone* 1991;12:219-224.

71. Tanck E, Homminga J, Van Lenthe GH, et al. Increase in bone volume fraction precedes architectural adaptation in growing bone. *Bone* 2001;28:650-654.

72. Goldstein SA. The mechanical properties of trabecular bone: dependence on anatomic location and function. *J Biomech* 1987;20:1055-1061.

73. Tanck E, Hannink G, Ruimerman R, et al. Cortical bone development under the growth plate is regulated by mechanical load transfer. *J Anat* 2006;208:73-79.

74. Frost HM. From Wolff's law to the mechanostat: a new "face" of physiology. *J Orthop Sci* 1998;3:282-286.

75. Ruegsegger P, Koller B, Muller R. A microtomographic system for the nondestructive evaluation of bone architecture. *Calcif Tissue Int* 1996;58:24-29.

76. Muller R, Van Campenhout H, Van Damme B, et al. Morphometric analysis of human bone biopsies: A quantitative structural comparison of histological sections and micro-computed tomography. *Bone* 1998;23:59-66.

77. Wolschrijn CF, Gruys E, Weijs WA. Microcomputed tomography and histology of a fragmented medial coronoid process in a 20-week-old golden retriever. *Vet Rec* 2005;157:383-386.

78. Wentink GH. Biokinetical analysis of hind limb movements of the dog. *Anat Embryol (Berl)* 1977;151:171-181.

79. Frost HM. A 2003 update of bone physiology and Wolff's Law for clinicians. *Angle Orthod* 2004;74:3-15.

80. Maierl J, Dickomeit M, Bohmisch R, et al. Spaltlinien am ellbogengelenk des hundes. *Verh Anat Ges* 2001;183:259.

81. Schon M, Eckstein F, Vogt S, et al. Subchondrale spaltlinien des menschlichen ellbogen und kniegelenks- Ausdruck der biegung und zugbeanspruchung des subchondralen knochens? *Osteologie* 1998;7:77-87.

82. Roth V, Mow VC. The intrinsic tensile behavior of the matrix of bovine articular cartilage and its variation with age. *J Bone Joint Surg Am* 1980;62:1102-1117.

83. Ekman S, Carlson CS. The pathophysiology of osteochondrosis. *Vet Clin North Am Small Anim Pract* 1998;28:17-32.

84. Carlson CS, Meuten DJ, Richardson DC. Ischemic necrosis of cartilage in spontaneous and experimental lesions of osteochondrosis. *J Orthop Res* 1991;9:317-329.

85. Ytrehus B, Ekman S, Carlson CS, et al. Focal changes in blood supply during normal epiphyseal growth are central in the pathogenesis of osteochondrosis in pigs. *Bone* 2004;35:1294-1306.

86. Wolschrijn CF, Kik MJ, Weijs WA. Cartilage-free areas in the elbow joint of young golden retrievers. *Anat Rec A Discov Mol Cell Evol Biol* 2003;275:990-996.

87. Hamrick MW. A chondral modeling theory revisited. *J Theor Biol* 1999;201:201-208.

88. Tillman B, Bartz B. Funktionelle anatomie des ellbogengelenks. *Aktuelle Probl Chir Orthop* 1989;37:20-27.

89. Eckstein F, Lohe F, Muller-Gerbl M, et al. Stress distribution in the trochlear notch. A model of bicentric load transmission through joints. *J Bone Joint Surg Br* 1994;76:647-653.

90. Eckstein F, Merz B, Muller-Gerbl M, et al. Morphomechanics of the humero-ulnar joint: II. Concave incongruity determines the distribution of load and subchondral mineralization. *Anat Rec* 1995;243:327-335.

91. Eckstein F, Lohe F, Schulte E, et al. Physiological incongruity of the humero-ulnar joint: a functional principle of optimized stress distribution acting upon articulating surfaces? *Anat Embryol (Berl)* 1993;188:449-455.

92. Collins KE, Cross AR, Lewis DD, et al. Comparison of the radius of curvature of the ulnar trochlear notch of Rottweilers and Greyhounds. *Am J Vet Res* 2001;62:968-973.

93. Dickomeit M, Maierl J, Bottcher P, et al. An anatomical and biomechanical analysis of the canine elbow joint. The 24th Congress of the European Association of Veterinary Anatomists (EAVA) 2002;52.

94. Kunzel W, Breit S, Probst A. Funktionell bedeutsame morphologische besonderheiten am olekranon des hundes. *Wien Tierarztl Mschr* 2002;89:157-162.

95. Probst A, Kunzel W, Breit S. The canine olecranon- are variations in shape of the articular surface incidental findings or expressions of different loading capacities? The 24th Congress of the European Association of Veterinary Anatomists (EAVA) 2002;53.

96. Grondalen J, Rorvik AM. Arthrosis in the elbow joint of young rapidly growing dogs. IV. Ununited anconeal process. A follow up investigation of operated dogs. *Nord Vet Med* 1980;32:212-218.

97. Grondalen J. Arthrosis in the elbow joint of young rapidly growing dogs. III. Ununited medial coronoid process of the ulna and osteochondritis dissecans of the humeral condyle. Surgical procedure for correction and postoperative investigation. *Nord Vet Med* 1979;31:520-527.

98. Rovesti GL, Fluckiger M, Margini A, et al. Fragmented coronoid process and incomplete ossification of the humeral condyle in a rottweiler. *Vet Surg* 1998;27:354-357.

99. Marcellin-Little DJ. Incomplete ossification of the humeral condyle in dogs. In: Bonagura JD, ed. *Kirk's Current Veterinary Therapy XIII*. Philadelphia: W. B. Saunders, 1999;1000-1004.

100. Robin D, Marcellin-Little DJ. Incomplete ossification of the humeral condyle in two Labrador retrievers. *J Small Anim Pract* 2001;42:231-234.

101. Rovesti GL, Biasibetti M, Schumacher A, et al. The use of computed tomography in the diagnostic protocol of the elbow in the dog: 24 joints. *Vet Comp Orthop Trauma* 2002;15:35-43.

102. Grondalen J, Lingaas F. Arthrosis in the elbow joint of young rapidly growing dogs: A genetic investigation. *J Small Anim Pract* 1991;32:460-464.

103. Guthrie S, Pidduck HO. Heritability of elbow osteochondrosis within a closed population of dogs. *J Small Anim Pract* 1990;31:93-96.

104. Padgett GA, Mostosky UV, Probst CW, et al. The inheritance of osteochondritis dissecans and fragmented coronoid process of the elbow joint in labrador retrievers. *J Am Anim Hosp Assoc* 1995;31:327-330.

105. Janutta V, Hamann H, Klein S, et al. Genetic analysis of three different classification protocols for the evaluation of elbow dysplasia in German shepherd dogs. *J Small Anim Pract* 2006;47:75-82.

106. Swenson L, Audell L, Hedhammar A. Prevalence and inheritance of and selection for elbow arthrosis in Bernese mountain dogs and Rottweilers in Sweden and benefit: cost analysis of a screening and control program. *J Am Vet Med Assoc* 1997;210:215-221.

107. Grondalen J. Arthrosis in the elbow joint of young rapidly growing dogs. VII. Occurrence in the Rottweiler breed. *Nord Vet Med* 1982;34:76-82.

108. Grondalen J, Lingaas F. Arthrosis of the elbow joint among Rottweiler dogs. Results from investigations into hereditary disposition. *Tijdschr Diergeneeskd* 1988;113 Suppl 1:49S-51S.

109. Studdert VP, Lavelle RB, Beilharz RG, et al. Clinical features and heritability of osteochondrosis of the elbow joint in Labrador retrievers. *J Small Anim Pract* 1992;32:557-563.

110. Beuing R, Mues CH, Tellhelm B, et al. Prevalence and inheritance of canine elbow dysplasia in German Rottweiler. *J Anim Breed Genet* 2000;117:375-383.

111. Guthrie S. Use of radiographic scoring technique for the assessment of dogs with elbow osteochondrosis. *J Small Anim Pract* 1989;30:639-644.

112. Meyer-Lindenberg A, Fehr M, Nolte I. Co-existence of ununited anconeal process and fragmented medial coronoid process of the ulna in the dog. *J Small Anim Pract* 2006;47:61-65.

113. van Ryssen B, van Bree H. Arthroscopic findings in 100 dogs with elbow lameness. *Vet Rec* 1997;140:360-362.

114. Meyer-Lindenberg A, Langhann A, Fehr M, et al. Prevalence of fragmented medial coronoid process of the ulna in lame adult dogs. *Vet Rec* 2002;151:230-234.

115. Everts RE, Hazewinkel HA, Rothuizen J, et al. Bone disorders in the dog: a review of modern genetic strategies to find the underlying causes. *Vet Q* 2000;22:63-70.

116. Maki K, Liinamo AE, Ojala M. Estimates of genetic parameters for hip and elbow dysplasia in Finnish Rottweilers. *J Anim Sci* 2000;78:1141-1148.

117. Lang J, Busato A, Baumgartner D, et al. Comparison of two classification protocols in the evaluation of elbow dysplasia in the dog. *J Small Anim Pract* 1998;39:169-174.

118. Mason TA, Lavelle RB, Skipper SC, et al. Osteochondrosis of the elbow joint in young dogs. *J Small Anim Pract* 1980;21:641-656.

119. (IEWG) IEWG. Elbow Protocol. 1999.

120. (OFA) OFfA. Elbow Registry. Columbia, MO, 1996.

121. Corley EA, Carlson WD. Radiographic, genetic and pathologic aspects of elbow dysplasia. *J Am Vet Med Assoc* 1965;147:1651.

122. Corley EA, Sutherland TM, Carlson WD. Genetic aspects of canine elbow dysplasia. *J Am Vet Med Assoc* 1968;153:543-547.

123. Kealy RD, Olsson SE, Monti KL, et al. Effects of limited food consumption on the incidence of hip dysplasia in growing dogs. *J Am Vet Med Assoc* 1992;201:857-863.

124. Hayes HM, Selby LA, Eilson GP, et al. Epidemiologic observations of canine elbow disease (emphasis on dysplasia). *J Am Anim Hosp Assoc* 1979;15:449-453.

125. Olsson SE. Pathophysiology, morphology, and clinical signs of osteochondrosis in the dog. In: Bojrab MS, Smeak DD,Bloomberg MS, eds. *Disease Mechanisms in Small Animal Surgery*. 2nd ed. Philadelphia: Lea & Febiger, 1993;777-796.

126. Guthrie S. Some radiographic and clinical aspects of ununited anconeal process. *Vet Rec* 1989;124:661-662.

127. Herron MR. Ununited anconeal process in the dog. *Vet Clin North Am* 1971;1:417-428.

128. Thacher C. Ununited anconeal process. In: Slatter D, ed. *Textbook of Small Animal Surgery*. 2nd ed. Philadelphia: W. B. Saunders, 1993;1977-1980.

129. Carlson WD. *Veterinary Radiology*. 2 ed. Philadelphia: Lea & Febiger, 1967.

130. Carlson WD, Severin G. Elbow dysplasia in the dog, A preliminary report. *J Am Vet Med Assoc* 1961;138:295.

131. Nap RC, Hazewinkel HA. Growth and skeletal development in the dog in relation to nutrition; a review. *Vet Q* 1994;16:50-59.

132. Richardson DC, Zentek J. Nutrition and osteochondrosis. *Vet Clin North Am Small Anim Pract* 1998;28:115-135.

133. Olsson SE. En ny typ av armbagledsdysplasi hos hund? En preliminar rapport. (A new type of elbow dysplasia in the dog. A preliminary report). *Svensk Vet-Tidn* 1974;26:152-157.

134. Bennett D, Duff SR, Kene RO, et al. Osteochondritis dissecans and fragmentation of the coronoid process in the elbow joint of the dog. *Vet Rec* 1981;109:329-336.

135. Reiland S. The effect of decreased growth rate on frequency and severity of osteochondrosis in pigs. *Acta Radiol Suppl* 1978;358:107-122.

136. Reiland S, Stromberg B, Olsson SE, et al. Osteochondrosis in growing bulls. Pathology, frequency and severity on different feedings. *Acta Radiol Suppl* 1978;358:179-196.

137. Poulos PW, Jr., Reiland S, Elwinger K, et al. Skeletal lesions in the broiler, with special reference to dyschondroplasia (osteochondrosis). Pathology, frequency and clinical significance in two strains of birds on high and low energy feed. *Acta Radiol Suppl* 1978;358:229-275.

138. Siffert RS. The osteochondroses. *Clin Orthop Relat Res* 1981:2-3.

139. Siffert RS. Classification of the osteochondroses. *Clin Orthop Relat Res* 1981:10-18.

140. Rejno S, Stromberg B. Osteochondrosis in the horse. II. Pathology. *Acta Radiol Suppl* 1978;358:153-178.

141. Stromberg B, Rejno S. Osteochondrosis in the horse. I. A clinical and radiologic investigation of osteochondritis dissecans of the knee and hock joint. *Acta Radiol Suppl* 1978;358:139-152.

142. Stromberg B. A review of the salient features of osteochondrosis in the horse. *Equine Vet J* 1979;11:211-214.

143. Patel N, Weiner SD. Osteochondritis dissecans involving the trochlea: report of two patients (three elbows) and review of the literature. *J Pediatr Orthop* 2002;22:48-51.

144. Grondalen J. Arthrosis with special reference to the elbow joint of young rapidly growing dogs. II. Occurrence, clinical and radiographical findings. *Nord Vet Med* 1979;31:69-75.

145. Johnston SA. Osteochondritis dissecans of the humeral head. *Vet Clin North Am Small Anim Pract* 1998;28:33-49.

146. Boudrieau RJ, Hohn RB, Bardet JF. Osteochondritis dissecans of the elbow in the dog. *J Am Anim Hosp Assoc* 1983;19:627-635.

147. Guthrie S, Plummer JM, Vaughan LC. Aetiopathogenesis of canine elbow osteochondrosis: a study of loose fragments removed at arthrotomy. *Res Vet Sci* 1992;52:284-291.

148. Olsson SE, Reiland S. The nature of osteochondrosis in animals. Summary and conclusions with comparative aspects on osteochondritis dissecans in man. *Acta Radiol Suppl* 1978;358:299-306.

149. Myers SL, Flusser D, Brandt KD, et al. Prevalence of cartilage shards in synovium and their association with synovitis in patients with early and endstage osteoarthritis. *J Rheumatol* 1992;19:1247-1251.

150. Baird DK, Hathcock JT, Kincaid SA, et al. Low-field magnetic resonance imaging of early subchondral cyst-like lesions in induced cranial cruciate ligament deficient dogs. *Vet Radiol Ultrasound* 1998;39:167-173.

151. Clanton TO, DeLee JC. Osteochondritis dissecans . History, pathophysiology and current treatment concepts. *Clin Orthop Relat Res* 1982:50-64.

152. Douglas G, Rang M. The role of trauma in the pathogenesis of the osteochondroses. *Clin Orthop Relat Res* 1981:28-32.

153. Nakano T, Aherne FX. Involvement of trauma in the pathogenesis of osteochondritis dissecans in swine. *Can J Vet Res* 1988;52:154-155.

154. Nakano T, Aherne FX. The pathogenesis of osteochondrosis--a hypothesis. *Med Hypotheses* 1994;43:1-5.

155. White SL, Rowland GN, Whitlock RH. Radiographic, macroscopic, and microscopic changes in growth plates of calves raised on hard flooring. *Am J Vet Res* 1984;45:633-639.

156. Stubbs MJ, Field LD, Savoie FH, 3rd. Osteochondritis dissecans of the elbow. *Clin Sports Med* 2001;20:1-9.

157. Shaughnessy WJ, Bianco AJ. Osteochondritis dissecans . In: Morrey BF, ed. *The elbow and its disorders*. 2nd ed. Philadelphia: W. B. Saunders, 1993;282-287.

158. Carlson CS, Hilley HD, Henrikson CK, et al. The ultrastructure of osteochondrosis of the articular-epiphyseal cartilage complex in growing swine. *Calcif Tissue Int* 1986;38:44-51.

159. Staiger BA, Beale BS. Use of arthroscopy for debridement of the elbow joint in cats. *J Am Vet Med Assoc* 2005;226:401-403, 376.

160. Ubbink GJ, van de Broek J, Hazewinkel HA, et al. Prediction of the genetic risk for fragmented coronoid process in labrador retrievers. *Vet Rec* 2000;147:149-152.

161. Morgan JP, Wind A, Davidson AP. Bone dysplasias in the labrador retriever: a radiographic study. *J Am Anim Hosp Assoc* 1999;35:332-340.

162. Ubbink GJ, van de Broek J, Hazewinkel HA, et al. Cluster analysis of the genetic heterogeneity and disease distributions in purebred dog populations. *Vet Rec* 1998;142:209-213.

163. Ubbink GJ, Hazewinkel HA, van de Broek J, et al. Familial clustering and risk analysis for fragmented coronoid process and elbow joint incongruity in Bernese Mountain Dogs in The Netherlands. *Am J Vet Res* 1999;60:1082-1087.

164. Lewis DD, Parker RB, Hager DA. Fragmented medial coronoid process of the canine elbow. *Compend Contin Educ Prac Vet* 1989;11:703-715.

165. Denny HR, Gibbs C. The surgical treatment of ostoechondritis dissecans and ununitied coronoid process in the canine elbow joint. *J Small Anim Pract* 1980;21:323-331.

166. Kapatkin AS, Volk SW, Keith DG, et al. Elbow dysplasia in a basset hound. *Vet Comp Orthop Trauma* 2003;16:11-15.

167. Henry WB, Jr. Radiographic diagnosis and surgical management of fragmented medial coronoid process in dogs. *J Am Vet Med Assoc* 1984;184:799-805.

168. Berzon JL, Quick CB. Fragmented coronoid process: Anatomical, clinical, and radiographic considerations with case analysis. *J Am Anim Hosp Assoc* 1980;16:241-251.

169. Tirgari M. Clinical radiographical and pathological aspects of arthritis of the elbow joint in dogs. *J Small Anim Pract* 1974;15:671-679.

170. Voorhout G, Hazewinkel HAW. Radiographic evaluation of the canine elbow joint with special reference to the medial humeral condyle and the medial coronoid process. *Vet Radiol* 1987;25:158-165.

171. Robins GM. Some aspects of the radiographic examination of the canine elbow joint. *J Small Anim Pract* 1980;21:417-428.

172. Remy D, Neuhart L, Fau D, et al. Canine elbow dysplasia and primary lesions in German shepherd dogs in France. *J Small Anim Pract* 2004;45:244-248.

173. Zentek J. [Skeletal diseases in young dogs: nutritionally determined pathogenesis]. *Dtsch Tierarztl Wochenschr* 1999;106:77-78.

174. Zentek J, Meyer H, Dammrich K. The effect of a different energy supply for growing Great Danes on the body mass and skeletal development. 3. Clinical picture and chemical studies of the skeleton. *Zentralbl Veterinarmed A* 1995;42:69-80.

175. Olsson SE. Lameness in the dog. A review of lesions causing osteoarthrosis of the shoulder, elbow, hip, stifle and hock joints. 42nd Annual Meeting of the American Animal Hospital Association 1975.

176. Bardet JF. Arthroscopy of the elbow in dogs. Part II: Cranial portals in the diagnosis and treatment of the lesions of the coronoid process. *Vet Comp Orthop Trauma* 1997;10:60-66.

177. Schwalder P. Osteochondrosekomplex am ellbogengelenk. Proc Annu Meet Schweiz Vereinig Kleintiermed 1990;52-64.

178. Setton LA, Mow VC, Muller FJ, et al. Altered structure-function relationships for articular cartilage in human osteoarthritis and an experimental canine model. *Agents Actions Suppl* 1993;39:27-48.

179. Fitzpatrick MN, Reuter R. Histopathology of cartilage and subchondral bone following subtotal coronoidectomy for the treatment of fragmented medial coronoid process. British Small Animal Veterinary Association (BSAVA) Congress 2004;586.

180. Preston CA, Schulz KS, Taylor KT, et al. In vitro experimental study of the effect of radial shortening and ulnar ostectomy on contact patterns in the elbow joint of dogs. *Am J Vet Res* 2001;62:1548-1556.

181. MacPherson GC, Lewis DD, Johnson KA, et al. Fragmented coronoid process associated with premature distal radial physeal closure in four dogs. *Vet Comp Orthop Trauma* 1992;5:93-99.

182. Bienz HA. Klinische and radiologische untersuchunger uber den fragmentievten processus coronoideus medialis in ellbogengelenk des berner sennenhunde und der anderen sennenhunde-vassen. Zurich, Switzerland: University of Zurich, 1985.

183. Nap RC. Pathophysiology and clinical aspects of canine elbow dysplasia. Abstract from the 7th Annual Meeting of the International Elbow Working Group 1995.

184. Pool RR. Unpublished necropsy study in 400 immature large breed dogs.: Department of Pathobiology and Population Medicine, College of Veterinary Medicine, Mississippi State University, MS, 2002.

185. Pool RR. Pathophysiology of elbow dysplasia- a new twist. 37th Annual Scientific Meeting of ACVS Veterinary Symposium- Small Animal Proceedings 2002;99-102.

186. Trostel CT. Canine lameness caused by developmental orthopedic diseases: Fragmented medial coronoid process and ununited anconeal process. *Compend Contin Educ Prac Vet* 2003;25:112-120.

187. Kramer A, Holsworth IG, Wisner ER, et al. Computed tomographic evaluation of canine radioulnar incongruence in vivo. *Vet Surg* 2006;35:24-29.

188. Gemmill TJ, Mellor DJ, Clements DN, et al. Evaluation of elbow incongruency using reconstructed CT in dogs suffering fragmented coronoid process. *J Small Anim Pract* 2005;46:327-333.

189. Viehmann B, Waibl H, Brunnberg L. Computergestutzte auswertung von rontgenbildern zur erfassung von parametern der ellbogengelenkdysplasie. Teil 1: Incisura trochlearis ulnae. *Kleintierprax* 1999;44:595-606.

190. Eckstein F, Lohe F, Hillebrand S, et al. Morphomechanics of the humero-ulnar joint: I. Joint space width and contact areas as a function of load and flexion angle. *Anat Rec* 1995;243:318-326.

191. Mason DR, Schulz KS, Fujita Y, et al. In vitro force mapping of normal canine humeroradial and humeroulnar joints. *Am J Vet Res* 2005;66:132-135.

192. Guthrie S, Buckland-Wright JC, Vaughan LC. Microfocal radiography as an aid to the diagnosis of canine elbow osteochondrosis. *J Small Anim Pract* 1991;32:503-508.

193. Hazewinkel HA, Voorhout G. [Examination and treatment of a loose medial coronoid process in dogs]. *Tijdschr Diergeneeskd* 1986;111:1234-1245.

194. Read RA, Armstrong SJ, Black AP, et al. Relationship between physical signs of elbow dysplasia and radiographic score in growing Rottweilers. *J Am Vet Med Assoc* 1996;209:1427-1430.

195. van Bree HJ, van Ryssen B. Diagnostic and surgical arthroscopy in osteochondrosis lesions. *Vet Clin North Am Small Anim Pract* 1998;28:161-189.

196. Keller GG, Kreeger JM, Mann FA, et al. Correlation of radiographic, necropsy and histologic findings in 8 dogs with elbow dysplasia. *Vet Radiol Ultrasound* 1997;38:272-276.

197. Miyabayashi T, Takiguchi M, Schrader SC, et al. Radiographic anatomy of the medial coronoid process of dogs. *J Am Anim Hosp Assoc* 1995;31:125-132.

198. van Bree H, van Ryssen B, Simoens P. Correlation between radiographic and arthroscopic findings in dogs with elbow arthrosis. 1st Conference of the European Veterinary Radiological Association 1992.

199. van Bree HJ, van Ryssen B. [Value of arthroscopy in the diagnosis and treatment of osteochondrosis in dogs]. *Tijdschr Diergeneeskd* 1997;122:710-714.

200. van Bree H, van Ryssen B. Imaging the canine elbow: Radiography, computed tomography and arthroscopy. *Vet Ann* 1995;35:118-129.

201. Vaughan LC, Robins GM. Surgical remodelling of the femoral trochlea: an experimental study. *Vet Rec* 1975;96:447-450.

202. Buckwalter JA, Hunziker EB. Orthopaedics. Healing of bones, cartilages, tendons, and ligaments: a new era. *Lancet* 1996;348 Suppl 2:sII18.

203. Shapiro F, Koide S, Glimcher MJ. Cell origin and differentiation in the repair of full-thickness defects of articular cartilage. *J Bone Joint Surg Am* 1993;75:532-553.

204. McIlwraith CW, Nixon AJ. Joint resurfacing- Attempts at repairing articular cartilage defects. In: Trotter GW,McIlwraith CW, eds. *Joint Diseases in the Horse*. 1st ed. Philadelphia: W. B. Saunders, 1996;317.

205. Salter RB. The physiologic basis of continuous passive motion for articular cartilage healing and regeneration. *Hand Clin* 1994;10:211-219.

206. Salter RB, Simmonds DF, Malcolm BW, et al. The biological effect of continuous passive motion on the healing of full-thickness defects in articular cartilage. An experimental investigation in the rabbit. *J Bone Joint Surg Am* 1980;62:1232-1251.

207. Probst CW, Flo GL, McLoughlin MA. A simple medial approach to the canine elbow for treatment of fragmented coronoid process and osteochondritis dissecans . *J Am Anim Hosp Assoc* 1989;25:331-334.

208. Bouck GR, Miller CW, Taves CL. A comparison of surgical and medical treatment of fragmented coronoid process and osteochondritis dissecans of the canine elbow. *Vet Comp Orthop Trauma* 1995;8:177-183.

209. Huibregtse BA, Johnson AL, Muhlbaeur MC, et al. The effect of treatment of fragmented medial coronoid process on the development of osteoarthritis of the elbow. *J Am Anim Hosp Assoc* 1994;30:190-195.

210. Ness MG. Treatment of fragmented coronoid process in young dogs by proximal ulnar osteotomy. *J Small Anim Pract* 1998;39:15-18.

211. Tobias TA, Miyabayaski T, Olmstead MI. Surgical removal of fragmented medial coronoid process in the dog: Comparative effects of surgical approach and age at time of surgery. *J Am Anim Hosp Assoc* 1994;30:360-368.

212. Meyer-Lindenberg A, Fehr M, Nolte I. Short- and long-term results after surgical treatment of ununited anconeal process in 17 dogs. *Vet Comp Orthop Trauma* 2001;14:101-110.

213. Pluhar GE. Surgical management of elbow dysplasia. 37th Annual Scientific Meeting of the ACVS Veterinary Symposium 1992;107-109.

214. Roy RG, Wallace LJ, Johnston GR. A retrospective long-term evaluation of ununited anconeal excision on the canine elbow. *Vet Comp Orthop Trauma* 1994;7:94-97.

215. Krotscheck U, Hulse DA, Bahr AM. Ununited anconeal process: Lag-screw fixation with proximal ulnar osteotomy. *Vet Comp Orthop Trauma* 2000;13:212-216.

216. Sinibaldi KR, Arnoczky SP. Surgical removal of the ununited anconeal process in the dog. *J Am Anim Hosp Assoc* 1975;11:192-198.

217. Beale BS, Hulse DA, Schulz KS, et al. Arthroscopically assisted surgery of the elbow joint. In: Kersey RR,LeMelledo D, eds. *Small Animal Arthroscopy*. Philadelphia: W. B. Saunders, 2003;51-79.

218. van Ryssen B, van Bree H, Simoens P. Elbow arthroscopy in clinically normal dogs. *Am J Vet Res* 1993;54:191-198.

219. Meyer-Lindenberg A, Staszyk C, Gasse H, et al. Caudomedial approach for removal of an ununited anconeal process and assessment of the medial coronoid process of the ulna. *J Vet Med A Physiol Pathol Clin Med* 2002;49:277-280.

220. Bubenik LJ, Johnson SA, Smith MM, et al. Evaluation of lameness associated with arthroscopy and arthrotomy of the normal canine cubital joint. *Vet Surg* 2002;31:23-31.

221. Schulz KS. Pressure, arthritis, and the canine elbow. 37th Annual Scientific Meeting of the ACVS Veterinary Symposium 2002;249-253.

222. Flo GL. Surgical removal of fragmented coronoid processes and fractured anconeal process in an older dog with evidence of severe degenerative joint disease. *J Am Vet Med Assoc* 1998;213:1780-1782, 1754.

223. Theyse LFH, Hazewinkel HAW, van den Brom WE. Force plate analyses before and after surgical treatment of unilateral fragmented coronoid process. *Vet Comp Orthop Trauma* 2000;13:135-140.

224. Puccio M, Marino DJ, Stefanacci JD, et al. Clinical evaluation and long-term follow-up of dogs having coronoidectomy for elbow incongruity. *J Am Anim Hosp Assoc* 2003;39:473-478.

225. Hazewinkel HA, Meij BP, Theyse LF. Surgical treatment of elbow dysplasia. *Vet Q* 1998;20 Suppl 1:S29-31.

226. Bardet JF, Bureau S. Fragmentation of the coronoid process in dogs. A case control study of 83 elbows treated by shortening osteotomy of the proximal ulna. *Pratique Medicale & Chirurgicale de l'Animal de Compagnie* 1996;31:451-463.

227. Bardet JF. Treatment of the coronoid process fragmentation in the dog. Proceedings of the 6th European Society of Veterinary Orthopaedics and Traumatology Conference 1992;15.

228. Thomson MJ, Robins GM. Osteochondrosis of the elbow: a review of the pathogenesis and a new approach to treatment. *Aust Vet J* 1995;72:375-378.

229. Snelling SR, Lavelle RB. Radiographic changes in elbow dysplasia following ulnar osteotomy--a case report and review of the literature. *Aust Vet J* 2004;82:278-281.

230. Berry CR. Radiology Corner: Evaluation of the canine elbow for fragmented medial coronoid process. *Vet Radiol Ultrasound* 1992;33:273-276.

231. Murphy ST, Lewis DD, Shiroma JT, et al. Effect of radiographic positioning on interpretation of cubital joint congruity in dogs. *Am J Vet Res* 1998;59:1351-1357.

232. Wosar MA, Lewis DD, Neuwirth L, et al. Radiographic evaluation of elbow joints before and after surgery in dogs with possible fragmented medial coronoid process. *J Am Vet Med Assoc* 1999;214:52-58.

233. Wood AK, McCarthy PH, Howlett CR. Anatomic and radiographic appearance of a sesamoid bone in the tendon of origin of the supinator muscle. *Am J Vet Res* 1985;46:2043-2047.

234. Kippenes H, Johnston G. Diagnostic imaging of osteochondrosis. *Vet Clin North Am Small Anim Pract* 1998;28:137-160.

235. Snaps FR, Balligand MH, Saunders JH, et al. Comparison of radiography, magnetic resonance imaging, and surgical findings in dogs with elbow dysplasia. *Am J Vet Res* 1997;58:1367-1370.

236. Fox SM, Roberts RE. Linear tomography in diagnosing fragmented coronoid processes in canine elbows. *Compend Contin Educ Prac Vet* 1987;9:61-65.

237. Knox VWt, Sehgal CM, Wood AK. Correlation of ultrasonographic observations with anatomic features and radiography of the elbow joint in dogs. *Am J Vet Res* 2003;64:721-726.

238. Haudiquet PR, Marcellin-Little DJ, Stebbins ME. Use of the distomedial-proximolateral oblique radiographic view of the elbow joint for examination of the medial coronoid process in dogs. *Am J Vet Res* 2002;63:1000-1005.

239. Marcellin-Little DJ, Strebbins ME, Haudiquet P. The mediodistal to lateroproximal oblique (MEDLAP) radiographic view enhances visualization of the medial coronoid process in dogs. 11th Annual ACVS Veterinary Symposium 2001.

240. Walde I, Tellhelm B. Fragmented medial coronoid process of the ulna (FCP) and osteochondritis dissecans (OCD) of the canine elbow and hock joint: A review of literature, diagnosis, and therapy. *Wien Tierarztl Monatsschr* 1991;78:414-421.

241. Yovich JC, Read RA. Traumatic fracture of the medial coronoid process in two dogs. *Vet Comp Orthop Trauma* 1994;7:173-176.

242. Gortz K, van Ryssen B, Taeymans O, et al. Traumatic fracture of the medial coronoid process in a dog. *Vet Comp Orthop Trauma* 2004;17:159-162.

243. Mason DR, Schulz KS, Samii VF, et al. Sensitivity of radiographic evaluation of radio-ulnar incongruence in the dog in vitro. *Vet Surg* 2002;31:125-132.

244. Blond L, Dupuis J, Beauregard G, et al. Sensitivity and specificity of radiographic detection of canine elbow incongruence in an in vitro model. *Vet Radiol Ultrasound* 2005;46:210-216.

245. Blond L, Dupuis J, Beauregard G, et al. Sensitivity and specificity of radiology in the detection of canine elbow incongruence in an in vitro model. Abstract from the annual scientific conference of the American College of Veterinary Radiology. *Vet Radiol Ultrasound* 2004;45:264.

246. DeCamp CE, Soutas-Little RW, Hauptman J, et al. Kinematic gait analysis of the trot in healthy greyhounds. *Am J Vet Res* 1993;54:627-634.

247. Maierl J, Hecht S, Bottcher P, et al. New aspects of the functional anatomy of the canine elbow joint. 10th ESVOT Congress 2000;90.

248. Samoy Y, van Ryssen B, Gielen IM, et al. Elbow incongruity in the dog: Review of the literature. *Vet Comp Orthop Trauma* 2006;19:1-8.

249. van Bree H, van Ryssen B. Diagnostic imaging of the canine elbow joint including radiology, arthroscopy and computed tomography. Abstract from the 10th meeting of the International Veterinary Radiology Association, Philadelphia, PA. *Vet Radiol Ultrasound* 1994;35:248.

250. Gibbs C. Linear Tomography in Veterinary Practice. *Vet Radiol Ultrasound* 1973;14:37-44.

251. Berry CR, Koblik PD. Evaluation of survey radiography, linear tomography, and computed tomography for detecting experimental lesions of the cribriform plate in dogs. *Vet Radiol Ultrasound* 1990;31:146-154.

252. Jeffcott LB. Radiographic appearance of equine lumbosacral and pelvic abnormalities by linear tomography. *Vet Radiol Ultrasound* 1983;24:201-213.

253. Jeffcott LB. Technique of linear tomography for the pelvic region of the horse. *Vet Radiol Ultrasound* 1983;24:194-200.

254. Voorhout G, Rijnberk A. Cisternography combined with linear tomography for visualization of pituitary lesions in dogs with pituitary-dependent hyperadrenocorticism. *Vet Radiol Ultrasound* 1990;31:74-78.

255. Voorhout G. Cisternography combined with linear tomography for visualization of the pituitary gland in healthy dogs. A Comparison with Computed Tomography. *Vet Radiol Ultrasound* 1990;31:68-73.

256. van Bree H. Epinephrine enhanced positive contrast shoulder arthrography in the dog. *Zentralbl Veterinarmed A* 1989;36:687-691.

257. van Bree H, van Ryssen B, Tshamala M, et al. Comparison of the nonionic contrast agents, iopromide and iotrolan, for positive-contrast arthrography of the scapulohumeral joint in dogs. *Am J Vet Res* 1992;53:1622-1626.

258. van Bree H. Evaluation of the prognostic value of positive-contrast shoulder arthrography for bilateral osteochondrosis lesions in dogs. *Am J Vet Res* 1990;51:1121-1125.

259. van Bree H, Verhaeghe B, Maenhout D. Positive contrast arthrography of the dog's shoulder with meglumine-sodium diatrizoate. *Zentralbl Veterinarmed A* 1989;36:421-430.

260. van Bree H. Comparison of the diagnostic accuracy of positive-contrast arthrography and arthrotomy in evaluation of osteochondrosis lesions in the scapulohumeral joint in dogs. *J Am Vet Med Assoc* 1993;203:84-88.

261. Suter PF, Carb AV. Shoulder arthrography in dogs- radiographic anatomy and clinical application. *J Small Anim Pract* 1969;10:407-413.

262. Story EC. Prognostic value of arthrography in canine shoulder osteochondrosis (osteochondritis dissecans) . *Vet Clin North Am* 1978;8:301-308.

263. Pavlov H, Ghelman B, Warren RF. Double-contrast arthrography of the elbow. *Radiology* 1979;130:87-95.

264. Hudson TM. Elbow arthrography. *Radiol Clin North Am* 1981;19:227-241.

265. Lowry JE. Radiographic anatomy and technique for arthrography of the cubital joint in clinically normal dogs. *J Am Vet Med Assoc* 1993;203:72-77.

266. Rantanen NW. Diagnostic Ultrasound. *Vet Clin North Am Equine Pract* 1986;2:127-226.

267. Spaulding K. Ultrasonic anatomy of the tendons and ligaments in the distal metacarpal-metatarsal region of the equine limb. *Vet Radiol Ultrasound* 1984;25:155-166.

268. Dik KJ. Ultrasonography of the equine crus. *Vet Radiol Ultrasound* 1993;34:28-34.

269. Dik KJ. Utrasonography of the equine tarsus. *Vet Radiol Ultrasound* 1993;34:36-43.

270. Pugh CR. A simple method to document the location of ultrasonographically detected equine tendon lesions. *Vet Radiol Ultrasound* 1993;34:211-212.

271. Long CD, Nyland TG. Ultrasonographic evaluation of the canine shoulder. *Vet Radiol Ultrasound* 1999;40:372-379.

272. Kramer M, Gerwing M. [The importance of sonography in orthopedics for dogs]. *Berl Munch Tierarztl Wochenschr* 1996;109:130-135.

273. Kramer M, Gerwing M, Sheppard C, et al. Ultrasonography for the diagnosis of diseases of the tendon and tendon sheath of the biceps brachii muscle. *Vet Surg* 2001;30:64-71.

274. Rivers B, Wallace LJ, Johnson GR. Biceps tenosynovitis in the dog: Radiographic and sonographic findings. *Vet Comp Orthop Trauma* 1992;5:51-57.

275. Kramer M, Stengel H, Gerwing M, et al. Sonography of the canine stifle. *Vet Radiol Ultrasound* 1999;40:282-293.

276. Reed AL, Payne JT, Constantinescu GM. Ultrasonographic anatomy of the normal canine stifle. *Vet Radiol Ultrasound* 1995;36:315-321.

277. Gnudi G, Bertoni G. Echographic examination of the stifle joint affected by cranial cruciate ligament rupture in the dog. *Vet Radiol Ultrasound* 2001;42:266-270.

278. Kramer A, Schimke E, Gerwing M, et al. Diseases of the achilles tendon in dogs and cats. *Tierarztl Prax* 1998;26:238-246.

279. Lamb CR, Duvernois A. Ultrasonographic anatomy of the normal canine calcaneal tendon. *Vet Radiol Ultrasound* 2005;46:326-330.

280. Lamb CR, Wong K. Ultrasonographic anatomy of the canine elbow. *Vet Radiol Ultrasound* 2005;46:319-325.

281. Garcia T, Hornof WJ, Insana MF. On the ultrasonic properties of tendon. *Ultrasound Med Biol* 2003;29:1787-1797.

282. Michele U, Gerwing M, Kramer M. Pathologic sonographical findings in the canine elbow. Abstract from the Annual Meeting of the European Association of Veterinary Diagnostic Imaging. Vienna, Austria. *Vet Radiol Ultrasound* 1999;40:559.

283. Kramer M, Gerwing M, Hach V, et al. Sonography of the musculoskeltal system in dogs and cats. *Vet Radiol Ultrasound* 1997;38:139-149.

284. Berg J, Lamb CR, O'Callaghan MW. Bone scintigraphy in the initial evaluation of dogs with primary bone tumors. *J Am Vet Med Assoc* 1990;196:917-920.

285. Forrest LJ, Thrall DE. Bone scintigraphy for metastasis detection in canine osteosarcoma. *Vet Radiol Ultrasound* 1994;35:124-130.

286. Lamb CR, Berg J, Bengtson AE. Preoperative measurement of canine primary bone tumors, using radiography and bone scintigraphy. *J Am Vet Med Assoc* 1990;196:1474-1478.

287. Clark GN, Boudrieau RJ, O'Callaghan MW. Scintigraphic evaluation of total hip arthroplasties using 99m technetium methyldiphosphonate in 10 dogs. *Vet Comp Orthop Trauma* 1994;7:60-61.

288. Goggin JM, Hoskinson JJ, Carpenter JW, et al. Scintigraphic assessment of distal extremity perfusion in 17 patients. *Vet Radiol Ultrasound* 1997;38:211-220.

289. Harari J, Roberts G, DeHaan D. Scintigraphic evaluation of tissue viability after gunshot injury in a dog. *J Am Vet Med Assoc* 1992;200:1507-1508.

290. Lamb CR. Bone scintigraphy in small animals. *J Am Vet Med Assoc* 1987;191:1616-1622.

291. Chambers MD. Bone imaging: The diphosphonates. In: Daniel GB,Berry CR, eds. *Handbook of Veterinary Nuclear Medicine*. Raleigh, NC: North Carolina State University, 1996;49-59.

292. Hoskinson JJ, Tucker RL. Diagnostic imaging of lameness in small animals. *Vet Clin North Am Small Anim Pract* 2001;31:165-180, vii.

293. Schwarz T, Johnson VS, Voute L, et al. Bone scintigraphy in the investigation of occult lameness in the dog. *J Small Anim Pract* 2004;45:232-237.

294. Lamb CR. Non-skeletal distribution of bone-seeking radiopharmaceuticals. *Vet Radiol* 1990;31:246-253.

295. Snaps FR, Saunders JH, Park RD, et al. Comparison of spin echo, gradient echo and fat saturation magnetic resonance imaging sequences for imaging the canine elbow. *Vet Radiol Ultrasound* 1998;39:518-523.

296. Wayne JS, Kraft KA, Shields KJ, et al. MR imaging of normal and matrix-depleted cartilage: correlation with biomechanical function and biochemical composition. *Radiology* 2003;228:493-499.

297. Carrino JA, Smith DK, Schweitzer ME. MR Arthrography of the Elbow and Wrist. *Semin Musculoskelet Radiol* 1998;2:397-414.

298. Kaplan LJ, Potter HG. MR imaging of ligament injuries to the elbow. *Magn Reson Imaging Clin N Am* 2004;12:221-232, v-vi.

299. Chung CB, Chew FS, Steinbach L. MR imaging of tendon abnormalities of the elbow. *Magn Reson Imaging Clin N Am* 2004;12:233-245, vi.

300. Kijowski R, Tuite M, Sanford M. Magnetic resonance imaging of the elbow. Part I: normal anatomy, imaging technique, and osseous abnormalities. *Skeletal Radiol* 2004;33:685-697.

301. Kijowski R, Tuite M, Sanford M. Magnetic resonance imaging of the elbow. Part II: Abnormalities of the ligaments, tendons, and nerves. *Skeletal Radiol* 2005;34:1-18.

302. Snaps FR, Park RD, Saunders JH, et al. Magnetic resonance arthrography of the cubital joint in dogs affected with fragmented medial coronoid processes. *Am J Vet Res* 1999;60:190-193.

303. Janach KJ, Breit SM, Kunzel WW. Assessment of the geometry of the cubital (elbow) joint of dogs by use of magnetic resonance imaging. *Am J Vet Res* 2006;67:211-217.

304. Tidwell AS, Jones JC. Advanced imaging concepts: a pictorial glossary of CT and MRI technology. *Clin Tech Small Anim Pract* 1999;14:65-111.

305. Disler DG. Fat-suppressed three-dimensional spoiled gradient-recalled MR imaging: assessment of articular and physeal hyaline cartilage. *AJR Am J Roentgenol* 1997;169:1117-1123.

306. Disler DG, McCauley TR, Kelman CG, et al. Fat-suppressed three-dimensional spoiled gradient-echo MR imaging of hyaline cartilage defects in the knee: comparison with standard MR imaging and arthroscopy. *AJR Am J Roentgenol* 1996;167:127-132.

307. Disler DG, McCauley TR, Wirth CR, et al. Detection of knee hyaline cartilage defects using fat-suppressed three-dimensional spoiled gradient-echo MR imaging: comparison with standard MR imaging and correlation with arthroscopy. *AJR Am J Roentgenol* 1995;165:377-382.

308. Disler DG, Recht MP, McCauley TR. MR imaging of articular cartilage. *Skeletal Radiol* 2000;29:367-377.

309. Eckstein F, Schnier M, Haubner M, et al. Accuracy of cartilage volume and thickness measurements with magnetic resonance imaging. *Clin Orthop Relat Res* 1998:137-148.

310. Eckstein F, Adam C, Sittek H, et al. Non-invasive determination of cartilage thickness throughout joint surfaces using magnetic resonance imaging. *J Biomech* 1997;30:285-289.

311. Fujita Y, Schulz KS, Mason DR, et al. Effect of humeral osteotomy on joint surface contact in canine elbow joints. *Am J Vet Res* 2003;64:506-511.

312. van Bree H, van Ryssen B, Degryse H, et al. Magnetic resonance arthrography of the scapulohumeral joint in dogs, using gadopentetate dimeglumine. *Am J Vet Res* 1995;56:286-288.

313. Grainger AJ, Elliott JM, Campbell RS, et al. Direct MR arthrography: A review of current use. *Clin Radiol* 2000;55:163-176.

314. Cotten A, Boutin RD, Resnick D. Normal anatomy of the elbow on conventional MR imaging and MR arthrography. *Semin Musculoskelet Radiol* 1998;2:133-140.

315. Yao L, Gentili A, Seeger LL. Saline versus gadolinium-enhanced magnetic resonance arthrography of porcine cartilage. *Acad Radiol* 1997;4:127-131.

316. Zanetti M, Hodler J. Contrast media in MR arthrography of the glenohumeral joint: intra-articular gadopentetate vs saline: preliminary results. *Eur Radiol* 1997;7:498-502.

317. van Bree H, Degryse H, van Ryssen B, et al. Pathologic correlations with magnetic resonance images of osteochondrosis lesions in canine shoulders. *J Am Vet Med Assoc* 1993;202:1099-1105.

318. Stickle RL, Hathcock JT. Interpretation of computed tomographic images. *Vet Clin North Am Small Anim Pract* 1993;23:417-435.

319. Braden TD, Stickle RL, Dejardin LM, et al. The use of computed tomography in fragmented coronoid disease: A case report. *Vet Comp Orthop Trauma* 1994;7:40-44.

320. Holsworth IG, Wisner ER, Scherrer WE, et al. Accuracy of Computerized Tomographic Evaluation of Canine Radio-Ulnar Incongruence In Vitro. *Vet Surg* 2005;34:108-113.

321. Gemmill TJ, Hammond G, Mellor D, et al. Use of reconstructed computed tomography for the assessment of joint spaces in the canine elbow. *J Small Anim Pract* 2006;47:66-74.

322. Marcellin-Little DL, Roe SC, DeYoung DJ. What is your diagnosis? Faint vertical condylar radiolucency, secondary to incomplete ossification of the humeral condyle. *J Am Vet Med Assoc* 1996;209:727-728.

323. Gielen IM, van Ryssen B, Buijtels J, et al. Canine elbow incongruity evaluated with computerized tomography, radiography and arthroscopy. Annual Meeting of the EAVDI and ECVDI 2001;359.

324. Samii VF, Dyce J. Computed tomographic arthrography of the normal canine stifle. *Vet Radiol Ultrasound* 2004;45:402-406.

325. Dubberley JH, Faber KJ, Patterson SD, et al. The detection of loose bodies in the elbow: the value of MRI and CT arthrography. *J Bone Joint Surg Br* 2005;87:684-686.

326. Waldt S, Bruegel M, Ganter K, et al. Comparison of multislice CT arthrography and MR arthrography for the detection of articular cartilage lesions of the elbow. *Eur Radiol* 2005;15:784-791.

327. Seeram E. Instrumentation. *Computed Tomography: Physical Principles, Clinical Applications, and Quality Control* 2ed. Philadelphia: W.B. Saunders Company, 2001;111-130.

328. Barnes GT, Lakshminarayanan AV. Computed tomography: Physical principles and image quality considerations. In: Lee JKT, Sagel SS,Stanley RJ, eds. *Computed Body Tomography with MRI Correlation*. 2 ed. New York: Raven Press, 1989;1-21, 31-37.

329. Curry TS, Dowdey JE, Murray RC. *Christensen's Physics of Diagnostic Radiology.* 4 ed. Philadelphia: Lea & Febiger, 1990.

330. Bushberg JT, Seibert JA, Leidholdt EM, et al. *The Essential Physics of Medical Imaging*. 2 ed. Philadelphia: Lippincott Williams & Wilkins, 2002.

331. Hathcock JT, Stickle RL. Principles and concepts of computed tomography. *Vet Clin North Am Small Anim Pract* 1993;23:399-415.

332. Jones JC, Wilson ME, Bartels JE. A review of high resolution computed tomography and a proposed technique for regional examination of the canine lumbosacral spine. *Vet Radiol Ultrasound* 1994;35:339-346.

333. Correia JA, Davis KR, Kharasch M, et al. Production of thin CT sections and coronal and sagittal images by spatial filtering. *Journal of Computer Assisted Tomography* 1980;4:83-90.

334. Mayo JR, Webb WR, Gould R, et al. High-resolution CT of the lungs: An optimal approach. *RSNA* 1987;163:507-510.

335. Twible DA, Judy PF, Swensson RG. Effects of the CT display window on detectability of large and small lesions. Society of Photo-optical Instrumentation and Engineering 1984;204-207.

336. Warren RC, Pandya YV. Effect of window width and viewing distance in CT display. *Br J Radiol* 1982;55:72-74.

337. Goodenough DJ. Assessment of image quality in diagnostic imaging systems. In: Hay GA, ed. *Medical Images: Formation, Perception, and Measurement*. London: Institute of Physics and John Wiley & Sons, 1976;263-277.

338. Warren RC. Detectability of low-contrast features in computed tomography. *Phys Med Biol* 1984;29:1-13.

339. Zwirewich CV, Terriff B, Muller NL. High-spatial-frequency (bone) algorithm improves quality of standard CT of the thorax. *AJR Am J Roentgenol* 1989;153:1169-1173.

340. Zerhouni EA, Spivey JF, Morgan RH, et al. Factors influencing quantitative CT measurements of solitary pulmonary nodules. *J Comput Assist Tomogr* 1982;6:1075-1087.

341. Stern EJ, Frank MS, Godwin JD. Chest computed tomography display preferences. Survey of thoracic radiologists. *Invest Radiol* 1995;30:517-521.

342. Fishman EK, Ney DR, Kawashima A, et al. Effect of image display on the quality of multiplanar reconstruction of computed tomography data. *Invest Radiol* 1993;28:146-149.

343. Wagner RC, Brown DG, Pastel MS. Application of information theory to the assessment of computed tomography. *Medical Physics* 1979;6:83-94.

344. Joseph P, M., Hilal SK, Schultz RA, et al. Clinical and experimental investigation of a smoothed CT reconstruction algorithm. *Radiology* 1980;134:507-516.

345. Krupinski EA. The future of image perception in radiology: Synergy between humans and computers. *Acad Radiol* 2003;10:1-3.

346. Schwencke M, van den Brom WE, Hazewinkel HAW. Morphological measurements for arthrosis risk in elbow dysplasia: a new method? *Vet Comp Orthop Trauma* 2004;17:225-231.

347. Gemmill T. Completing the picture: use of CT to investigate elbow dysplasia. *J Small Anim Pract* 2004;45:429-430.

348. Barnes JE. Characteristics and control of contrast in CT. *Radiographics* 1992;12:825-837.

349. Loo LD, Doi K, Metz CE. A comparison of physical image quality indices and observer performance in the radiographic detection of nylon beads. *Phys Med Biol* 1984;29:837-856.

350. Welsh EM, Gettinby G, Nolan A. Comparison of a visual analogue scale and numerical rating scale for assessment of lameness, using sheep as a model. *Am J Vet Res* 1993;54:976-983.

351. Zisapel N, Nir T. Determination of the minimal clinically significant difference on a patient visual analog sleep quality scale. *J Sleep Res* 2003;12:291-298.

352. Hudson JT, Slater MR, Taylor L, et al. Assessing repeatability and validity of a visual analogue scale questionnaire for use in assessing pain and lameness in dogs. *Am J Vet Res* 2004;65:1634-1643.

353. Rohleder JJ, Jones JC, Duncan RB, et al. Comparative performance of radiography and computed tomography in the diagnosis of middle ear disease in 31 dogs. *Vet Radiol Ultrasound* 2006;47:45-52.

354. MacDonald NJ, Burton CA, White RN. Comparison of visual analog and numeric scoring scales for assessing intraoperative mesenteric portovenography. *Vet Radiol Ultrasound* 2002;43:534-540.

355. Ishida M, Doi K, Loo LN, et al. Digital image processing: Effect on detectability of simulated low-contrast radiographic patterns. *Radiology* 1984;150:569-575.

APPENDIX 1

CT CHARACTERISTICS OF THE NORMAL CANINE ELBOW

(Opposing page) Transverse images of an elbow at the level of the MCP (A-C) and humeral condyle (D-F); dorsal plane images of the elbow at the level of the MCP (G-I); and sagittal plane images of the elbow (J-L). Images in the column 1 are displayed in a window width of 1500 HU; column 2 in 2500 HU; and column 3 in 3500 HU.

1 2 3

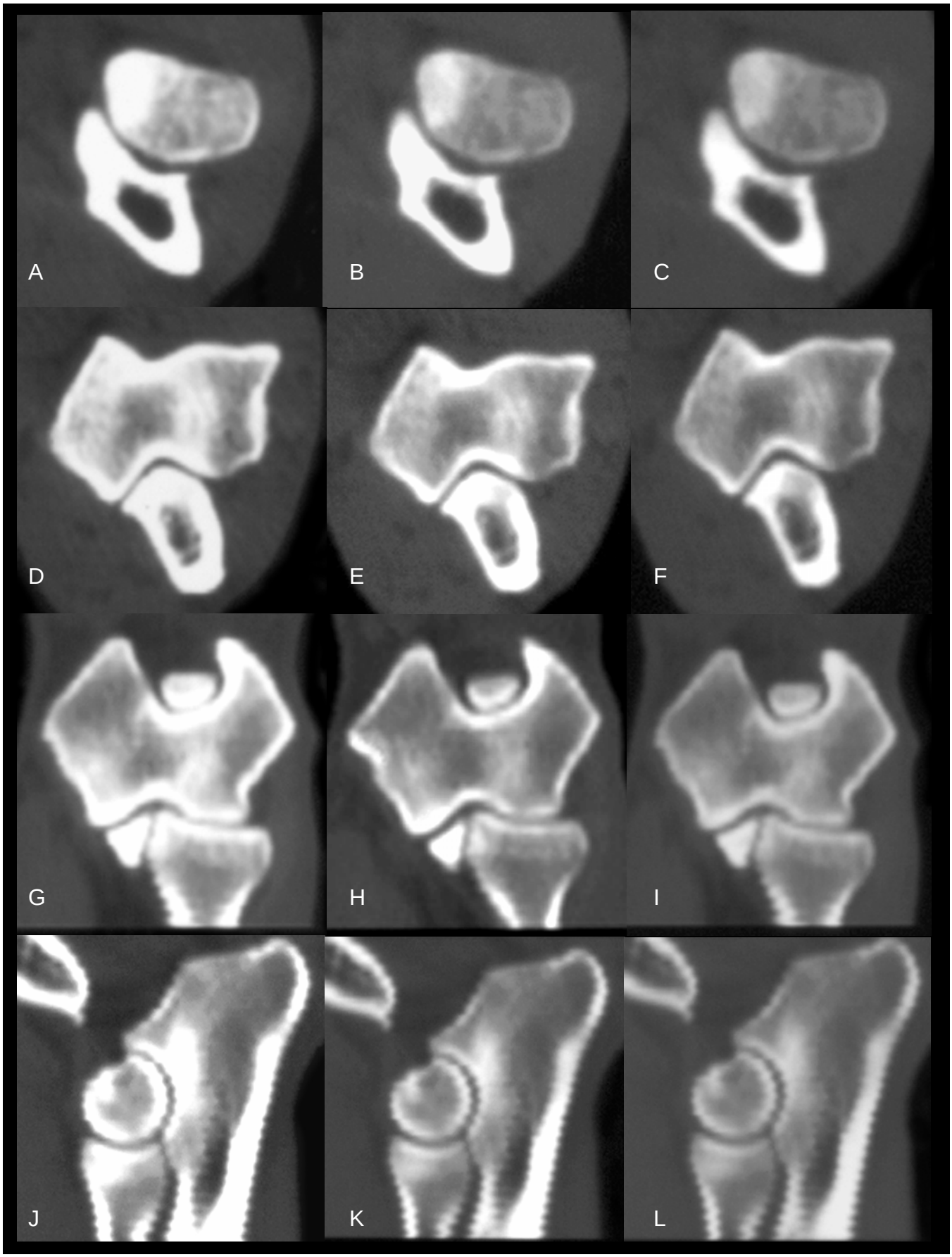

APPENDIX 2

SECTIONAL ANATOMY OF THE ELBOW

TRANSVERSE PLANE
Orientation is distal to proximal

AC- anconeus m.
AP- anconeal process of ulna
B- biceps brachii m.
BA- brachial artery, vein, and nerve
BB- tendons of biceps and brachialis mm.
BR- brachialis m.
C- capitulum humeri
CDE- common digital extensor m.
CL- lateral collateral ligament
CV- cephalic vein
DDF- deep digital flexor m.
ECR- extensor carpi radialis m.
EX- origin of carpal extensor mm.
FCR- flexor carpi radialis m.
FCU- flexor carpi ulnaris m.
FL- origin of carpal flexor mm.
H- humerus
HU- humeroulnar joint space
JC- joint capsule
LCP- lateral coronoid process of ulna
LDE- lateral digital extensor m.
LE- lateral epicondyle of humerus
MA- median artery, vein, and nerve
MCP- medial coronoid process of ulna
ME- medial epicondyle of humerus
MT- medial head of triceps m.
O- olecranon of ulna
OF- olecranon fossa of humerus
OL- oblique ligament
PQ- pronator quadratus m.
PT- pronator teres m.
R- radius
RI- radial incisure of ulna
RU- radioulnar joint space
SB- subtendinous bursa
SDF- superficial digital flexor m.
SU- supinator m.
T- trochlea humeri
TN- trochlear notch of ulna
TT- tendon of triceps m.
U- ulna
UL- ulnaris lateralis m.
UT- ulnar tuberosity

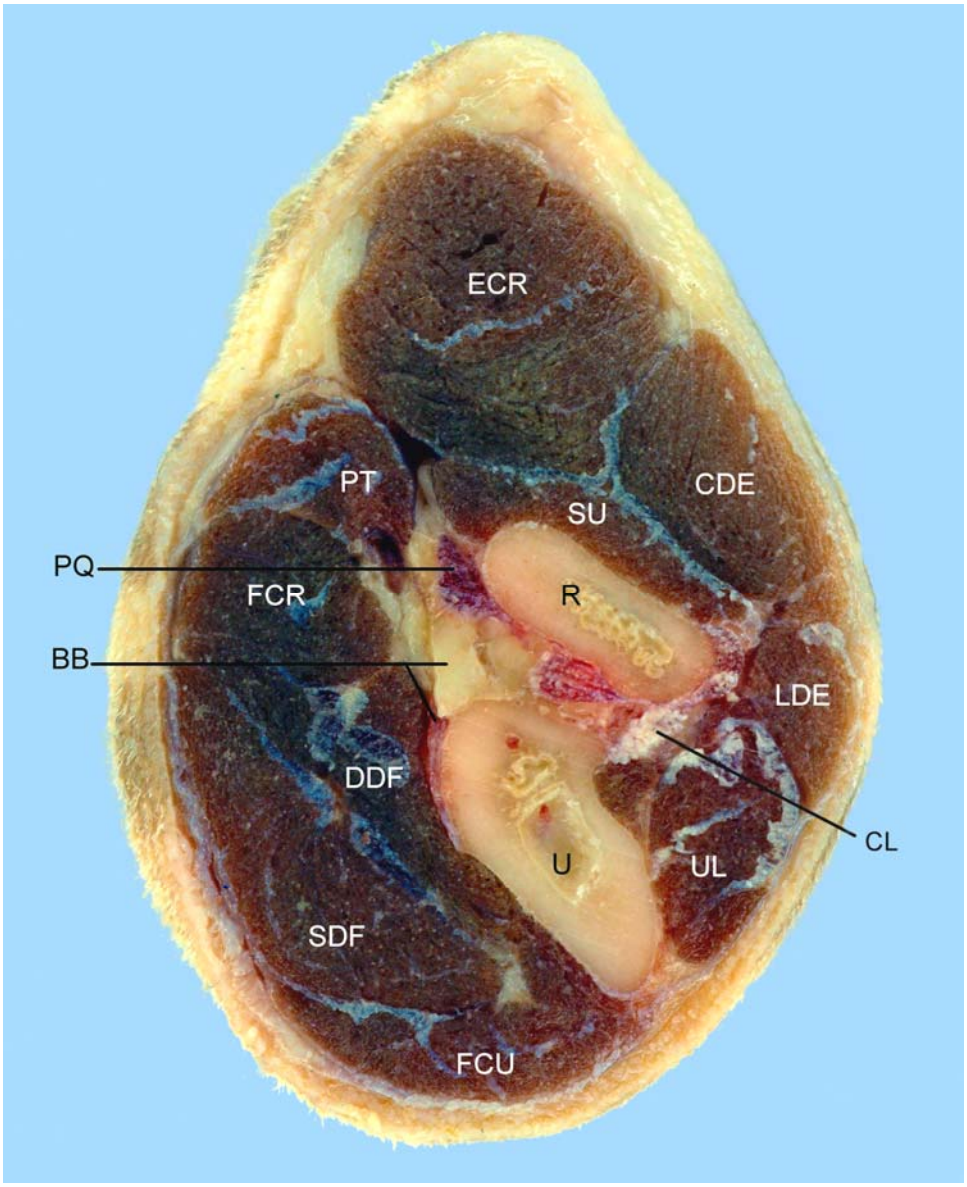
ECR
PT
CDE
SU
PQ
FCR
R
BB
LDE
DDF
CL
U
UL
SDF
FCU

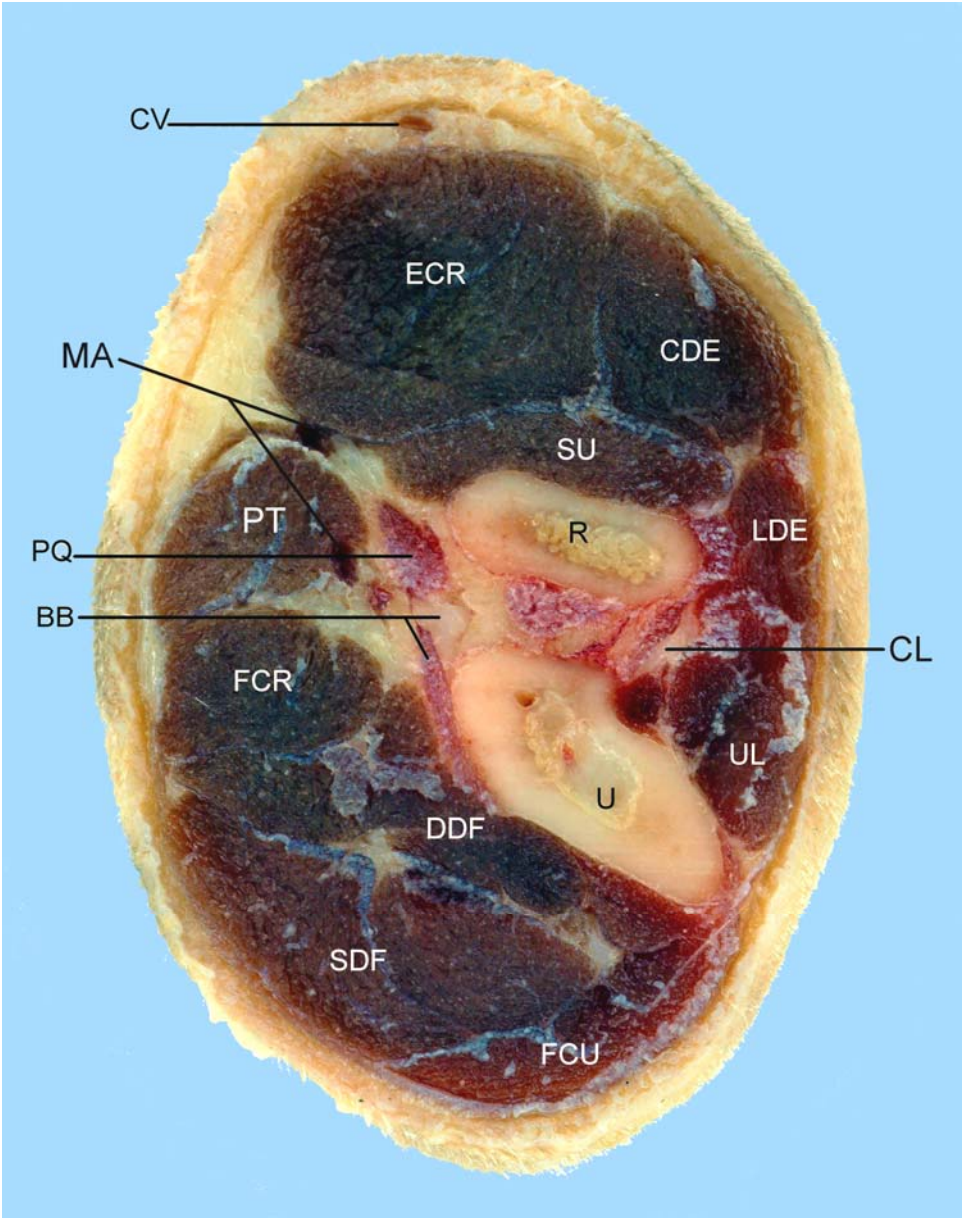
CV
ECR
MA
CDE
SU
PT
R
LDE
PQ
BB
CL
FCR
UL
U
DDF
SDF
FCU

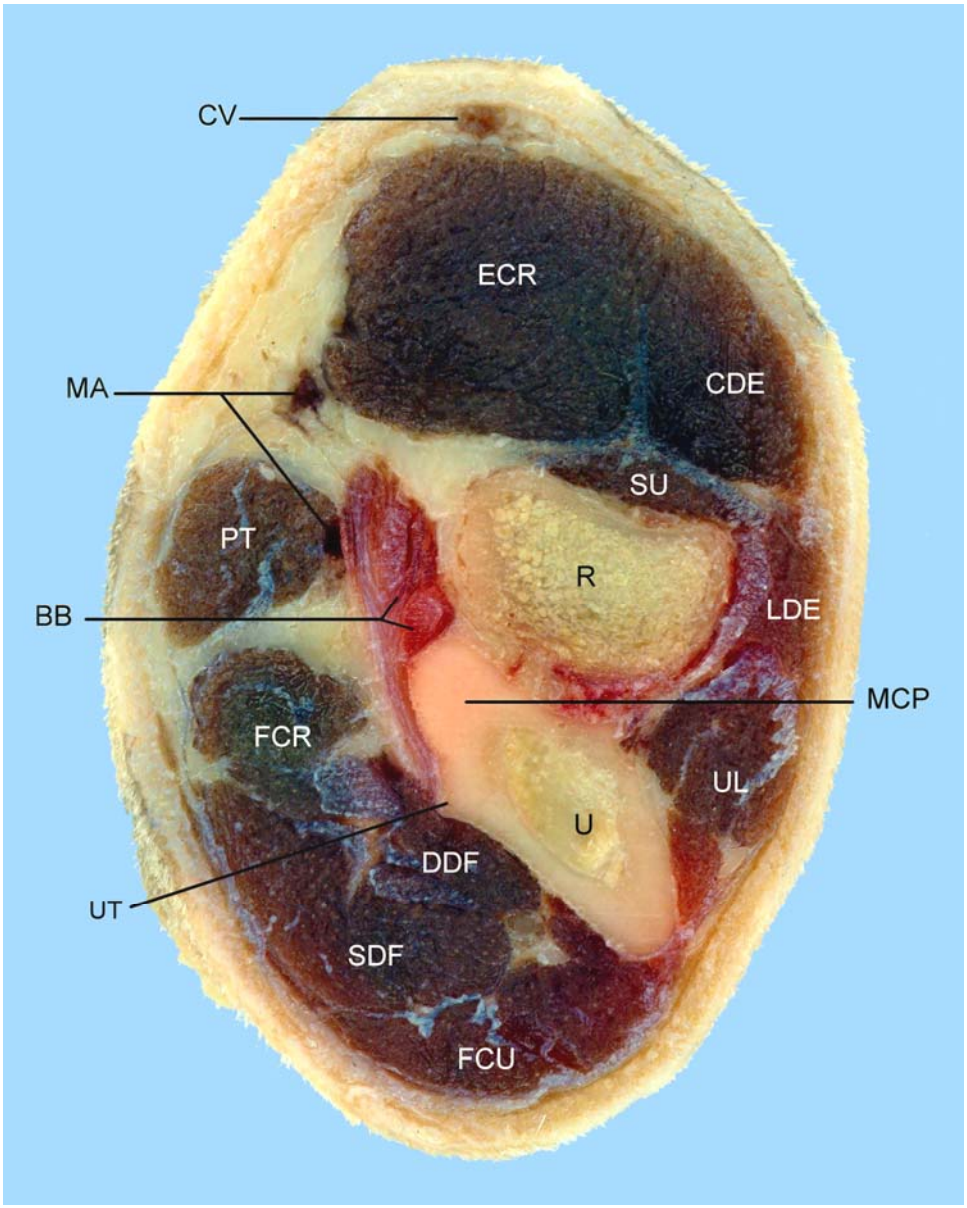
CV
ECR
MA
CDE
SU
PT
R
BB
LDE
MCP
FCR
UL
U
DDF
UT
SDF
FCU

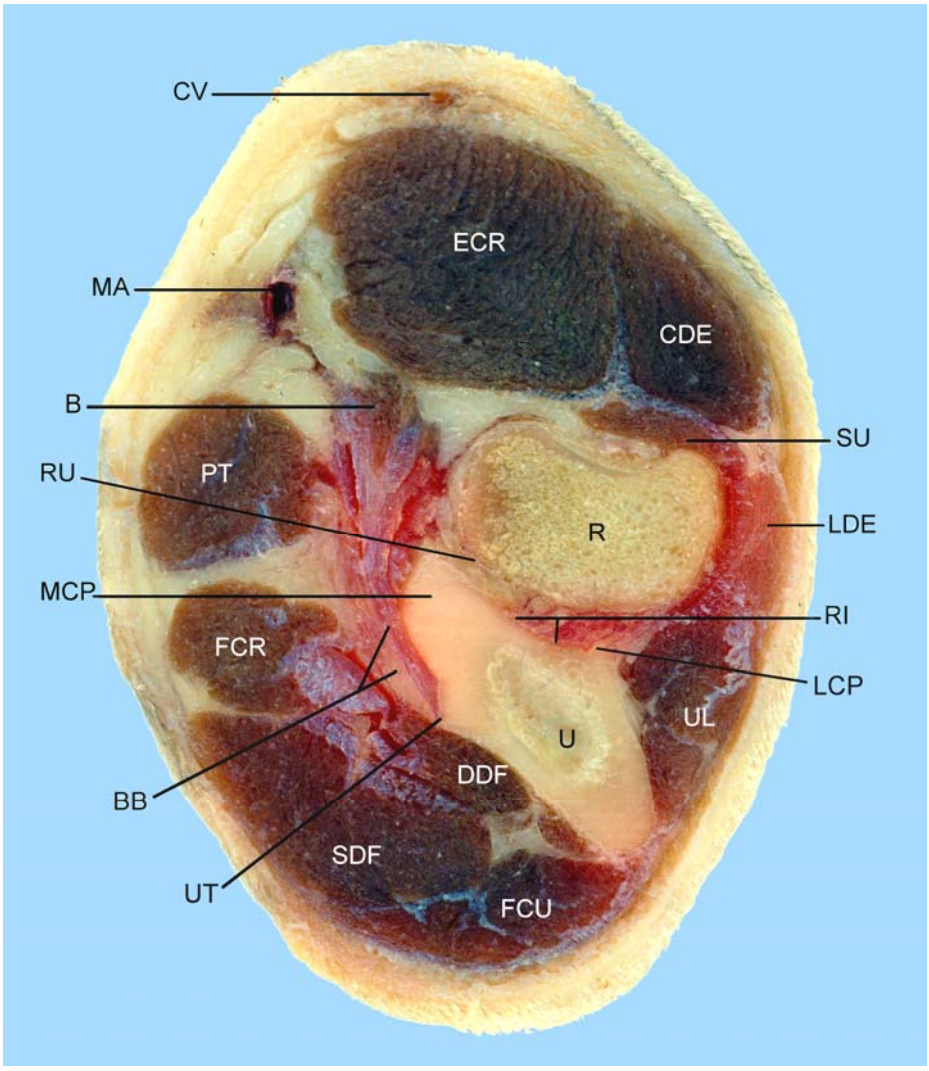
CV
ECR
MA
CDE
B
SU
RU
PT
R
LDE
MCP
RI
FCR
LCP
UL
U
DDF
BB
SDF
UT
FCU

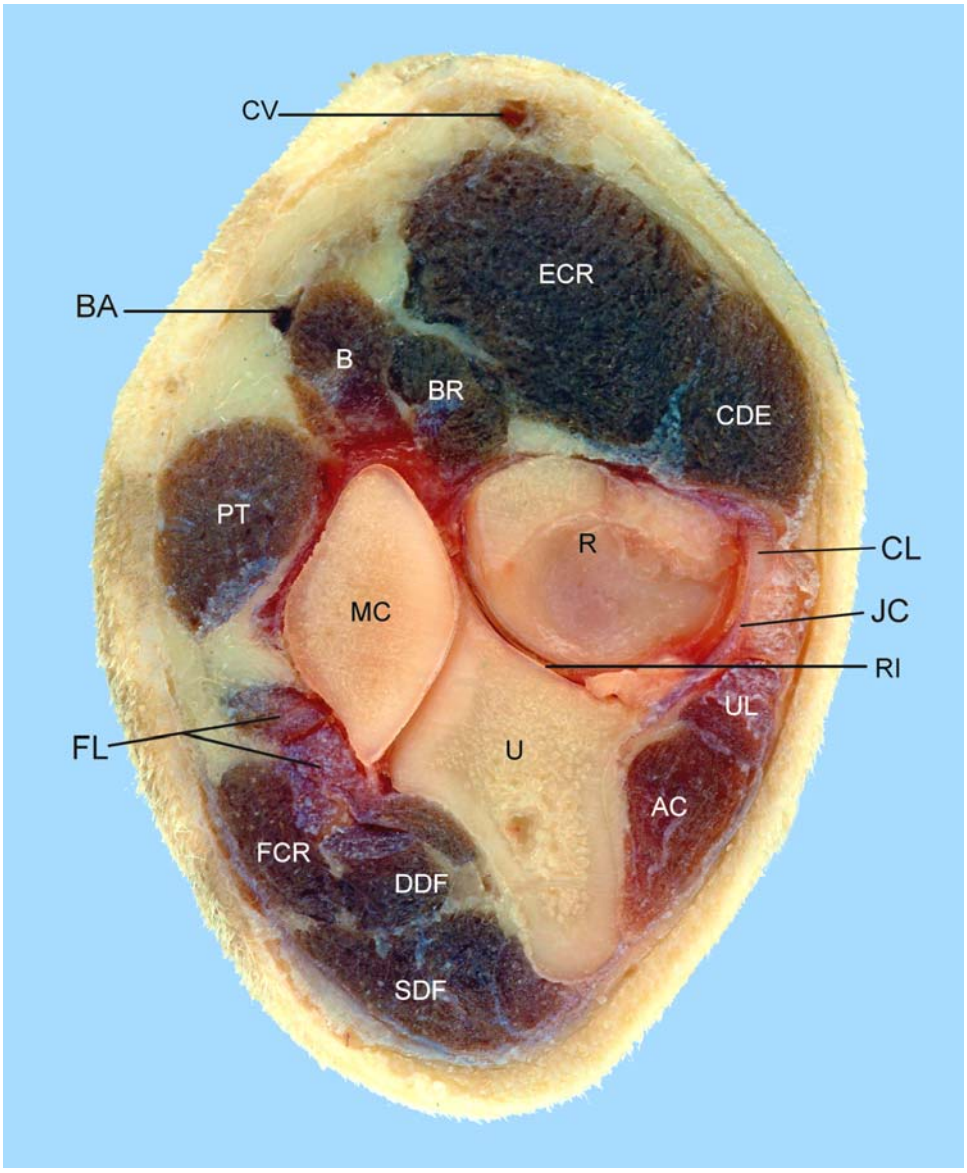
CV
ECR
BA
B
BR
CDE
PT
R
CL
MC
JC
RI
UL
FL
U
AC
FCR
DDF
SDF

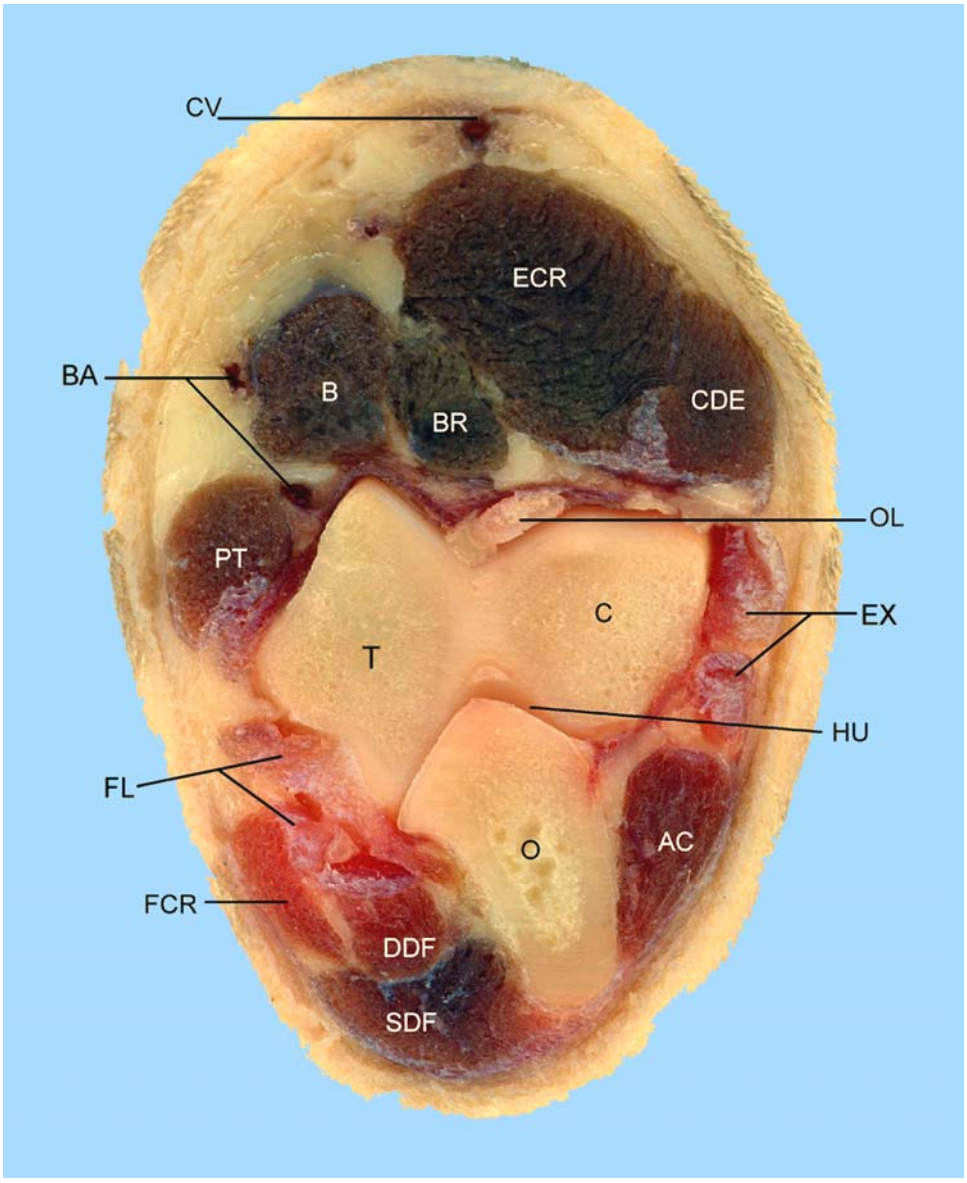
CV
ECR
BA
B
BR
CDE
OL
PT
C
EX
T
HU
FL
O
AC
FCR
DDF
SDF

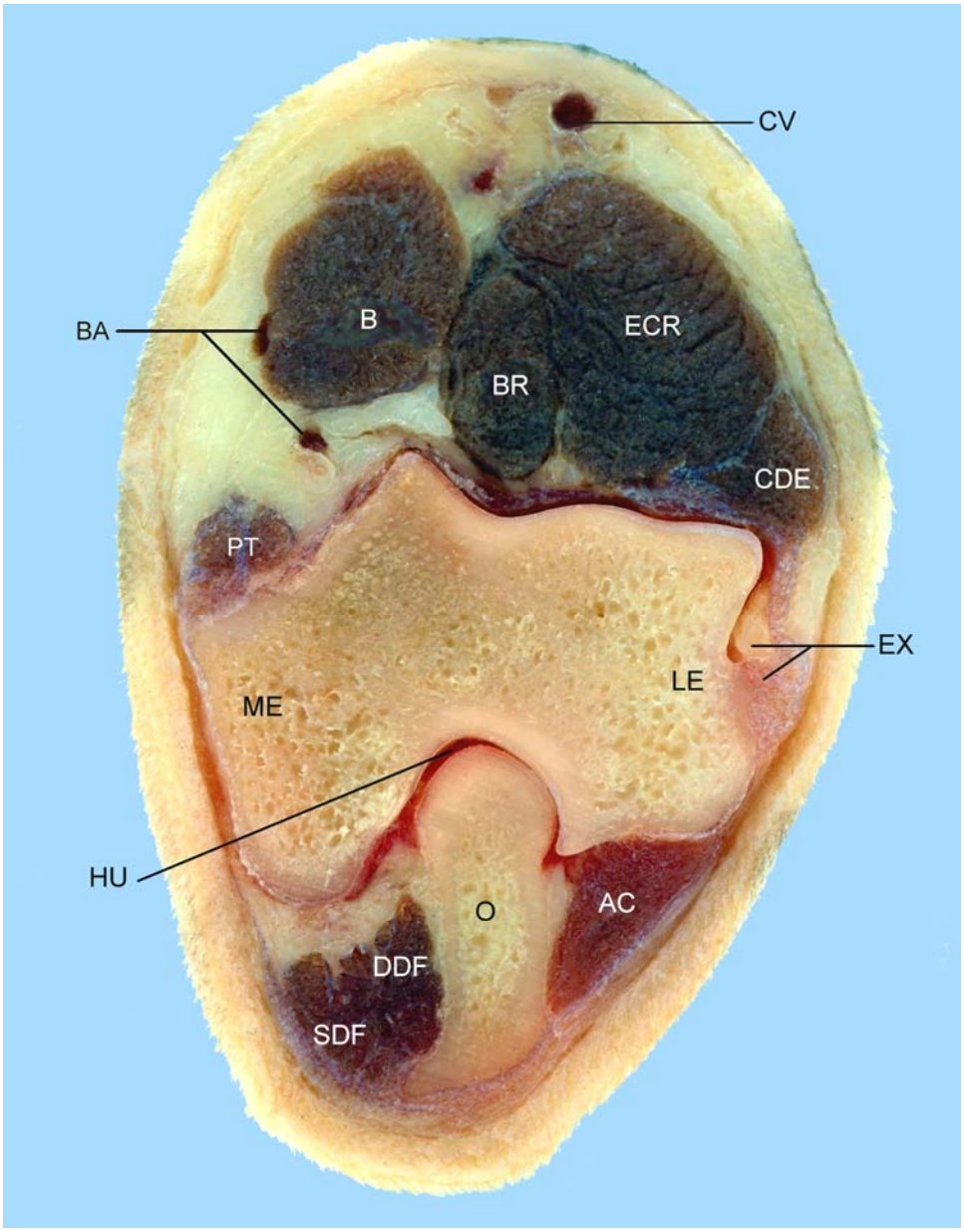
CV
BA
B
ECR
BR
CDE
PT
EX
LE
ME
HU
O
AC
DDF
SDF

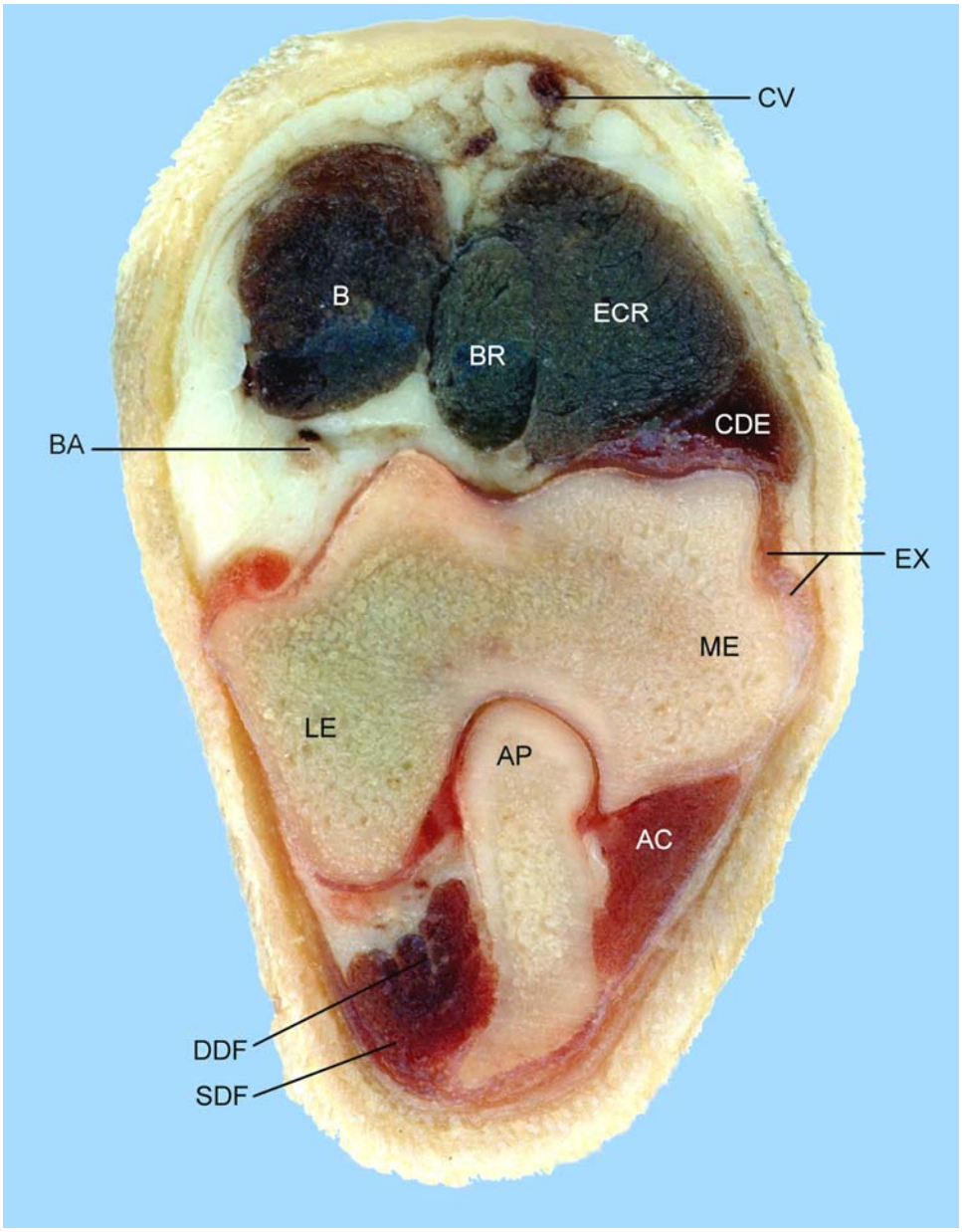
CV
B
ECR
BR
CDE
BA
EX
ME
LE
AP
AC
DDF
SDF

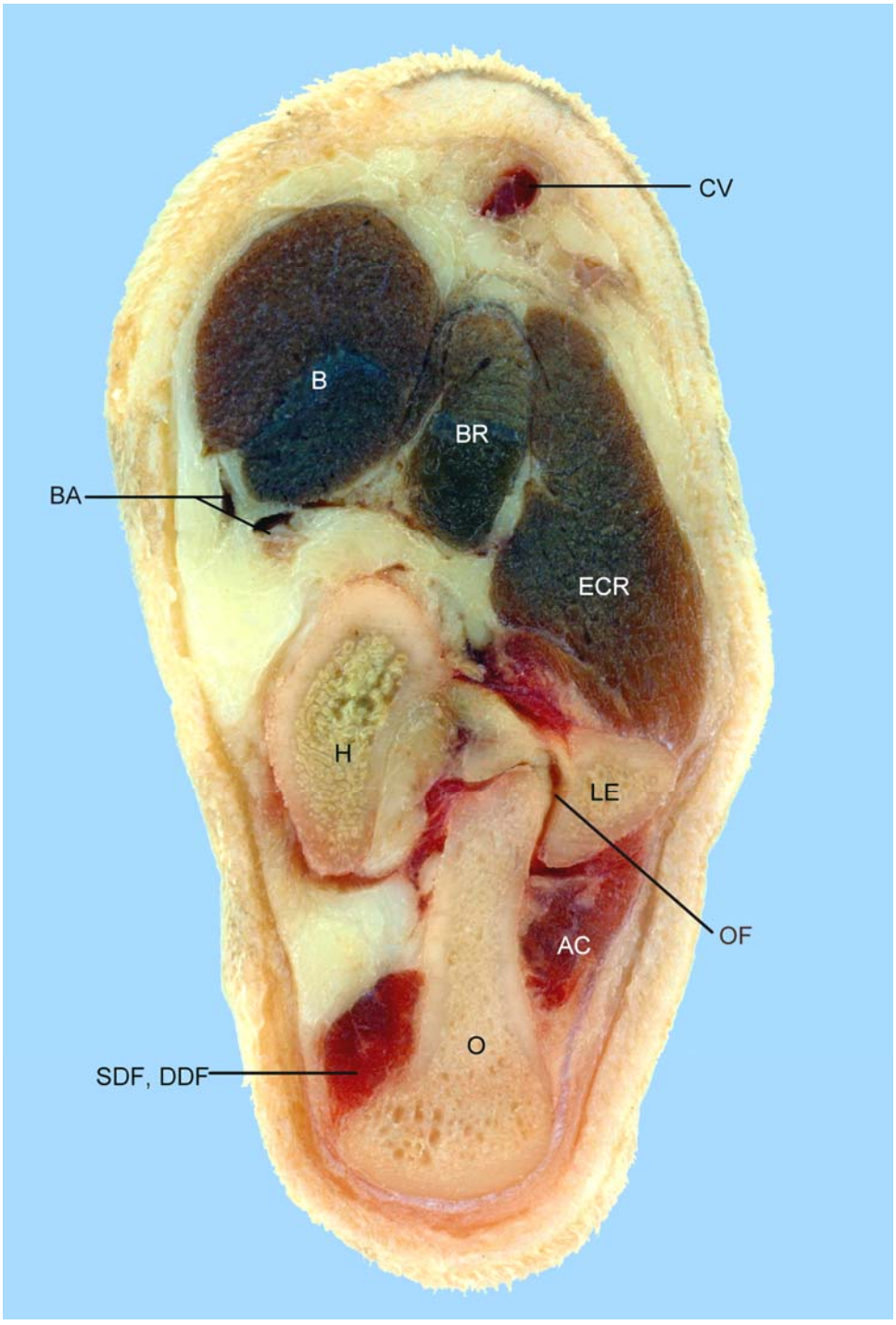
CV
B
BR
BA
ECR
H
LE
OF
AC
O
SDF, DDF

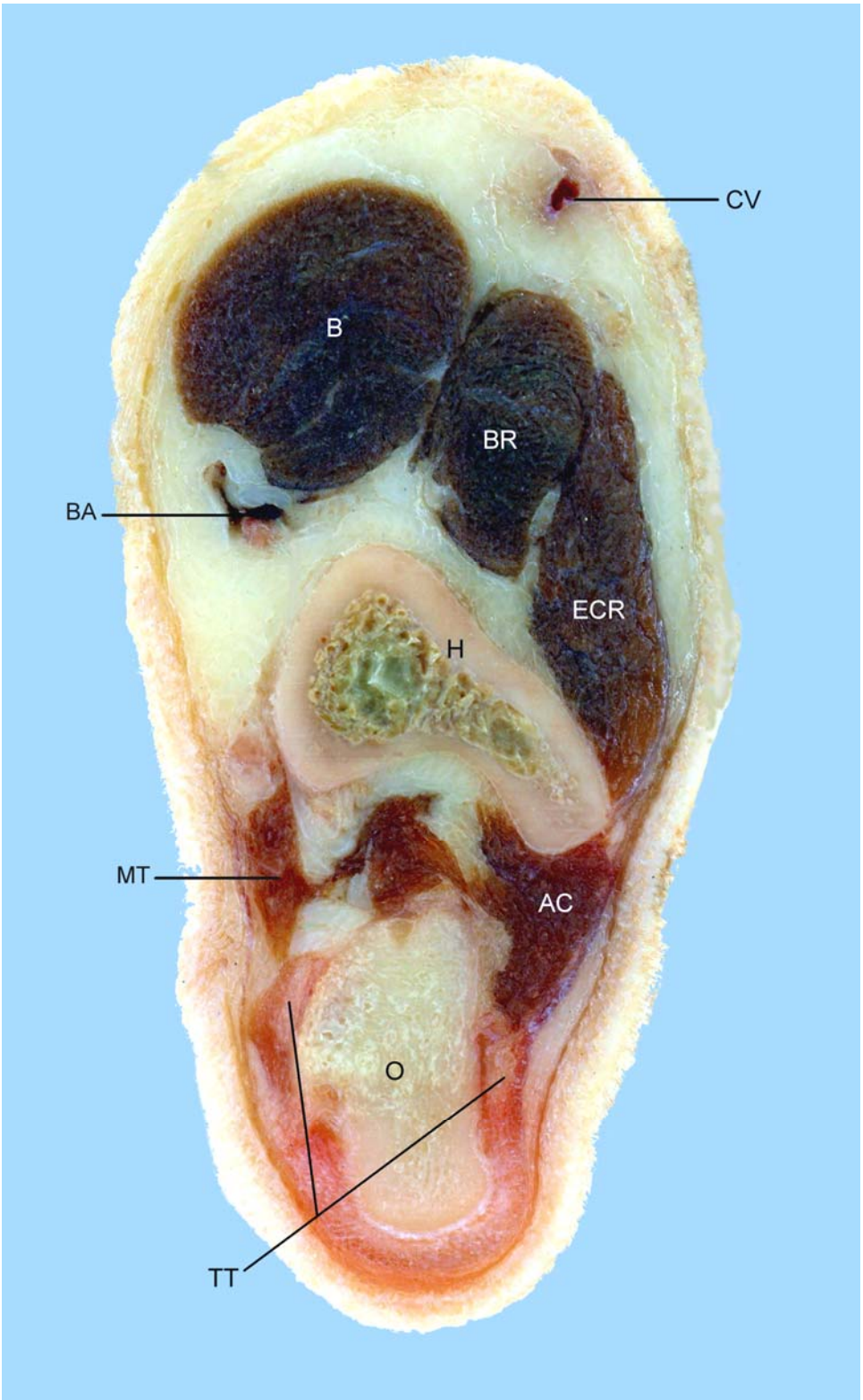
CV
B
BR
BA
ECR
H
MT
AC
O
TT

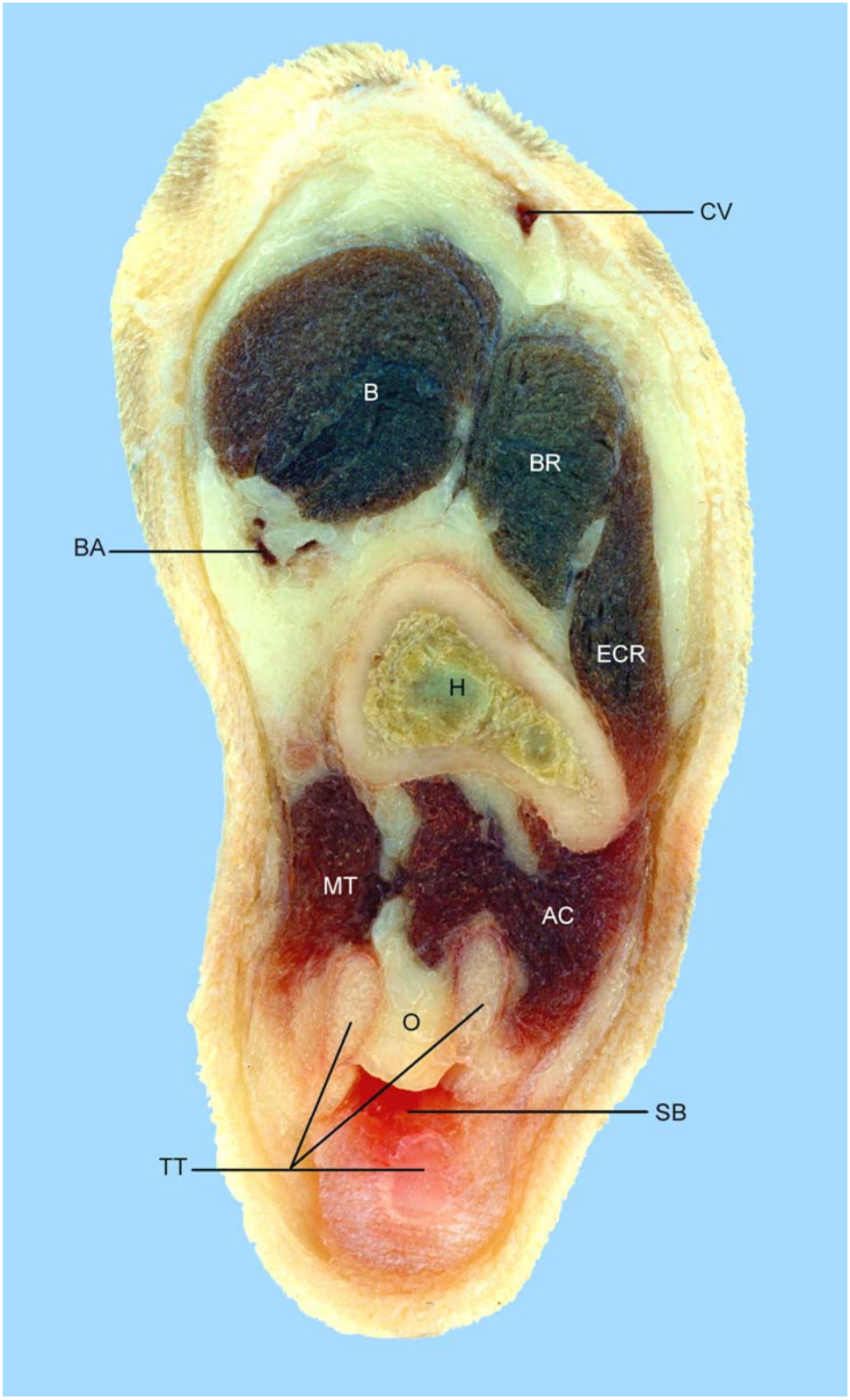
CV
B
BR
BA
ECR
H
MT
AC
O
SB
TT

SAGITTAL PLANE
Orientation is medial to lateral

AC- anconeus m.
AP- anconeal process of ulna
B- biceps brachii m.
BB- tendons of biceps and brachialis mm.
BR- brachialis m.
C- capitulum humeri
DDF- deep digital flexor m.
ECR- extensor carpi radialis m.
FCU- flexor carpi ulnaris m.
H- humerus
HR- humeroradial joint space
HU- humeroulnar joint space
JC- joint capsule
LaT- lateral head of triceps m.
LCP- lateral coronoid process of ulna
MCP- medial coronoid process of ulna
MT- medial head of triceps m.
O- olecranon of ulna
OF- olecranon fossa of humerus
PQ- pronator quadratus m.
R- radius
RU- radioulnar joint space
SB- subtendinous bursa
SDF- superficial digital flexor m.
SU- supinator m.
T- trochlea humeri
TN- trochlear notch of ulna
TT- tendon of triceps m.
U- ulna
UL- ulnaris lateralis m.

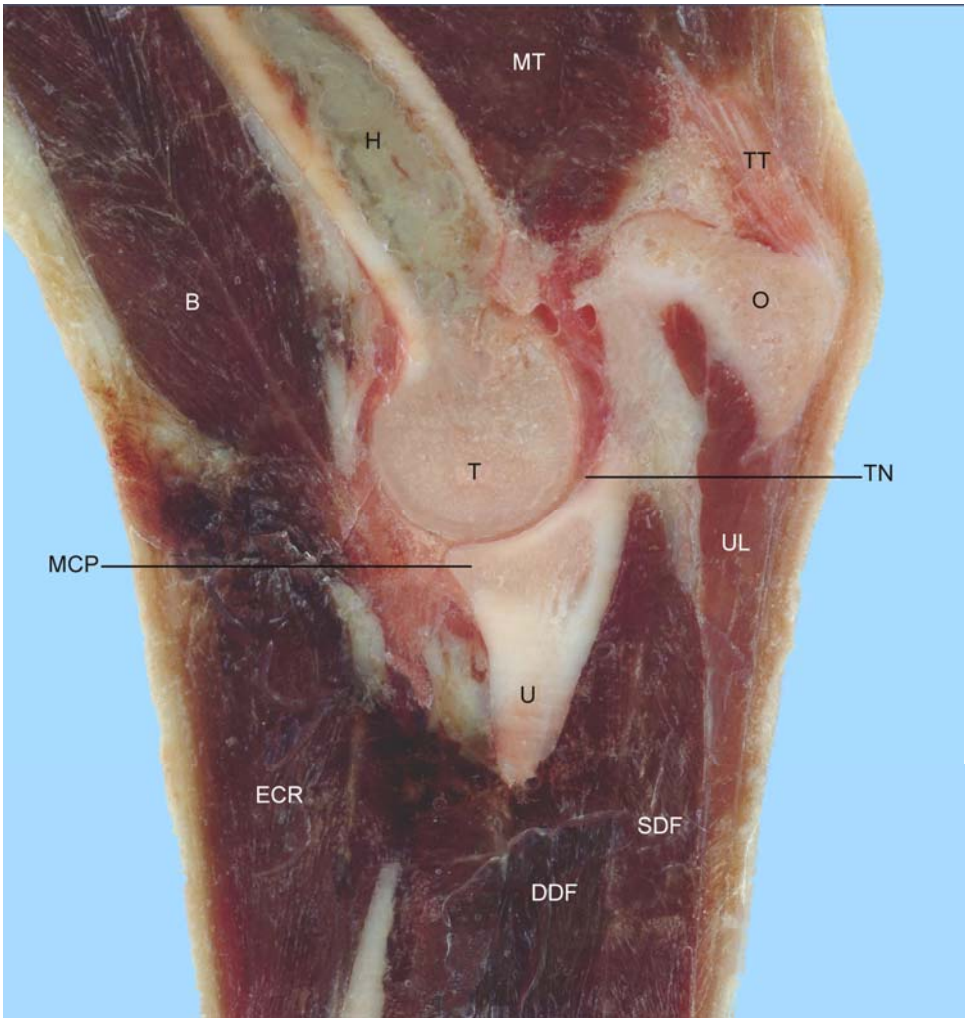
MT
H
TT
B
O
T
TN
MCP
UL
U
ECR
SDF
DDF

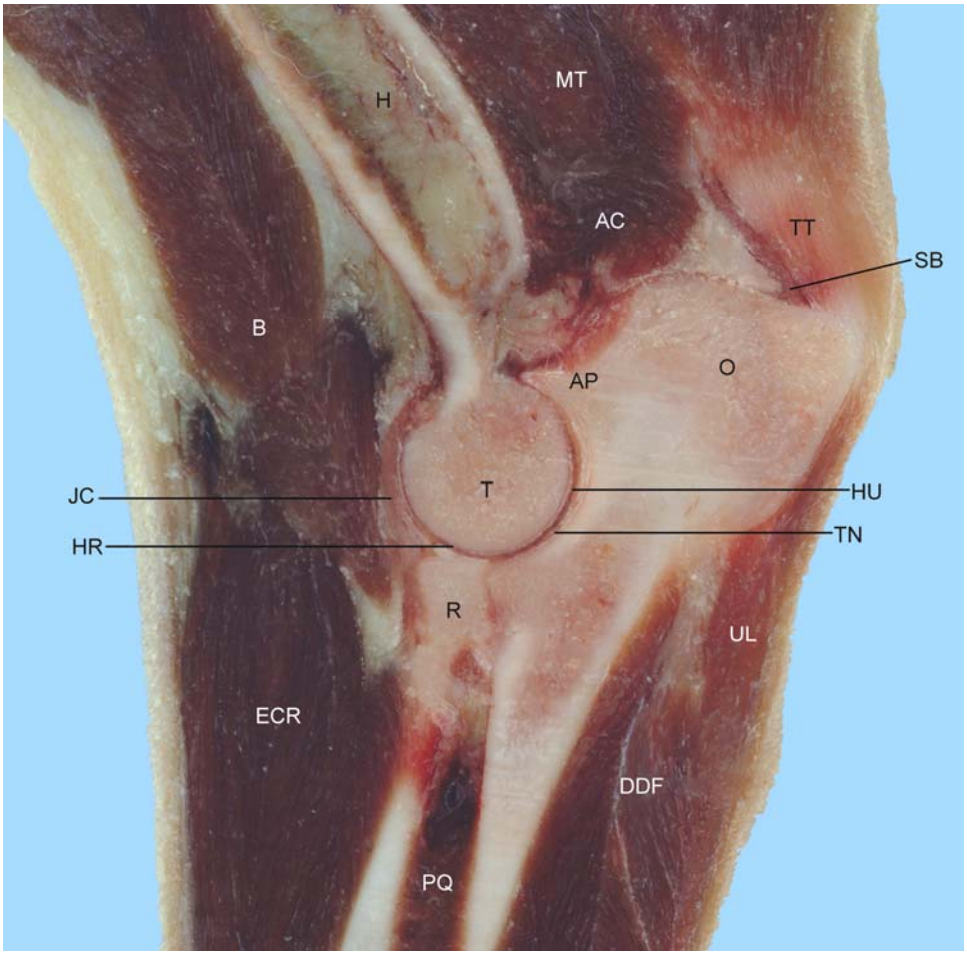
MT
H
AC
TT
SB
B
AP
O
JC
T
HU
HR
TN
R
UL
ECR
DDF
PQ

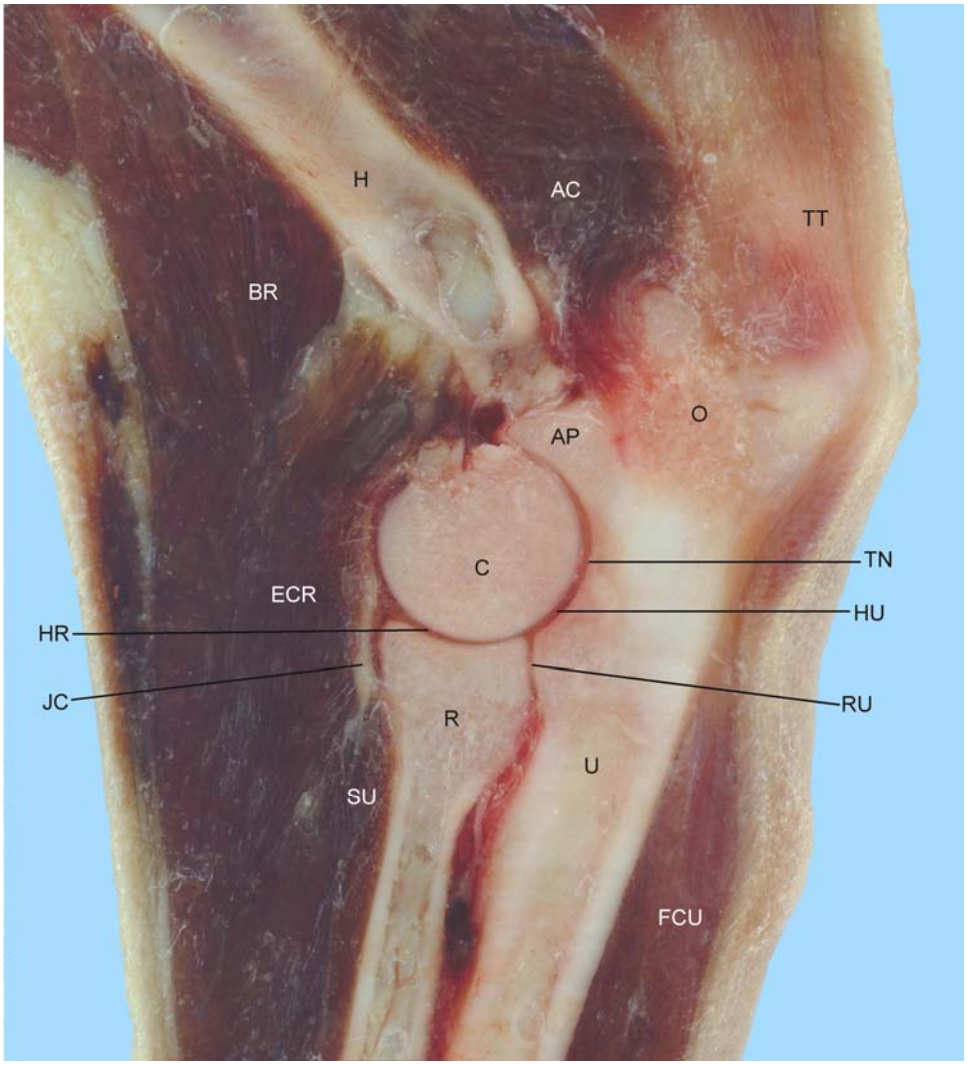
H
AC
TT
BR
O
AP
C
TN
ECR
HU
HR
JC
RU
R
U
SU
FCU

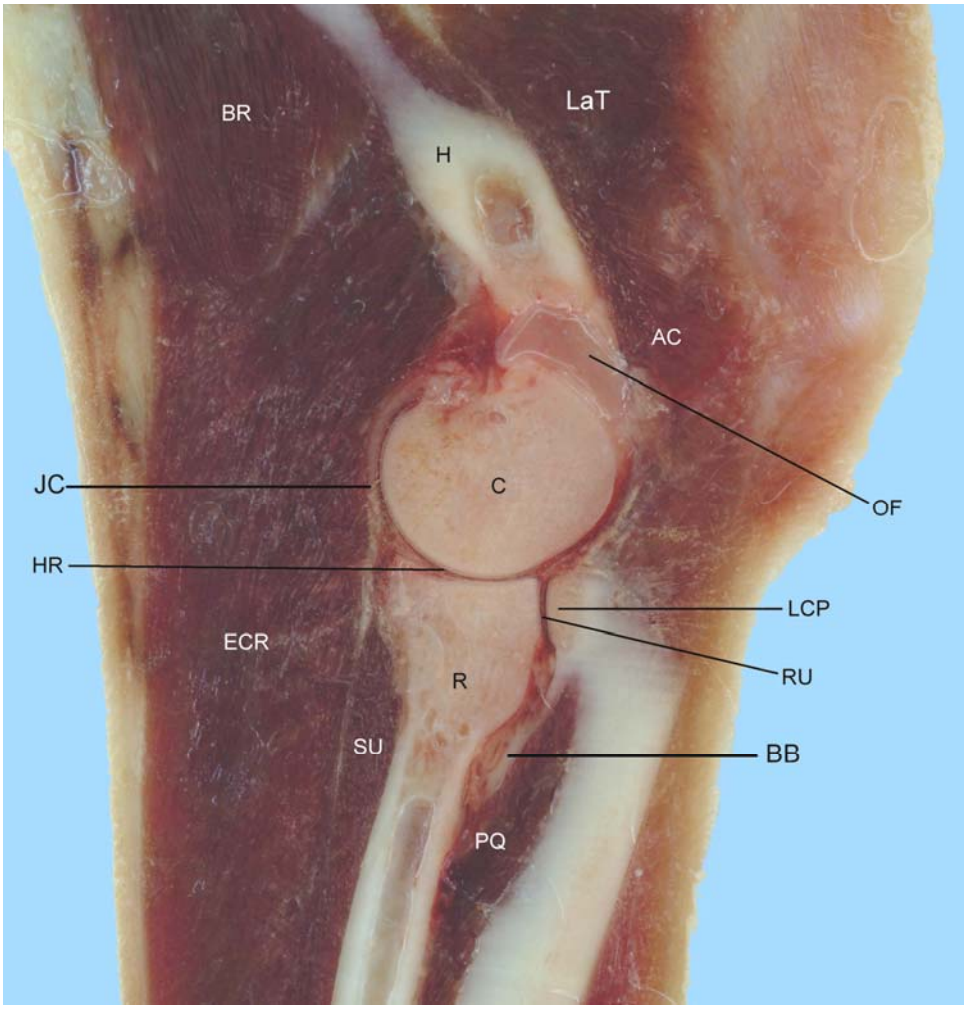
BR
LaT
H
AC
JC
C
OF
HR
LCP
ECR
RU
R
SU
BB
PQ

DORSAL PLANE

Orientation is cranial to caudal

AC- anconeus m.
AP- anconeal process of ulna
BB- tendons of biceps and brachialis mm.
C- capitulum humeri
CDE- common digital extensor m.
CL- lateral collateral ligament
DDF- deep digital flexor m.
FCR- flexor carpi radialis m.
FCU- flexor carpi ulnaris m.
H- humerus
HR- humeroradial joint space
HU- humeroulnar joint space
JC- joint capsule
LaT- lateral head of triceps m.
LCP- lateral coronoid process of ulna
LDE- lateral digital extensor m.
LE- lateral epicondyle of humerus
LoT- long head of triceps m.
MCP- medial coronoid process of ulna
ME- medial epicondyle of humerus
MT- medial head of triceps m.
O- olecranon of ulna
PQ- pronator quadratus m.
R- radius
SDF- superficial digital flexor m.
SU- supinator m.
T- trochlea humeri
TN- trochlear notch of ulna
TT- tendon of triceps m.
U- ulna
UL- ulnaris lateralis m.

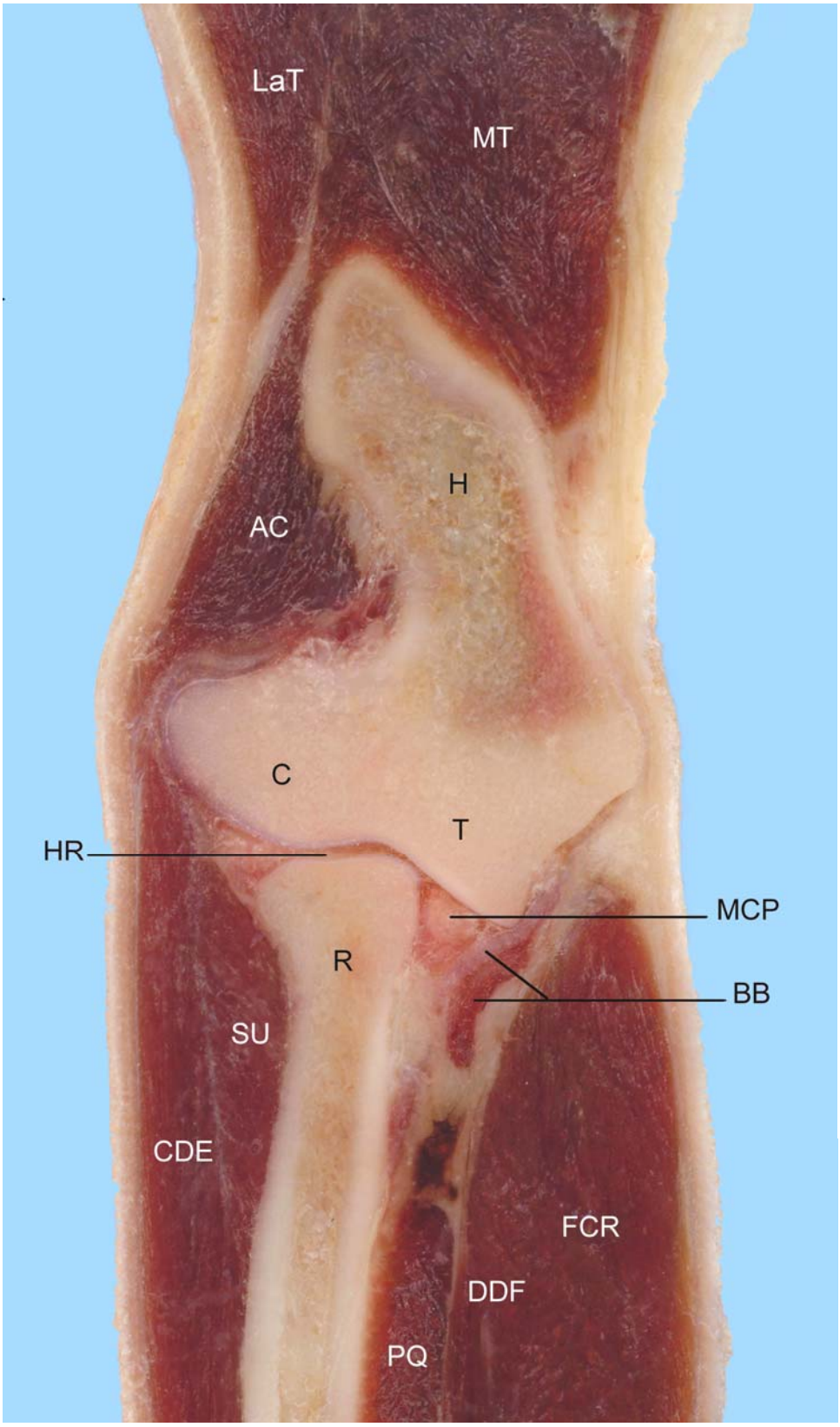
LaT
MT
H
AC
C
T
HR
MCP
R
BB
SU
CDE
FCR
DDF
PQ

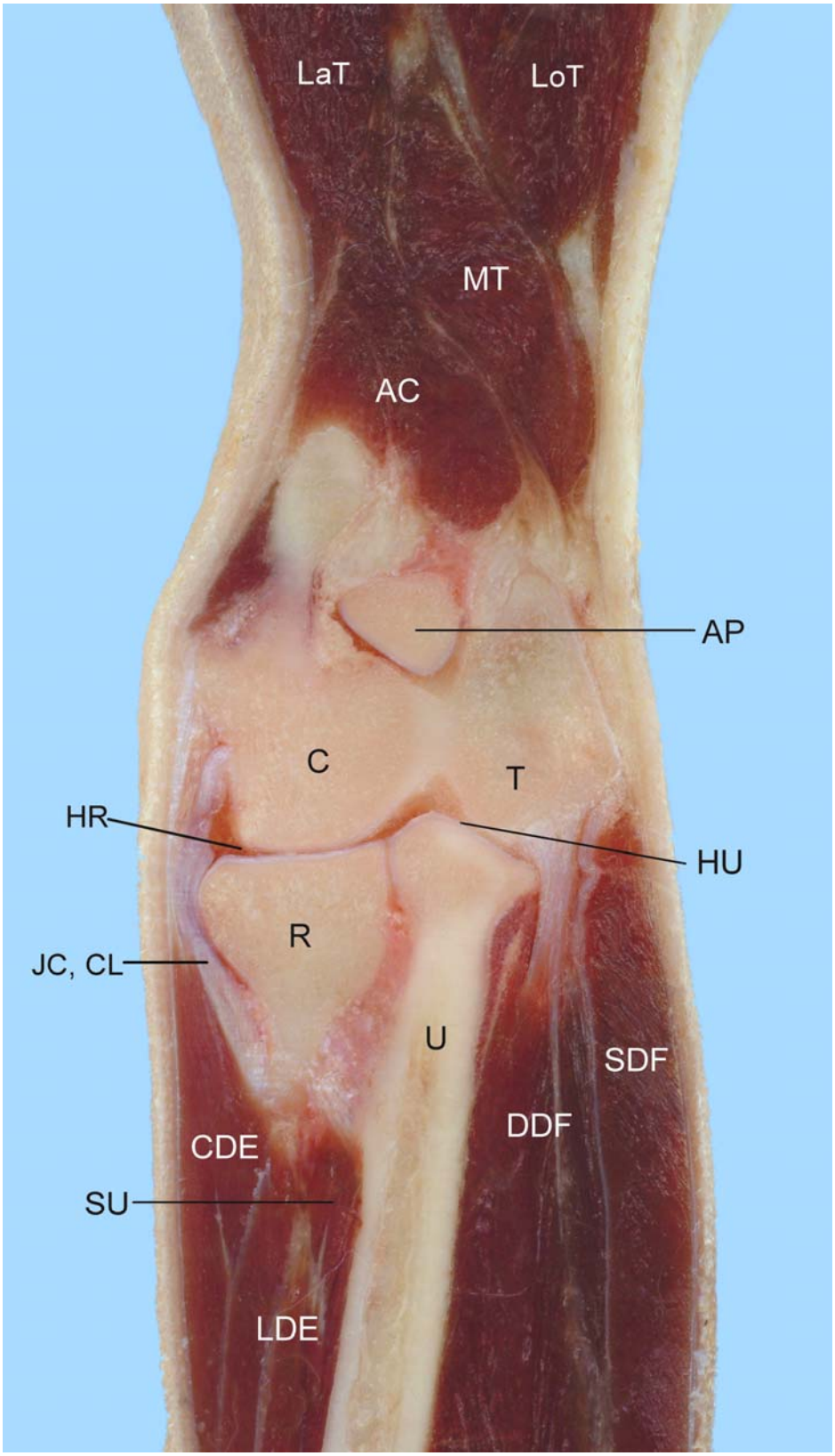
LaT
LoT
MT
AC
AP
C
T
HR
HU
R
JC, CL
U
SDF
DDF
CDE
SU
LDE

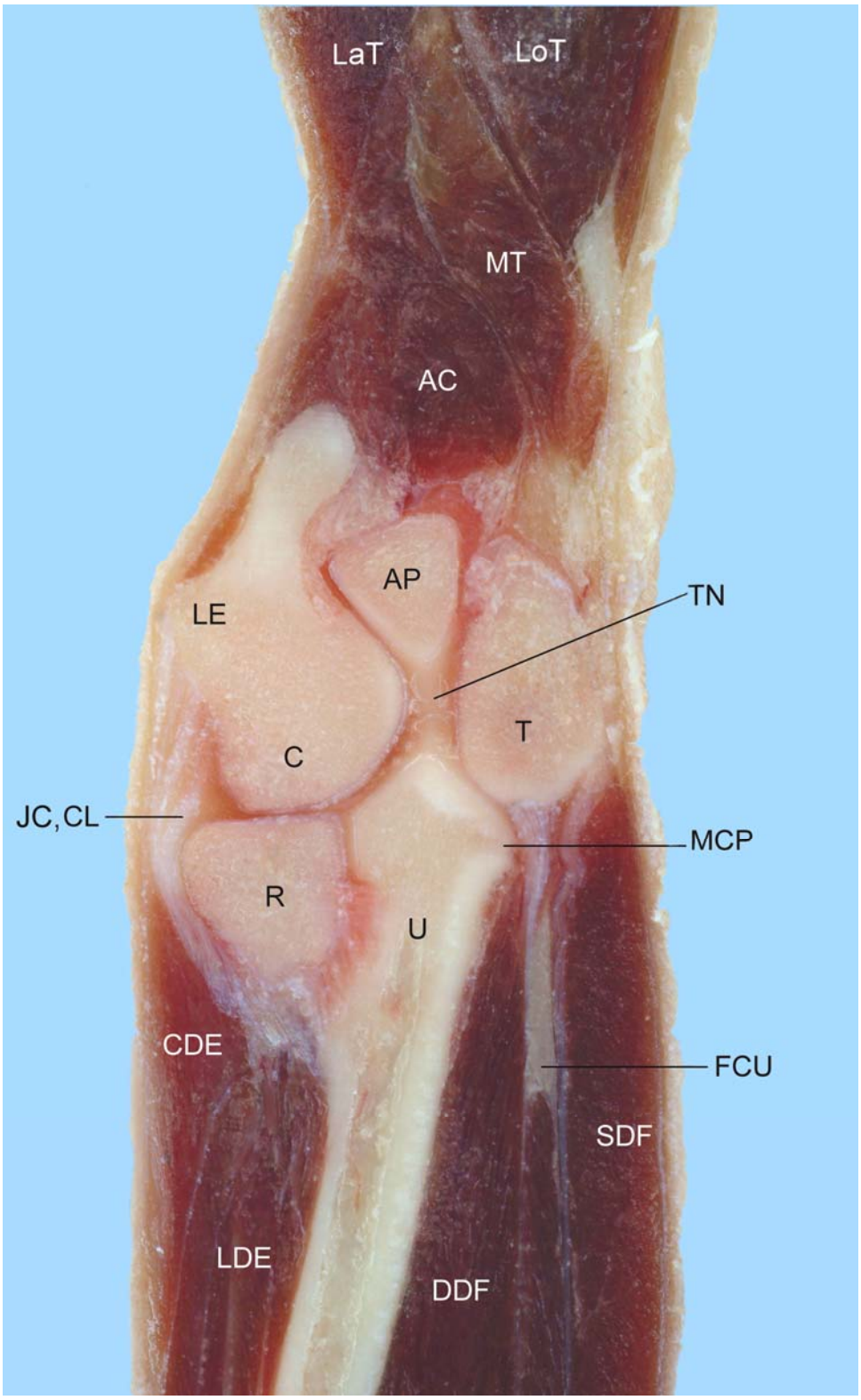
LaT
LoT
MT
AC
AP
LE
TN
T
C
JC, CL
MCP
R
U
CDE
FCU
SDF
LDE
DDF

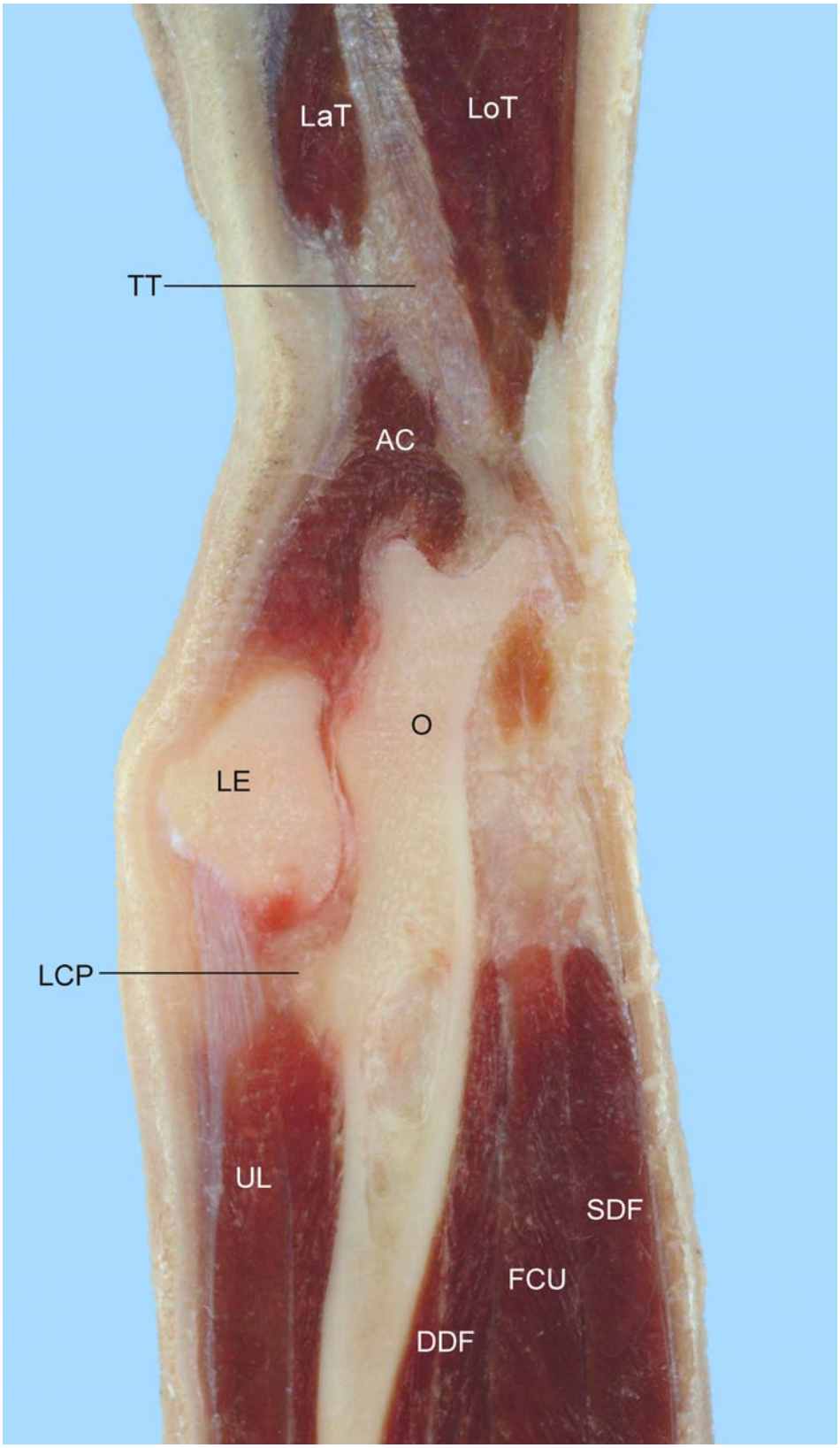
LaT
LoT
TT
AC
O
LE
LCP
UL
SDF
FCU
DDF